Studies on Anionic Platinum(II) Complexes: Phosphorescence Properties and Phase Control by Counter Cations

（アニオン性白金錯体に関する研究：対カチオンによる相制御とりん光特性）

Tomohiro Ogawa

Graduate School of Chemical Sciences and Engineering
Hokkaido University

Contents

Chapter 1
General Introduction

1-1. Introduction

Light is one of the most important source of our daily life. Scientists and industries have continuously researched physical properties of light and application to optoelectronic devices in order to develop our living for more convenient human society. For the last 20 years, optoelectronic devices became smaller, thicker and high-performing, which allows us to use high performance consumer electronics in our living nowadays. To control optoelectronic devices, excited state properties of materials play a key role in various conditions and media. The materials science has contributed to development of recent human society.

Although science and technology have been rapidly developed, international society still faces severe problems. One of critical issues is energy problem, which scientists can contribute to resolve. From the view point of sustainability and pollution of environment, utilization the energy of sun light is a promising candidate as clean energy resource. As one promising approach to convert solar energy to electricity, photovoltaic cell is now used for energy conversion from light to electricity by the photovoltaic effect.

Among these materials used in application, metal complexes play a key role in the development of optoelectronic applications. For example, the singlet and triplet excitons are theoretically generated in a 1:3 ratio by electronic excitation in organic light emitting diodes (OLEDs).[1] Therefore, fluorescent aromatic organic molecules can emit only 25% of excitons as photons. When metal complexes were used as emitter in OLEDs, theoretically 100% of excitons were extracted as photon due to phosphorescence properties of metal complexes.[2]

In the case of solar energy conversion, organic and inorganic dyes have been used as a photosensitizer in photovoltaic cells. Organic dyes are relatively low-cost and rich in variety, but photodegradation and long-term stability are inferior to inorganic dyes. In contrast, metal complexes show better stability and high performance,[3] however, the precious metals such as ruthenium and platinum are necessary for efficient sensitization. Other outstanding approach to utilize solar energy as energy source of human life is photochemical energy conversion called as artificial photosynthesis. Small molecule conversion reactions such as H_2 evolution,[4] CO_2 reduction,[5] and water splitting have been investigated with various metal complexes.

As mentioned above, metal organic chromophores have been received much attention due to their photophysical properties and diversity from designability of combination between metal atoms and organic ligands. Therefore, the research field of synthesis and physicochemical properties of metal complexes is considered one of important subjects.

1-2. Phosphorescent metal complexes

Phosphorescence is a type of luminescence which emits photons from excited triplet state (Figure 1). In the past decade, the interests of photofunctional metal complexes for wide range of application increased strongly. These materials are utilized emitters in OLEDs[6] and light-emitting electro-chemical cells (LEECs),[7] photosensitizer in dye-sensitized solar cells,[8] chemosensors,[9] bio-imaging,[10] chemical photo-catalysts.[11] Whilst high potential to be used for many application, the excited triplet states of metal complexes were less understood than pure organic materials.[12]

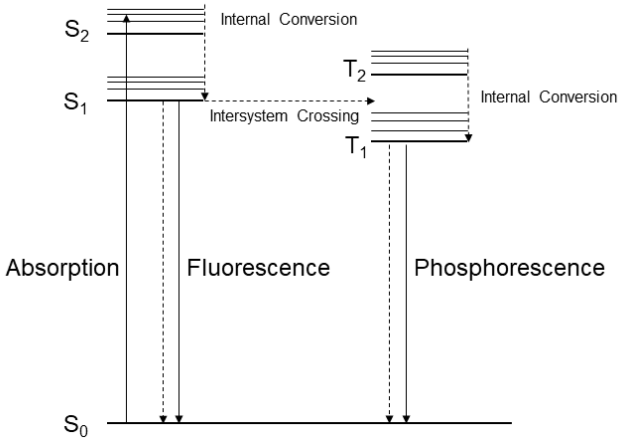

Figure 1. Jablonski diagram of fluorescence and phosphorescence.

In formation and phosphorescence properties of triplet states, spin-orbit coupling (SOC) plays a key role in both intersystem crossing (ISC) from excited singlet states to excited triplet states and phosphorescence from excited triplet states to ground states. Theoretically, such transition pathways are spin forbidden process, but mixing singlet states by spin-orbit coupling allow spin forbidden processes. In excited singlet states of organic molecules without any heavy atoms, rate constant of ISC is very competitive with radiative rate constant of fluorescence. On the other hand, for transition metal complexes, rate constant of ISC is significantly faster than that of fluorescence, and thus quantum yield of ISC is higher than that of organic molecules.[13] In radiative process from excited triplet states, radiative rate constant of phosphorescence of transition metal complexes are significantly faster than that of organic molecules. The rate constant of ISC from S_1 to $T_{1i\,(I = x, y, z)}$ is expressed by eq. 1, where, $\hbar$, $\widehat{H}_{SO}$, and Ψ, are Dirac constant, spin-orbit coupling Hamiltonian and wavefunction of each state, and δ function expresses the law of conservation of energy.

$$k_{ISC} = \frac{2\pi}{\hbar}\left|\left\langle \Psi_{S1}\left|\widehat{H}_{SO}{}^{i}\right|\Psi_{T1i}\right\rangle\right|^{2}\delta\big(E(S_1) - E_v(T_1)\big)\ (eq.\,1)$$

For simplified rate constant of phosphorescence is given by eq. 2, where, E is emission energy and n, h, ε_0 M_T are refractive index of medium, Plank constant, and the vacuum permittivity, respectively.

According to the first perturbation theory, transition dipole moment of phosphorescence M_T is given by eq. 3, where, Ψ_S , E_S and M_{S_n} are eigenfunction, eigenvalues, and transition dipole moment from *n*th singlet state to the ground states, respectively.[14]

$$k_T = \frac{16\pi^3 \times 10^6 E^3 n^3}{3\mathrm{h}\varepsilon_0} |M_T|^2 \ (eq. 2)$$

$$M_T = \sum \frac{\langle \Psi_T | \hat{H}_{SO} | \Psi_{S_n} \rangle}{{}^3E_T - {}^1E_{S_n}} M_{S_n} \ (eq. 3)$$

Both equation contain spin-orbit coupling Hamiltonian, which is given by eq. 4, where, ζ, $\hat{\boldsymbol{l}}$, and $\hat{\boldsymbol{s}}$ are spin-orbit coupling constant, angular momentum operator and spin operator, respectively.

$$\hat{H}_{SO} = \zeta \hat{\boldsymbol{l}} \cdot \hat{\boldsymbol{s}} \ (eq. 4)$$

The spin-orbit coupling constants of several atoms were listed in Table 1. These constants were calculated by using spin-restricted Hartree-Fock wavefunctions.[15] Therefore, large spin orbit coupling constants of heavy transition metals reveal very different excited character from light organic molecules, which is well-known as a heavy atom effect.

The equations 1-4 were simplified description, and it cannot be used in calculation of SOC efficiency of realistic measurements and experiments. To determine degree of SOC effect experimentally, zero-field splitting (ZFS) energy of excited triplet states is used. The energy level of triplet sublevels of ^{3}MLCT states is given by equation 5.

$$E(i) = E_{T_1} + \sum_{nj} \frac{|\langle T_n(j)|H_{SO}|T_1(i)\rangle|^2}{E[T_1] - E[T_n]} + \sum_{m} \frac{|\langle S_m|H_{SO}|T_1(i)\rangle|^2}{E[T_1] - E[S_m]} \ (eq. 5)$$

According to eq 5, the information of degree of SOC in excited triplet states can be obtained by energy splitting of triplet sublevels. At very low temperature, thermal equilibrium of three sublevels of triplet states depends on the temperature. Therefore, temperature dependence of phosphorescence lifetime measurement at wide range measurements have been used to determine the zero-field splitting in transition metal complexes. However, although the detailed phosphorescence studies need the information of ZFS parameters of excited triplet states, the reported ZFS parameters was significantly limited to several very famous transition metal complexes such as, $[Ru(bpy)_3]^{2+}$,[16] $[Ir(ppy)_3]$,[17] and [Pt(ppy)(acac)].[18]

Table 1 Atomic Masses and Spin-Orbit Coupling Constants

	Atomic Mass/u	ζ /cm^{-1}
Hydrogen	1.00794	0.24
Carbon	12.0107	32
Nitrogen	14.0067	78
Ruthenium	101.07	1042
Iridium	192.217	3909
Platinum	195.078	4481

1-3. Phosphorescence properties of platinum(II) complexes

Platinum is an element in third low of group 10 in the periodic table. The divalent Pt atom has d^8 electron configuration, which favor to adopt square planar coordination geometry. Consideration of a simple ligand field splitting diagram reveals why d^8 electron configuration frequently form square planar complexes with strong ligand field. For Pt(II), the ligand field is sufficiently large to form square planar with any ligands, whereas, weak ligand field ensure to adopt octahedral geometry in nickel(II) complexes with the same d^8 electronic configuration. The photophysical properties of Pt(II) complexes with four-coordinate square-planar geometry are remarkably different from the other metal complexes[19] such as, Ru(II), Ir(III), Rh(I), Os(II), Re(I) (octahedral, d^6 electron configuration) and Cu(I) (tetrahedral, d^{10} electron configuration), Ag(I), Au(I) (linear, d^{10} electron configuration) and lanthanide (7 or 8 coordinate). Flat molecular structure allows Pt(II) complexes to interact either with other Pt(II) complexes or other molecules. Ground state stacking of Pt(II) complexes cause metal-metal interactions when Pt-Pt distance is shorter than twice of van der Waals radius of Pt atom (3.5 Å). As shown in Figure 2, the overlap of two $5d_z^2$ orbitals form weakly bonding and antibonding dσ and dσ* molecular orbitals. Therefore, highest occupied molecular orbitals of emissive triplet states switch from ligand p orbital to metal based dσ* orbitals. Such charge-transfer excited state from metal dσ* to ligand π* is known as metal-metal-to-ligand charge-transfer (MMLCT) states.

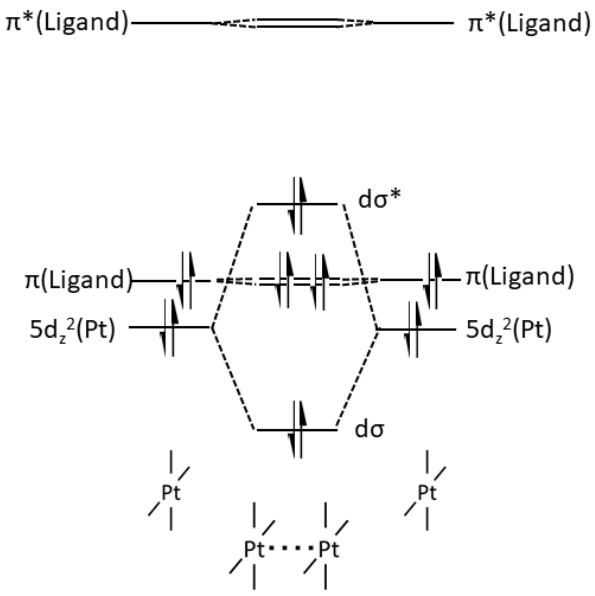

Figure 2. Simplified frontier molecular orbital diagram of monomer and dimer with Pt-Pt interaction.

As important instances, $[Pt(CN)_4]^{2-}$ exhibits concentration dependence of absorption spectra.[20] The MMLCT absorption band around 300 nm increases, and the broad emission is observed with increasing concentration in solution (Figure 3).

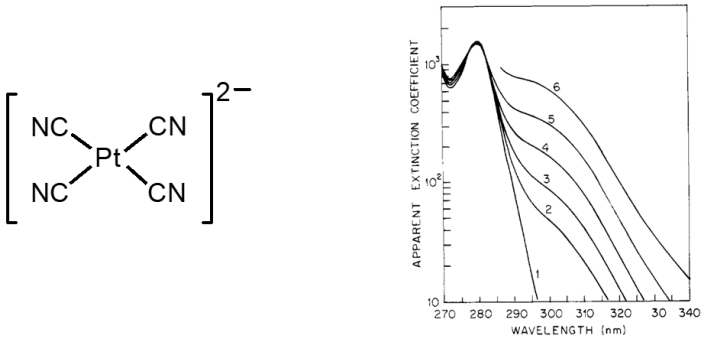

Figure 3. Structural formula of $[Pt(CN)_4]^{2-}$ and its concentration dependence of absorption spectra in solution.

In the crystalline sate, $[PtCl_2(bpy)]$ (bpy = 2,2'-bipyridine) displays temperature dependent emission.[21] The emission energy decreases linearly with R^{-3} (R = Pt-Pt distance from variable-temperature X-ray crystallography) (Figure 4).[22] After these pioneering works, many MMLCT emitter based on Pt(II) complexes have been reported because of the characteristic chromic behavior based on presence and degree of Pt-Pt interactions.[23]

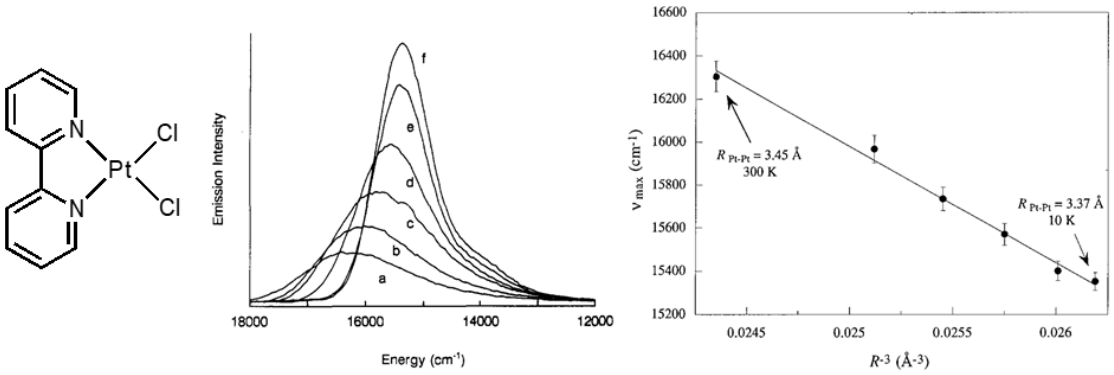

Figure 4. Structural formula of $[PtCl_2(bpy)]$ (left) and the temperature dependence of emission spectra (center)[21] and Pt-Pt distance (right).[22]

Furthermore, monomer emission from triplet ligand centered excited states (^{3}LC) is observed when ligand with strong σ donor ability is introduced in Pt(II) complexes. In Pt(II) complexes without metal-metal interaction, ligand field (d-d) excited states play key role in non-radiative pathways of excited states. To suppress such non-radiative pathway, strong ligand fields are necessary to form strong emitter. Phenylpyridine and its derivatives are most studied ligands which provide strong

ligand field derived from both strong σ donation of C^- and π acceptor ability of pyridyl group. Since systematic study of cyclometalated complexes [Pt(C^N)(O^O)] (C^N = phenyulpyridine and its derivatives; O^O = acetylacetonate or dipivaloylmethane, Figure 5) reported by Thompson and co-workers in 2002,[24] many cyclometalated Pt(II) complexes have been studied, because both ^{3}MMLCT and ^{3}LC can be utilized in OLEDs (Figure 6).[25] From the view point of emitters for OLEDs, numerous neutral Pt(II) complexes have been investigated, because ionic materials cannot be utilized in vacuum deposition process of OLEDs. Although the neutral Pt(II) complexes have been studied intensively, ionic materials based on phosphorescence Pt(II) complexes have been less reported. To investigate novel functional materials, using Pt(II) complexes as ionic materials is one of great possibility to create novel unique photo-functional materials.

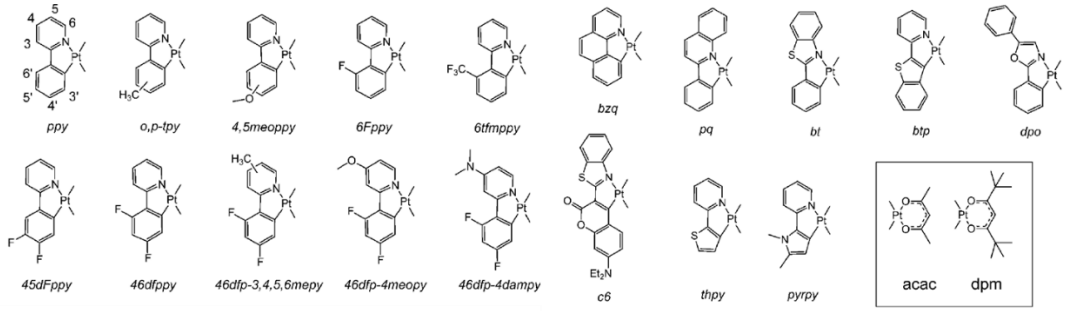

Figure 5. Variation of cyclometalating ligands used to prepare [Pt(C^N)(O^O)] complexes in Ref 24.

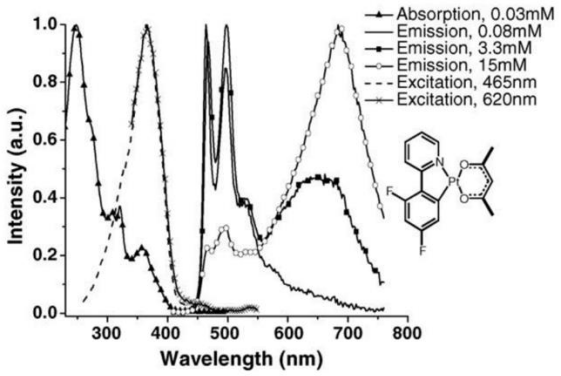

Figure 6. Emission spectra of various concentration of [Pt(dFppy)(acac)][25]

1-4. Soft material

Soft materials are substance that are deformed and/or structurally transformed by external stimuli such as, thermal, mechanical, magnetic, at around room temperature. The soft materials include liquid crystals, liquids, sols, gels, polymers, as well as biological materials. In the last three decades, liquid crystalline materials have been developed as functional soft materials. Liquid crystalline states are considered as the forth states of materials. Liquid crystalline phase has fluidity like a liquid, but they are anisotropic unlike a liquid. Most of liquid crystals are organic molecules with long alkyl chains. Recently, ionic liquid crystals have also been received considerable attention due to their additional function derived from ionic characters and diversity of combination of anions and cations.[26] In liquid crystals, metal complexes can be used as mesogenic cores known as metallomesogens.[27] Such metallomesogens were functionalized by magnetic, redox, and photoluminescent properties of metal complexes.

In addition to liquid crystals, liquid organic molecules have also attracted much attention as a soft material. For liquid materials, ionic liquid is much popular because of high designability. Ionic liquid is liquid materials that contain anion and anion, and either or both ions are composed of organic molecules.[28]

Although photophysical properties of transition metal complexes have been intensively studied in the past two decades, however, these reported photophysical properties were measured under limited condition, such as in solution state, crystalline states, or polymer host materials. Studies on photofunctional metal complexes as soft materials have been less investigated, while enormous photofunctional organic soft materials have been reported as versatile materials. For luminescent metallomesogens composed of Pt(II) complexes, Swager and co-worker reported columnar liquid crystalline phase of cationic Pt(II) complexes ([Pt(ppy)(L)]X: ppy = 2-phenylpyridine; L = 2-(1-hexyl-1,2,3-triazole-4-yl)-pyridine or 2-(1-dodecyl-1,2,3-triazole-4-yl)-pyridine; X = SbF_6^-, PF_6^-, BF_4^-, or OTf^-, Figure 7).[29] These complexes display thermotropic mesophase between crystalline and liquid states in spite of having a single side chain. The crystalline states of that compounds undergo mechanochromic transformation which is reversed with solvent exposure.

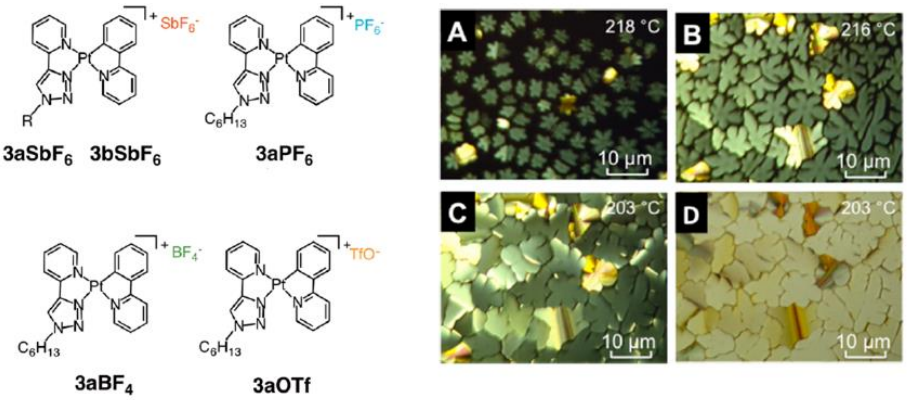

Figure 7. Structural formula of [Pt(ppy)(L)]X and poPolarized optical microscopy images of the hexagonal columnar liquid crystalline phase (Col_h) of $3aSbF_6$.[29]

Bruce and co-workers reported neutral liquid crystalline Pt(II) complexes [Pt(Rdpb)Cl] (HRdpb = 4,6-difluoro-1,3-di(5-dodecyl-2-pyridyl)-benzene or 4,6-difluoro-1,3-di(5-pentadecyl-2-pyridyl)-benzene, Figure 8).[30] These Pt(II) metellomesogens showed absorption and emission color change depending on the structural phase which can be controlled thermal treatment.

Most Pt(II) metallomesogens exhibit chromic emission behavior based on physical properties of the stimulus-sensitive mesophase, however, emission change of liquid crystalline Pt(II) complexes is attributed to degree of intermolecular interactions.

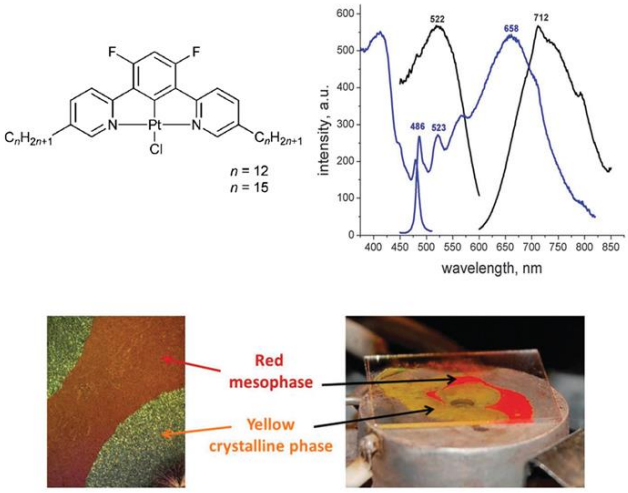

Figure 8. Structural formula of [Pt(Rdpb)Cl] and their photophysical properties.[30]

These results suggest that monomeric phosphorescence is not observed in liquid crystalline phase because planar Pt(II) mesogens are clarified to discotic liquid crystals which tend to form stacking liquid crystalline phase such as columnar and lamellar liquid crystalline phase. Therefore, to use both emission from monomer and aggregated Pt(II) complexes, more disordered structure is necessary to suppress formation of excited and ground state metallophilic interaction. For more dimensionally disordered materials, ionic liquid or liquid materials are candidate to create Pt(II) soft materials with both monomer and dimer/excimer emission. To synthesize low melting point molecules, introduction of long and/or branched alkyl chain is most frequently used approach. However, unlike organic molecules, most long alkyl chain substituted metal complexes form liquid crystalline phase, and no liquid phase have been reported in neutral metal complexes with long alkyl chain.

1-5. Ionic liquid composed of metal complexes

To create liquid materials with various functionality, one promising approach is using ionic complexes as ionic liquids. Ionic liquids are easily functionalized by electronic, magnetic, and optical properties of metal complexes when ionic metal complexes were used as ions in ionic liquid. For example of photophysical application of room temperature ionic liquids, Nockemann and co-workers reported ionic liquid materials using Lanthanide anionic complexes with di-alkyl imidazolium cations ($[C_4mim]_{x-3}[Ln(NCS)_x(H_2O)_y]$ (x = 6-8; y = 0-2; x + y < 10; Ln = Y, La-Yb); C_4mim = 1-butyl-3-methylimidazolium). Resulting liquid materials have absorption properties based on f-f transition of lanthanide complexes (Figure 9).[31]

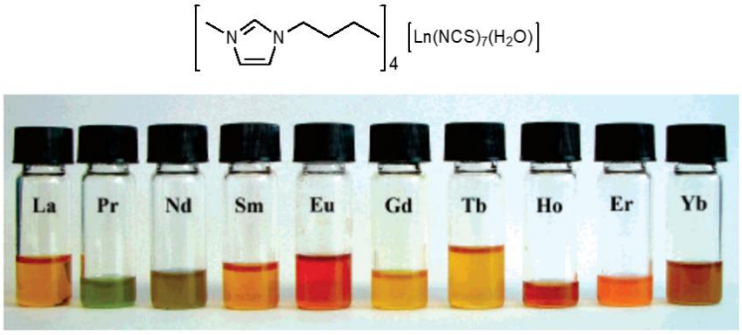

Figure 9. Structural formula of $[C_4mim]_4[Ln(NCS)_7(H_2O)]$ and photograph of ionic liquids which color is due to metal ions.[31]

Mudring and co-workers reported photoluminescent ionic liquids ($[R]_x[Eu(Tf_2N)_{3+x}]$ (Tf_2N = bis-(trifluoromethanesulfonyl) amide; x = 1 for R = 1-propyl-3-methylimidazolium (C_3mim) and 1-butyl-3-methylimidazolium(C_4mim); x = 2 for R = 1-butyl-1-methylpyrrolidinium (C_4mpyr)) as luminescent soft materials, and metal-centered f-f emission was observed in liquid states (Figure 10).[32]

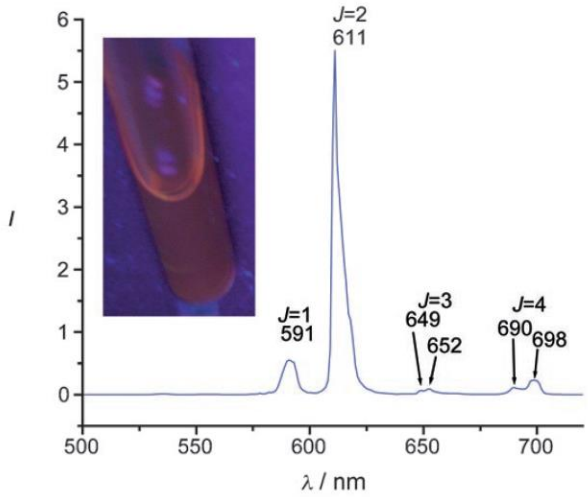

Figrue 10. photograph and emission spectra of liquid states of $[C_3mim][Eu(Tf_2N)_4]$.[32]

In addition to these examples, photoluminescent ionic liquid composed of Mg(II), Au(I), Ag(I), Ru(II), have been observed. To liquify ionic metal complexes, di-alkyl imidazolium cations were frequently used as a cation, which is most well-studied cation in organic ionic liquid.[32] Two different length of alkane, low molecular structural symmetry, as well as delocalization of cationic charge cause significant destabilization of crystalline phase. Besides using as a cation, few reports used imidazolium moieties as functional groups attached in ligands to obtain liquid materials. As described above, several pioneering reports focused on liquid materials using metal complexes, however, reported room temperature ionic liquids composed of metal complexes are still far less than that of organic ionic liquids.

In this thesis, the ionic liquids composed of metal complexes does not include the mixtures of metal complexes and ionic liquids. There are many reports about mixture of metal complexes and ionic liquid.[33] Dissolving metal complexes into ionic liquid is easier method to obtain non-volatile liquid materials. However, the major properties of such mixture are similar to those of metal complexes measured in organic polar solvents except for conductivity and volatility. To develop novel phosphorescent liquid materials, it is desirable that characteristic properties only observed in condensed liquid materials are described clearly.

1-6. Purpose of this thesis

A number of phosphorescent Pt(II) complexes have been reported until now because of characteristic photophysial properties. However, there is only a few examples for anionic Pt(II) complexes, which can be synthesized as functional ionic soft materials with many functional organic cations. Furthermore, ionic liquid Pt(II) complexes at room temperature have not been reported so far, although several liquid crystalline Pt(II) complexes and their photophysical properties have been reported.[29, 30] If Pt(II) complexes can be used as cation or anion of ionic liquids, condensed Pt(II) liquid materials are obtained. In liquid states of Pt(II) complexes, both monomer (^{3}LC) emission and dimer or excimer (^{3}MMLCT) emission might be observed due to coexistence of monomer and dimer structure in fluid liquid state. From the view point of luminescent liquid materials, ionic liquid Pt(II) complexes have a potential to exhibit chromic luminescence behavior depends on the ratio of monomer and dimer emission. As the mentioned this introduction, ionic liquid Pt(II) complex can be considered as one promising candidate for novel photofunctional soft materials.

In this thesis, synthesis, photophysical properties and thermal phase transition of ionic liquid Pt(II) complexes were studied. To synthesize first ionic liquid Pt(II) complex, anionic Pt(II) complexes was used as anion of ionic liquids with alkyl imidazolium cations. To synthesize anionic Pt(II) complexes, totally tri valent anionic ligands should coordinate to four coordination cites of Pt metal center. Not only charge but also ligand field strength should be considered to design phosphorescent Pt(II) complexes. Therefore, one anionic Pt(II) complex skeleton was chosen as anion used in this thesis, which have well-studied mono anionic bidentate phenylpyridine derivatives and two cyanides which is monoanionic monodentate ligand with strong ligand field.[34]

For anionic Pt(II) complexes, packing structure of crystalline states can be controlled by combination of various cations. Photophysical properties of monomer (^{3}LC) emission and dimer (^{3}MMLCT) emission can be determined by using corresponding crystalline complexes. When the potassium ion was used as a cation, obtained complexes have Pt-Pt interaction. On the other hand, bulky tetrabutyl ammonium cation suppress the Pt-Pt interaction due to alternative stacking structure of cations and anions.[35]

In order to investigate a variation of Pt(II) ionic liquids, a series of novel anionic Pt(II) complexes are necessary to be investigated. Anionic cyclometalated Pt(II) complexes with various N-heterocyclic carbene were synthesized and their detailed photophysical properties were studied as new anionic Pt(II) complexes. Furthermore, to develop phosphorescent ionic liquid, increasing photoluminescence quantum yields is an important issue. The criteria of strong emissive Pt(II) complexes was also studied.

1-7. Outline of this thesis

This thesis consists of 6 chapters, which was briefly described in this section.

In chapter 1, the background and purpose of this research thesis are described with important references. As key aspects,

In chapter 2, an ionic liquid Pt(II) complex $[C_2mim][Pt(CN)_2(ptpy)]$ (Hptpy = *p*-tolylpyridine) was reported as first ionic liquid composed of Pt(II) complexes. Photophysical properties and thermal phase transition as well as variable-temperature photoluminescence properties are described. Resulting ionic liquid Pt(II) complex exhibit dual emission from both monomer and dimer, which clearly demonstrate characteristic emission properties only observed in liquid states of luminescent Pt(II) complex.

In chapter 3, novel anionic Pt(II) complexes with N-heterocyclic carbenes *n*-$Bu_4N[Pt(CN)_2(NHC)]$ (H_2NHC^+ = 1-methyl-3-phenylimidazolium, 1-methyl-3-phenyl-benzimidazolium, 1-methyl-3-(naphtharene-2-yl)-1*H*-imidazolium, 1-methyl-3-(naphtharene-1-yl)-1*H*-imidazolium) were reported. The synthesis and photophysical properties were described. The thermal activation to higher lying non-radiative properties and zero-field splitting parameter of phosphorescence properties were studied in detail by wide range variable-temperature photoluminescence lifetime measurements. Furthermore, regioselective π extension effect was presented by three isomers derived from regioselective benzanulion.

In chapter 4, two ionic liquids $[C_4mim][Pt(CN)_2(L)]$ (H_2L = 1-methyl-3-phenylimidazolium, HL = benzo[h]quinoline) were described. Photophysical properties and thermal phase transition of two ionic liquid were described. Two ionic liquid materials have thermochromic photoluminescence properties. Such chromic behavior is attributed to both monomer and dimer emission. Therefore, ionic liquids based on Pt(II) anionic complexes have thermochromic photoluminescence properties not only one compounds reported in chapter 2.

In chapter 5, Photophysical properties of anionic Pt(II) complexes with tridentate C^N^C cyclometalating ligands (*n*-$Bu_4N[Pt(dFphpy)L]$ (H_2dFphpy = 2,6-bis(2,4-difluorophenyl)-pyridine; L = CN^- or Cl^-) were studied. Although Pt(II) complexes with N^C^N tridentate ligands exhibit strong phosphorescence with high quantum yields, Pt(II) C^N^C complexes show weak photoluminescence which was assigned to intra-ligand charge transfer (ILCT). To obtain further information about weak emissive C^N^C cyclometalated Pt(II) complexes, fluorine substitution was conducted. The detailed photophysical properties as well as

In chapter 6, the general conclusion and future perspective of this thesis were summarized.

1-8 References

1. L. J. Rothberg and A. J. Lovinger, *J. Mater. Res.*, 1996, **11**, 3174.
2. M. A. Baldo, D. F. O'Brien, Y. You, A. Shoustikov, S. Sibley, M. E. Thompson, and S. R. Forrest, *Nature*, 1998, **395**, 151.
3. B. O'Regan and M. Grätzel, *Nature*, 1991, **353**, 737.
4. (a) H. B. Gray and A. W. Maverick, *Science*, 1981, **214**, 1201. (b) A. F. Heyduk and D. G. Nocera, *Science*, 2001, **293**, 1639.
5. J. Hawecker, J.-M. Lehn, and R. Ziesse, *Helv. Chim. Acta*, 1986, **69**, 1990.
6. (a) P.T. Chou, and Y. Chi, *Chem. Eur. J*, 2007, **13**, 380; (b) C. Borek, K. Hanson, P.I. Djurovich, M.E. Thompson, K. Aznavour, R. Bau, Y. Sun, S.R. Forrest, J. Brooks, L. Michalski, and J. Brown, *Angew. Chem. Int. Ed.* 2007, **46**, 1109; (c) R.C. Evans, P. Douglas, and C.J. Winscom, *Coord. Chem. Rev*., 2006, **250**, 2093; (d) J.A.G. Williams, S. Develay, D.L. Rochester, and L. Murphy, *Coord. Chem. Rev*., 2008, **252**, 2596; (e) L. Xiao, Z. Chen, B. Qu, J. Luo, S. Kong, Q. Gong, and J. Kido, *Adv. Mater*, 2011, **23**, 926; (f) H. Yersin, A. F. Rausch, R. Czerwieniec, T. Hofbeck, and T. Fischer, *Coord. Chem. Rev*., 2011, **255**, 2622.
7. (a) H.J. Bolink, E. Coronado, R.D. Costa, N. Lardiés, and E. Ortí, *Inorg. Chem.*, 2008, **47**, 9149; (b) J. Slinker, D. Bernards, P.L. Houston, H.D. Abruña, S. Bernhard, and G.G. Malliaras, *Chem. Commun.* 2003, 2392; (c) R. Costa, E. Ortí, H. J. Bolink, F. Monti, G. Accorsi, and N. Armaroli, *Angew. Chem. Int. Ed.*, 2012, **51**, 8178.
8. (a) A. S. P. Polo, M. K. Itokazu, and N. Y. M. Iha, *Coord. Chem. Rev.*, 2004, **248**, 1343; (b) N. Robertson, *Angew. Chem. Int. Ed.,* 2006, **45**, 2338; (c) M. Grätzel, *Inorg. Chem*., 2005, **44**, 6841.
9. (a) K.K.-W. Lo, M.-W. Louie, and K.Y. Zhang, *Coord. Chem. Rev*., 2010, **254**, 2603; (b) M. Kato, *Bull. Chem. Soc. Jpn*., 2007, **80**, 287; (c) A. Kobayashi and M. Kato, *Eur. J. Inorg. Chem.,* 2014, 4469.
10. (a) Q. Zhao, C. Huang, and F. Li, *Chem. Soc. Rev.*, 2011, **40**, 2508; (b) K. K.-W. Lo and S. P.-Y. Li, *RSC Adv*., 2014, **4**, 10560.
11. (a) N. Hoffmann, *Chem. Rev.,* 2008, **108**, 1052; (b) S. Losse, J.G. Vos, and S. Rau, *Coord. Chem. Rev*., 2010, **254**, 2492.
12. M. Montalti, A. Credi, L. Prodi and M. T. Gandolfi, Handbook of photochemistry, 3rd ed., CRC press; US, 2006.
13. L. S. Forster, *Coord. Chem. Rev.*, 2006, **250**, 2023.
14. S. Obara, M. Itabashi, F. Okuda, S. Tamaki, Y. Tanabe, Y. Ishii, K. Nozaki, and M.-A. Haga, *Inorg. Chem.*, 2006, **45**, 8907.
15. S. Fraga, K. M. S. Saxena, and J. Karwowski, Handbook of Atomic Data. Physical Sciences Data; Elsevier: Amsterdam, The Netherlands, 1976, **5**, 551.

16. W. H. Elfring and G. A. Crosby, *J. Am. Chem. Soc.* 1981, **103**, 2683.
17. W.J. Finkenzeller and H. Yersin, *Chem. Phys. Lett*., 2003, **377**, 299.
18. A. Bossi, A. F. Rausch, M. J. Leitl, R. Czerwieniec, M. T. Whited, P. I. Djurovich, H. Yersin, and M. E. Thompson, *Inorg. Chem.*, 2013, **52**, 12403.
19. J. A. G. Williams, *Top. Curr. Chem.*, 2007, **281**, 205.
20. J. W. Schindler, R. C. Fukuda, and A. W. Adamson, *J. Am. Chem. Soc.,* 1982, **104**, 3596.
21. V. M. Miskowski, V. H. Houlding, C.-M. Che, and Y. Wang, *Inorg. Chem.,* 1993, **32**, 2518.
22. W. B. Connick, L. M. Henling, R. E. Marsh, and H. B. Gray, *Inorg. Chem.,* 1996, **35**, 6261.
23. (a) A. Aliprandi, D. Genovese, M. Mauro, and L. De Cola, *Chem. Lett*., 2015, **44**, 1152; (b) K. M.-C. Wong and V. W.-W. Yam, *Acc. Chem. Res*., 2011, **44**, 424.
24. J. Brooks, Y. Babayan, S. Lamansky, P. I. Djurovich, I. Tsyba, R. Bau, and M. E. Thompson, *Inorg. Chem.*, 2002, **41**, 3055.
25. B. W. D'Andrade, J. Brooks, V. Adamovich, M. E. Thompson, and S. R. Forrest, *Adv. Mater*., 2002, **14**, 1032.
26. (a)K. Binnemans, *Chem. Rev.,* 2005, **105**, 4148; (b) K. Goossens, K. Lava, C. W. Bielawski, and K. Binnemans, *Chem. Rev*., 2016, **116**, 4643.
27. (a) R. Giménez, D.P. Lydon, and J.L. Serrano, *Curr. Opin. Solid State Mater. Sci*., 2002, **6**, 527; (b) K. Binnemans and C. Görller-Walrand, *Chem. Rev.,* 2002, **102**, 2303.
28. (a) J. P. Hallett and T. Welton, *Chem. Rev.* 2011, **111**, 3508; (b) P. Wasserscheid and W. Keim, *Angew. Chem. Int. Ed*., 2000, **39**, 3772; (c) M. Armand, F. Endres, D. R. MacFarlane, H. Ohno, and B. Scrosati, *Nat. Mat*. 2009, **8**, 621; (d) S.-G. Lee, *Chem. Commun.*, 2006, 1049.
29. M. Krikorian, S. Liu, and T. M. Swager, *J. Am. Chem. Soc.,* 2014, **136**, 2952.
30. V. N. Kozhevnikov, B. Donnio, B. Heinrich, and D. W. Bruce, *Chem. Commun.,* 2014, **50**, 14191.
31. P. Nockemann, B. Thijs, N. Postelmans, K. Van Hecke, L. Van Meervelt, and K. Binnemans, *J. Am. Chem. Soc*., 2006, **128**, 13658.
32. S. Tang, A. Babai, and A.-V. Mudring, *Angew. Chem. Int. Ed*., 2008, **47**, 7631.
33. J. Estager, J. D. Holbrey, and M. Swadźba-Kwaśny, *Chem. Soc. Rev.*, 2014, **43**, 847.
34. J. Forniés, S. Fuertes, J. A. López, A. Martín and V. Sicilia, *Inorg. Chem*., 2008, **47**, 7166.
35. (a) J. R. Berenguer, E. Lalinde, and J. Torroba, *Inorg. Chem.*, 2007, **46**, 9919; (b) A. F. Rausch, U. V. Monkowius, M. Zabel, and H. Yersin, *Inorg. Chem.*, 2010, **49**, 7818.

Chapter 2
Ionic Liquid Based on an Anionic Platinum(II) Complex

2-1. Introduction

In the last two decades, ionic liquids have received considerable attention due to their wide liquid range, electric conductivity, large electrochemical window, and potential for use as alternative solvents for organic reactions.[1] To add higher functionalities to ionic liquids, metal-containing ionic liquids are attractive because of their diverse magnetic,[2a] electrochemical,[2b,c,d] or spectroscopic[2e] properties generated by metal ions and organic ligands. In particular, metal-containing ionic liquids are very intriguing as novel luminescent soft materials with unique properties such as low vapour pressure, high conductivity, and simple processability. Until now, several metal-containing ionic liquids showing notable luminescent properties have been reported. Well-known examples of luminescent room-temperature ionic liquids containing metal complexes are based on lanthanide complexes, especially Eu(III) complexes.[3] Although some other luminescent ionic liquids containing Mn(II),[4] Ru(II),[5] Cu(I),[6] Ag(I),[7a] Au(I),[7a,b] or Sb(III)[8] have also been developed, their luminescence intensities in the liquid state are too weak to utilize them as photofunctional materials with high flexibility and amorphousness at room temperature, and the exploration of luminescent ionic liquids is still a challenging subject.

To bring out photofunctional properties in ionic liquids, i.e., in flexible condensed matter, the introduction of luminescent Pt(II) complexes is considered as a promising candidate. Some Pt(II) complexes are known to exhibit remarkable luminescence color changes depending on their aggregation forms with different intermolecular Pt···Pt and π···π interactions not only in the solid state but also in the solution state.[9] These properties would be advantageous for organic light-emitting diodes (OLEDs), especially white light-emitting OLEDs, because the color changes could be achieved by controlling the emitter concentration in the host media.[10] Therefore, ionic liquids consisting of Pt(II) complexes are expected to exhibit sensitive but controllable luminescent properties that could be applicable to light-emitting electrochemical cells (LECs), promising easily fabricated light-emitting devices.[11]

In this chapter, the first Pt(II) complex-based ionic liquid, $[C_2mim][Pt(CN)_2(ptpy)]$ (**1**) (Hptpy = 2-(*p*-tolyl)pyridine, C_2mim = 1-ethyl-3-methylimidazolium ion) (Figure 1) and its temperature-dependent luminescence properties were reported. Complex **1** shows dual-emissive properties because of the coexistence of monomer and dimer moiety in the disordered structure of the liquid and glass states. The unique properties of ionic liquid **1** were investigated by comparing the properties with those of corresponding crystalline complex salts containing different cations, *n*-$Bu_4N[Pt(CN)_2(ptpy)]$ (**2**) and $K[Pt(CN)_2(ptpy)]$ (**3**).

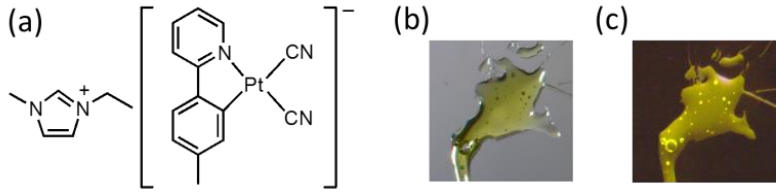

Figure 1. (a) Structural formula of $[C_2mim][Pt(CN)_2(ptpy)]$ (**1**). Photographs of liquid **1** under (b) bright field and (c) UV light. The ring-shaped and small dotted spots are bubbles in the ionic liquid.

2-2. Experimental

2-2-1. Physical measurements

^{1}H NMR spectroscopy was performed using a JEOL EX-270 NMR spectrophotometer. Elemental analyses were carried out at the analysis center in Hokkaido University. Thermogravimetry-differential thermal analysis (TG-DTA) measurements were recorded using a Rigaku Thermoplus EVO TG-DTA 8120 with Al sample pans under a N_2 flow. Differential scanning calorimetry (DSC) measurements were performed using a METTLER DSC 1 under a N_2 flow. Variable-temperature powder X-ray diffraction measurements (VT-PXRD) were measured with Cu Kα using a Bruker D8 Advance diffractometer equipped with a graphite monochrometer, a one dimensional LinxEye detector and Anton Paar TTK 450 low-temperature chamber. Absorption spectra were measured using a Shimadzu UV-2500PC Spectrophotometer under N_2 atmosphere using quartz cells with a thickness of either 1 cm or 1 mm.

2-2-2. Luminescence measurements

All luminescence measurements of neat **1** were performed under N_2 atmosphere. Luminescence spectra were measured using a JASCO FR-6600 spectrofluorometer at room temperature and 77 K. Slit widths of the excitation and emission light were 5 or 6 nm. Variable Temperature luminescence spectra were measured by single photon counting using a Hamamatsu Absolute PL Quantum Yield Measurement System C9920-02. Luminescence quantum yields were recorded on a Hamamatsu Photonics C9920-02 absolute photoluminescence quantum yield measurement system equipped with an integrating sphere apparatus and 150 W CW Xenon light source. Hamamatsu Photonics A10095-03 non-luminescent quartz sample holder was used for absolute photoluminescence quantum yield measurements. The accuracy of the instrument was confirmed by the measurement of quantum yield of anthracene in ethanol solution (Φ = 0.27).[12] Emission life time measurements were recorded using a Hamamatsu Photonics, C4334 system equipped with a streak camera as a Photo detector and a nitrogen laser for the 337 nm excitation. Liquid N_2 cryostat (Optistat-DN optical Dewar and ITC-503 temperature controller, Oxford Instruments) was used for the temperature control.

2-2-3. Single crystal X-ray diffraction measurements

All single crystal X-ray diffraction measurements were performed using a Rigaku AFC-7R diffractometer with a Mercury CCD area detector and graphite monochromatized Mo Kα radiation (λ = 0.71069 Å) at 200 K (complex **2**) and 150 K (complex **3**), respectively. Each single-crystal was mounted on a MicroMount using liquid paraffin. These crystals were cooled using a N_2-flow type temperature controller. Diffraction data were collected and processed using the Crystal-Clear software.[13] The structures were solved by direct methods (SIR2004[14] for **2**, SIR2011[15] for **3**).

Structural refinements were conducted by the full-matrix least-squares method using SHELXL-97.[16] Non-hydrogen atoms were refined anisotropically, and all hydrogen atoms were refined using the rigid model. All calculations were performed using the CrystalStructure crystallographic software package[17] except for refinement. The crystallographic data of **2** and **3** are summarized in Table 1.

Table 1. Crystallographic data of **2**·CH_3CN and **3**·$2H_2O$·CH_3COCH_3

	n-$Bu_4N[Pt(CN)_2(ptpy)]$·CH_3CN (**2**·CH_3CN)	$K[Pt(CN)_2(ptpy)]$·$2H_2O$·CH_3COCH_3 (**3**·$2H_2O$·CH_3COCH_3)
Formula	$C_{32}H_{48}N_5Pt$	$C_{31}H_{30}K_2N_6O_3Pt_2$
Formula Weight	697.85	1002.99
Crystal system	monoclinic	Monoclinic
Space group	$P2_1/c$	$P2_1/c$
a (Å)	22.614(8)	19.743(5)
b (Å)	8.529(3)	12.197(3)
c (Å)	17.808(6)	14.509(4)
α (°)	90	90
β (°)	107.887(5)	108.445(3)
γ (°)	90	90
V (Å^3)	3269(2)	3314(2)
T (K)	200	150
Z	4	4
D_{calc} (g cm^{-3})	1.418	2.010
F(000)	1412.00	1904.00
measured reflns	21244	25015
unique refns	7163	7536
GOF on F^2	1.074	1.068
R_{int}	0.0393	0.0524
R_1[a]	0.0365	0.0458
wR_2[b](all data)	0.0961	0.1278

[a] $R_1 = \Sigma||F_o| - |F_c||/\Sigma|F_o|$. [b] $wR_2 = [\Sigma w(F_o^2 - F_c^2)/\Sigma w(F_o)^2]^{1/2}$, $w = [\sigma_c^2(F_o^2) + (xP)^2 + yP]^{-1}$, $P = (F_o^2 - 2F_c^2)/3$.

2-2-4. Materials

2-(*p*-tolyl)pyridine (Hptpy), $AgClO_4$, KCN, *n*-Bu_4NClO_4, *N*-methylimidazole, bromoethane and 2-ethoxyethanol were purchased from Wako Pure Chemical Industries. Potassium tetrachloroplatinate(II) ($K_2[PtCl_4]$) was purchased from Tanaka Holdings Co., Inc. All solvents were purchased from Kanto Chemical Co., Inc. All of solvents for the measurements were distilled by standard methods under a N_2 atmosphere.

1-methyl-3-ethylimidazolium Bromide ([C_2mim][Br]) was synthesized by the literature method.[18] $[Pt(ptpy)(\mu\text{-}Cl)]_2$ was synthesized according to the synthetic method reported previously.[19] All of the solvents for syntheses were used without further purification. All measurements were performed under a N_2 atmosphere.

2-2-5. Synthesis

K[Pt(CN)$_2$(ptpy)] (3)

$K[Pt(CN)_2(ptpy)]$ was synthesized according to the literature method[20(a)] with slight modifications as follows. To the suspension of $[Pt(ptpy)(\mu\text{-}Cl)]_2$ (163 mg, 0.20 mmol) in acetonitrile (45 mL) was added $AgClO_4$ (85 mg, 0.41 mmol). After stirred for 7 h in the dark condition, the mixture was filtered through celite. The resulting yellow solution was evaporated to dryness. The yellow solid was suspended in methanol (45 mL), and KCN (53 mg, 0.82 mmol) was added. After stirring for 2h, the reaction mixture was filtered through celite and evaporated to dryness. Luminescent yellow powder was produced. By the recrystallization from acetone/Et_2O, yellow crystals suitable for the single X-ray crystallography were obtained as **3**·$2H_2O$·CH_3COCH_3, although the included acetone and water molecules were easily released in the air.

Yield, 140 mg (0.31 mmol, 74%). ^{1}H NMR (Acetone-d_6, 270 MHz): δ = 9.42 (td, J = 15.1, 1.6 Hz, 1H), 8.01 (d, J = 7.8 Hz, 1H), 7.98 (t, J = 25.1 Hz, 1H), 7.88 (d, J = 8.4 Hz, 1H), 7.51 (d, J = 7.9 Hz, 1H), 7.24 (td, J = 5.4, 1.3 Hz, 1H), 6.85 (d, J = 8.0 Hz, 1H), 2.27 (s, 3H). Anal. Calc. for $C_{14}H_{10}N_3PtK\cdot1.5H_2O$: C, 34.93; H, 2.72; N, 8.73%. Found: C, 35.09; H, 2.72; N, 8.45%

[C$_2$mim][Pt(CN)$_2$(ptpy)] (1)

$K[Pt(CN)_2(ptpy)]$ (181 mg, 0.40 mmol) and [C_2mim][Br] (76 mg, 0.40 mmol) were dissolved in dichloromethane (50 mL) and stirred for 1h at room temperature. The yellow suspension was filtrated using celite, and then the yellow solution was washed with water until no bromine ions were detected in $AgNO_3$ test. The organic layer was evaporated and dried under reduced pressure at 100°C for 12h. The yellow viscous liquid was yielded. Yield, 134 mg (0.152 mmol, 38%). ^{1}H NMR ($CDCl_3$, 270 MHz): δ = 9.65 (s, 1H), 9.28 (td, J = 16.7, 7.8 Hz, 1H), 7.90 (t, J = 24.9 Hz, 1H), 7.72 (t, J = 8.0 Hz, 1H), 7.60 (d, J = 8.0 Hz, 1H), 7.36 (d, J = 8.0 Hz, 1H), 7.18 (m, 2H), 7.00 (t, J = 7.2 Hz, 2H), 6.86 (d, J = 7.6 Hz, 1H), 4.41 (q, J = 7.2 Hz, 2H), 4.06 (s, 3H), 2.26 (s, 3H), 1.55 (s, 3H). Anal. Calc. for

$C_{20}H_{22}N_5Pt \cdot 0.5H_2O$: C, 44.86; H, 4.14; N, 13.08%. Found: C, 44.94; H, 3.89; N, 12.90%. Included water molecules were checked by thermogravimetry-differential thermal analysis.

n-$Bu_4N[Pt(CN)_2(ptpy)]$ (2)

n-$Bu_4N[Pt(CN)_2(ptpy)]$ was synthesized according to the literature method with slight modifications as follows. To the suspension of $[Pt(ptpy)(\mu\text{-}Cl)]_2$ (144 mg, 0.18 mmol) in acetonitrile (35 mL) was added $AgClO_4$ (75 mg, 0.36 mmol). After stirred for 7 h in the dark condition, the mixture was filtered through celite. The resulting yellow solution was evaporated to dryness. The yellow solid was suspended in methanol (35 mL), and KCN (45 mg, 0.70 mmol) was added. After stirring for 2h, the reaction mixture was filtered through celite and evaporated to dryness. The resulting yellow solid was suspended in acetone (35 mL) and n-Bu_4NClO_4 (119 mg, 0.35 mmol) was added. Then, the suspension was filtered through celite and evaporated under reduced pressure. By the recrystallization from $MeCN/Et_2O$, pale yellow crystals were obtained as the acetonitrile solvated form.

Yield, 205 mg (0.31 mmol, 90%). ^{1}H NMR (Acetone-d_6, 270 MHz): δ = 9.46 (td, J = 15.1, 1.6 Hz, 1H), 8.03 (d, J = 7.8 Hz, 1H), 7.96 (t, J = 25.1 Hz, 1H), 7.87 (d, J = 8.4 Hz, 1H), 7.50 (d, J = 7.9 Hz, 1H), 7.23 (td, J = 5.4, 1.3 Hz, 1H), 6.84 (d, J = 8.0 Hz, 1H), 3.46 (m, 8H), 2.27 (s, 3H), 1.83(m, 8H), 1.45 (m, 8H), 0.97 (t, J = 7.3 Hz, 12H). Anal. Calc. for $C_{30}H_{46}N_4Pt \cdot 0.5CH_3CN$: C, 54.89; H, 7.06; N, 9.29%. Found: C, 54.71; H, 7.06; N, 9.26%.

2-3. Results and discussion

2-3-1. Phase transition behavior of Pt(II) ionic liquid

Complex **1** was synthesized by a metathesis method as follows: Stoichiometric amounts of complex **3** and [C_2mim]Br were mixed in dichloromethane, followed by washing with water for removal of the inorganic salts and drying under vacuum at 100°C. The resulting yellow substance was found to be a liquid at room temperature in an inert atmosphere, although it exhibited hygroscopicity. Therefore, in order to elucidate its properties in the anhydrous state, complex **1** was dried under reduced pressure at 90°C overnight and then stored under inert atmosphere at room temperature for several hours prior to use. The thermal behaviour of **1** was investigated by measurements thermogravimetry-differential thermal analyses (TG-DTA) (Figure 2), as well as differential scanning calorimetry (DSC) (Figure 3). TG curve suggests that complex **1** is stable under 150°C, which is less stable than crystalline Pt(II) complexes.

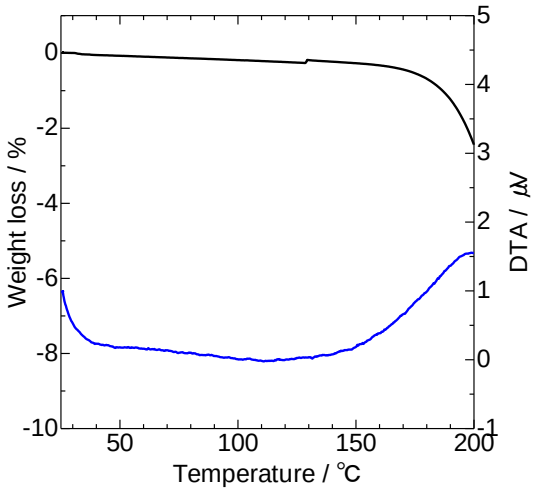

Figure 2. Thermogravimetry-differential thermal analyses of **1** at scan rate of 5 K min^{-1} (TG (black), DTA (blue)).

As shown in Figure 2, the DSC curves exhibited glass transition behaviour in both cooling and heating processes after the first heating from 25 to 60°C, and no other thermal events such as crystalline phase transitions were observed between −30 and 60°C. The glass transition temperature (T_g) of **1** was estimated to be −10°C from the first cooling process.

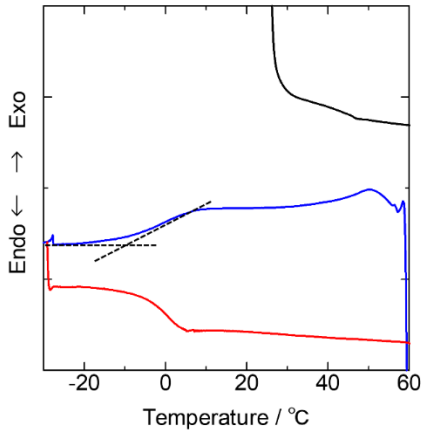

Figurer 3. DSC curves of **1** [first heating (black line), first cooling (blue line), second heating (red line)]. Scan rate: 5 K min^{-1}.

The X-ray diffraction measurements supported that the sample of **1** did not crystallize at all until −192°C, and only one peak at approximately $2\theta = 24.2°$ ($d = 3.67$ Å) was detected at low temperatures, suggesting that the glass state of **1** included a local periodic structure such as weak π–π stacking without forming any other long-range order (Figure 4).

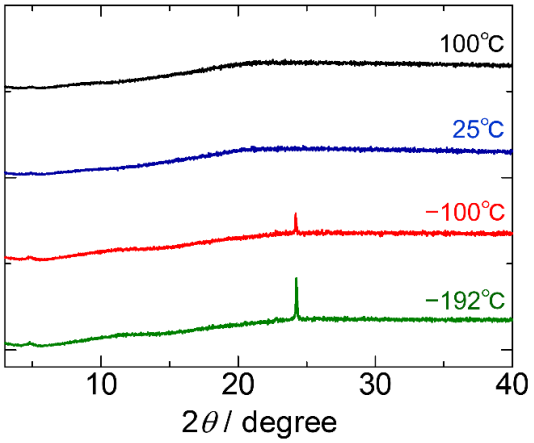

Figure 4. VT-PXRD patterns of **1** at 100°C (black), 25°C (blue), –100°C (red) and –192°C (green).

Although the π systems of $[Pt(CN)_2(ptpy)]^-$ and $[C_2mim]^+$ are considered to stabilize a crystalline state, the dialkyl-imidazolium cation of $[C_2mim]^+$ would significantly destabilize its crystalline state because of the poor symmetry and charge delocalization. As a result, the liquid state of the Pt(II) complex was realized at room temperature, and an amorphous glass phase was formed at low temperature instead of a crystalline state.

2-3-2. Photoluminescence properties of Pt(II) ionic liquids

Ionic liquid **1** emitted yellow luminescence under UV light irradiation at room temperature. As shown in Figure 5, it exhibited a broad emission spectrum with several peaks (Table 2). It was quite different from the methanol solution (1.0×10^{-3} M), in that **1** showed a vibronically structured emission spectrum with the maximums at approximately 486 and 517 nm, assignable to the ligand-centered $^3\pi$–π^* transition (^{3}LC) with some mixing of ^{3}MLCT character.[20] The emission spectrum is characteristic of discrete mononuclear complexes without intermolecular interactions. In fact, essentially the same monomeric emission spectrum was observed for the crystal of the *n*-Bu_4N^+ salt **2** [Figure 6(b)], which includes discrete Pt(II) complex anions surrounded by *n*-Bu_4N cations, as shown in Figure 7(a). On the other hand, a broad emission spectrum with a maximum of 558 nm was observed for the potassium salt **3** [Figure 6(b)], in which an interesting dimeric structure of $[Pt(CN)_2(ptpy)]^-$ anions with a short Pt···Pt contact [3.2785(7) Å] was found [Figure 7 (b)].

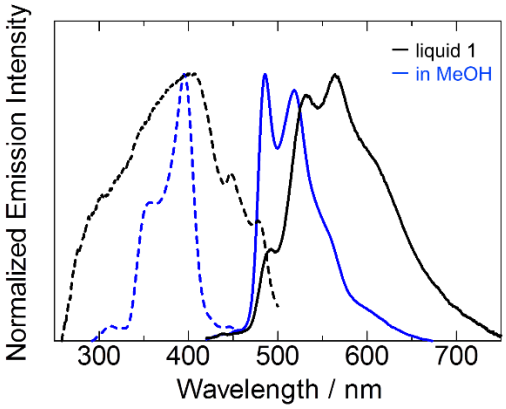

Figure 5. Emission (solid lines) and excitation (dotted lines) spectra of **1** in liquid state (black, λ_{ex} = 400 nm, λ_{em} = 560 nm) and a MeOH solution (1.0×10^{-3} mol L^{-1}) (blue, λ_{ex} = 400 nm, λ_{em} = 480 nm) at 298 K under N_2 atmosphere.

Table 2. Emission data of **1** in neat liquid state and MeOH solution.

	[C_2mim][Pt(CN)$_2$(ptpy)] (**1**)	
Condition	Neat liquid	in MeOH
λ_{max} / nm	493, 532, 564	486, 518, 560(sh)
Φ_{em}	0.06	0.03

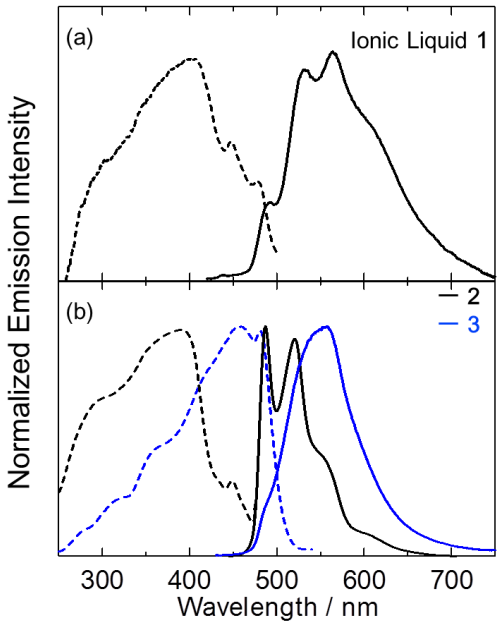

Figure 6. Emission (solid lines) and excitation (dotted lines) spectra of (a) **1** in liquid state (λ_{ex} = 400 nm, λ_{em} = 560 nm) and (b) **2** (black, λ_{ex} = 400 nm, λ_{em} = 480 nm) and **3** (blue, λ_{ex} = 400 nm, λ_{em} = 560 nm) at room temperature.

Table 3. Emission spectral data of **2**

	n-Bu_4N[$Pt(CN)_2$(ptpy)] (**2**)	
Temperature	77 K	298 K
λ_{max} / nm	486, 520, 550(sh)	487, 521, 560(sh)
Φ_{em}	0.95	0.72

Table 4. Emission spectral data of **3**

	K[$Pt(CN)_2$(ptpy)] (**3**)	
Temperature	77 K	298 K
λ_{max} / nm	561	558
Φ_{em}	0.32	0.09

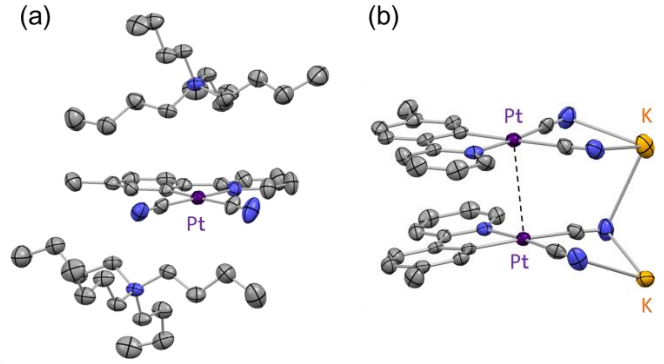

Figure 7. ORTEP drawings showing the environment of $[Pt(CN)_2(ptpy)]^-$ for (a) the *n*-Bu_4N^+ salt (**2**) and (b) the K^+ salt (**3**). Displacement parameters are drawn at the 50% probability level. Hydrogen atoms are omitted for clarity. Color code: Pt, purple; C, grey; N, blue; K, orange.

Thus, the broad emission spectrum can be assigned to that from the triplet metal-metal-to-ligand charge transfer (^{3}MMLCT) state of the dimerized Pt(II) complexes.[20a] These results suggest that the emission spectrum of ionic liquid **1** could be an overlapped one of an aggregate species of the platinum complexes and the monomeric species. The emission spectrum of **1** changed slightly by excitation at wavelengths longer than 490 nm, which would be due to preferential excitation of the aggregated species (Figure 8). For the excitation spectra, however, distinct differences depending on the monitoring emission wavelength could not been observed (Figure 9) as observed for crystalline samples **2** and **3** [Figure 6(b)]. Also, in the absorption spectrum of ionic liquid **1**, no detectable bands for the assembled species were observed (Fig. 10). These features suggest that the assembled species in the ionic liquid should be much less in the amount compared with the monomer species, and thus the dual emission of **1** at room temperature would be attributable to the energy transfer from the excited state of the monomeric species to that of the aggregated species.

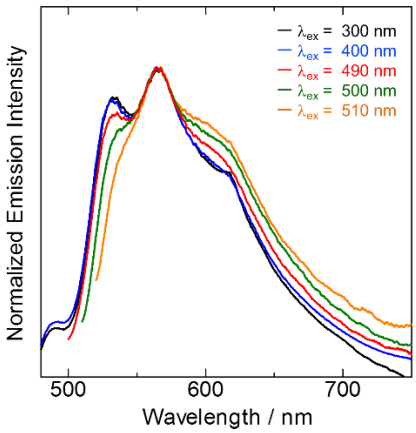

Figure 8. Excitation wavelength dependency for emission spectra of **1**. Thin liquid membrane condition of neat **1** sandwiched in two quartz plates were measured under N_2 atmosphere at 298 K.

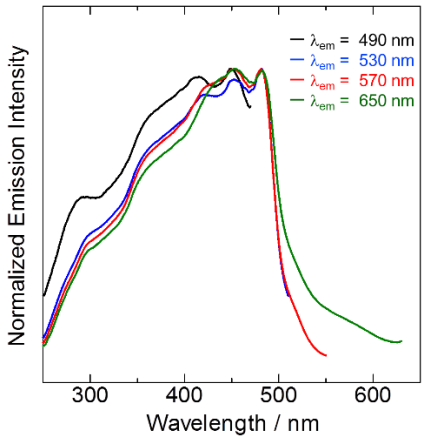

Figure 9. Excitation spectra of **1** detected at different emission wavelengths at 298 K.

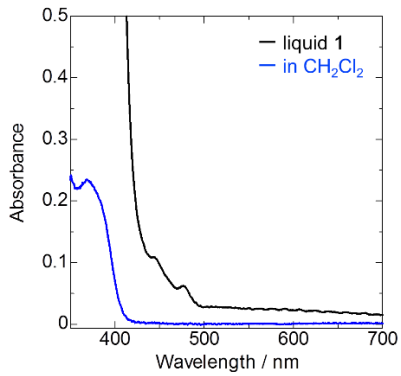

Figure 10. Absorption spectra of neat liquid **1** (black line) and **1** in CH_2Cl_2 (blue line, 1.0×10^{-4} M)

2-3-3. time-resolved emission behaviour

For further insight, time-resolved emission behaviours were investigated (Table 5). As shown in Figure 11, the emission decay curves from the different wavelength regions clearly indicated the existence of several components (Table 6). A fast decay component with a lifetime (τ) of *ca.* 0.2 μs was observed mainly in the short-wavelength region (486–500 nm), where the emission came from the monomeric species, whereas the relatively slow decay components (τ = *ca.* 1 and 4 μs) increased in the ratio in the longer-wavelength regions (501–550 nm and 551–629 nm). Taking into account that the emission decay of the monomeric species is much slower in a diluted MeOH solution (10^{-4} M) as a fluid medium [Figure 9(b)], the fast decay for the monomeric species in **1** indicates the existence of an additional process in the ionic liquid. It would be reasonable to consider the energy transfer from the monomeric to the aggregated species because the overall quantum yield of **1** (Φ_{em} = 0.06, Table 5) is slightly higher than that in the dilute MeOH solution containing only the monomeric species (Φ_{em} = 0.03, Table 7). Assuming that the emission lifetime in the dilute MeOH solution (τ_{av} = 2.53 μs) is same as that for the monomeric species of **1** in fluid media, the energy transfer rate constant from the monomeric to the aggregated species is roughly estimated from the difference in the lifetime value of the monomeric species in the ionic liquid (τ = 0.19 μs, Table S2) to be *ca.* 4.8×10^6 s^{-1}, which is a reasonable value typical for the triplet energy transfer rate constants (10^{6-7} s^{-1}). [21]

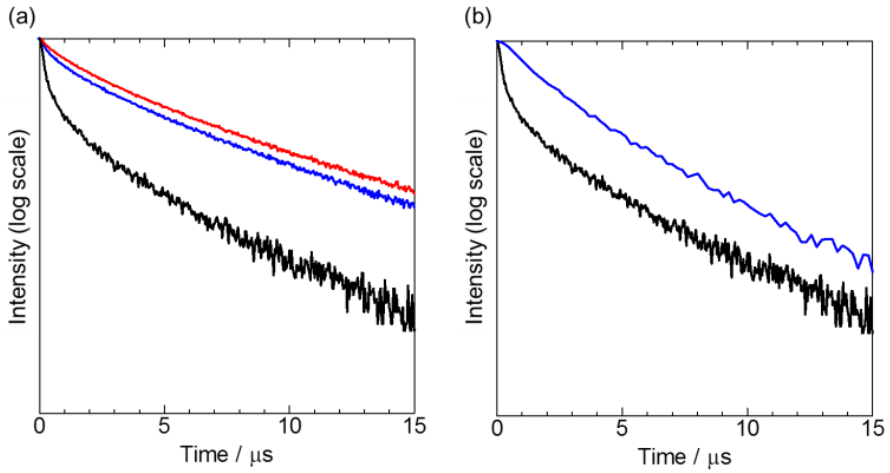

Figure 11. (a) Emission decay curves of ionic liquid **1** at 298 K detected at 486–500 nm (black line), 501–550 nm (blue line), and 551–629 nm (red line). (b) Comparison of the emission decay curve of **1** (black line, detected at 486–500 nm) with that in MeOH (blue line, 1.0×10^{-4} M). λ_{ex} = 337 nm.

Table 5. Luminescence data of neat **1** at 298 K and 77 K.

Temperature	λ_{em}[a] (nm)	Φ[b]	τ[c] [μs (A[d])]	χ^2[e]	τ_{av}[f] (μs)	k_r[g](s^{-1})	k_{nr}[h] (s^{-1})
298 K	493, 532, 564	0.06	0.91 (0.86), 3.57 (0.362)	1.185	2.57	2.3×10^4	3.6×10^5
77 K	494, 532, 561	0.47	9.72 (0.646), 22.09(0.449)	1.023	17.2	2.7×10^4	3.1×10^4

[a] Emission maxima. [b] Photoluminescence quantum yield. [c] Emission lifetimes; Emission decays were analyzed with two components: $I = A_1\exp(-t/\tau_1) + A_2\exp(-t/\tau_2)$. [d] Pre-exponential factors. [e] Fitting parameter. [f] Average emission lifetimes were determined by using the equation 1.[22] [g] Radiative rate constants k_r were estimated by Φ/τ_{av}. [h] Nonradiative rate constants k_{nr} were estimated by $k_{nr.} = -k_r + 1/\tau_{av}$.

$$\tau_{av} = \frac{A_1\tau_1^2 + A_2\tau_2^2}{A_1\tau_1 + A_2\tau_2} \qquad (1)$$

Table 6. Emission lifetime data of neat **1** at 298 K recorded by different wavelength.

λ_{det} (nm)		486 - 500	501 - 550	551 - 629
T[u] [μs (A[c])]	$\tau_1(A_1)$	0.192 (0.760)	1.035 (0.285)	1.330 (0.401)
	$\tau_2(A_2)$	0.849 (0.243)	3.565 (0.467)	4.164 (0.485)
	$\tau_3(A_3)$	3.240 (0.154)		
τ_{av} (μs)		2.14	3.18	3.57
χ^2		1.009	1.172	1.149
k (s^{-1})		5×10^6, 1.2×10^6, 3.1×10^5	9.6×10^5, 2.8×10^5	7.5×10^5, 2.4×10^5

[a]Average emission lifetimes determined using equation 1 or 2.[22]

$$\tau_{av} = \frac{A_1\tau_1^2 + A_2\tau_2^2 + A_3\tau_3^2}{A_1\tau_1 + A_2\tau_2 + A_3\tau_3} \qquad (2)$$

Table 7. Luminescence data of **1** at 298 K in MeOH (1.0×10^{-4}).

λ_{em} (nm)	Φ	τ [μs (A[d])]	χ^2	τ_{av} (μs)	k_r(s^{-1})	k_{nr} (s^{-1})
486, 518, 560(sh)	0.03	1.335 (0.636) 3.196 (0.486)	1.198	2.53	1.2×10^4	3.8×10^5

2-3-4. temperature dependence of luminescence properties

The ionic liquid exhibited distinct emission color changes depending on temperature (Figure 12 inset). With decreasing temperature, the emission intensity at shorter wavelength regions increased remarkably, and at 77 K, the luminescent spectrum of **1** reached that of the monomeric species, with the vibronic structure as shown in Figure 10. The monomeric emission decay rate decreased at 77 K (5.8×10^4 s^{-1}, Figure 13, Table 5), which supports the claim that the energy transfer was almost suppressed at 77 K due to some energy barrier. However, the spectral change at around the glass-phase transition point (−10°C) was not distinct, indicating that the fluidity or translational motion were not important factors for the dual emission.[23] On the other hand, the excitation spectra monitored at emission wavelengths of 490–650 nm did not exhibit any notable changes in the range from room temperature to 77 K (Figure 14). This would be reasonable for the energy transfer emission system, as mentioned above.

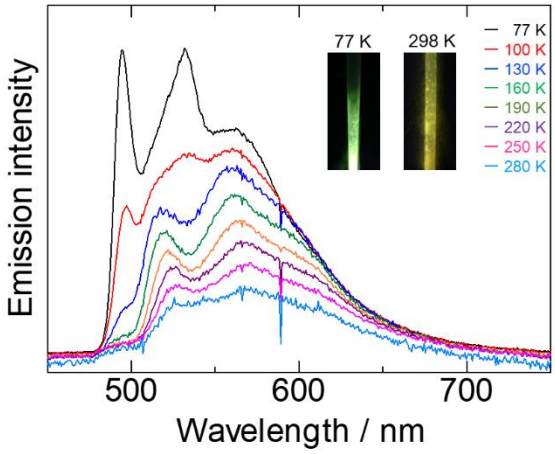

Figure 12. Emission spectra of **1** at different temperatures. λex = 337 nm. The relative emission intensities were adjusted for clarity. Inset: luminescence images of the sample at 77 K and 298 K.

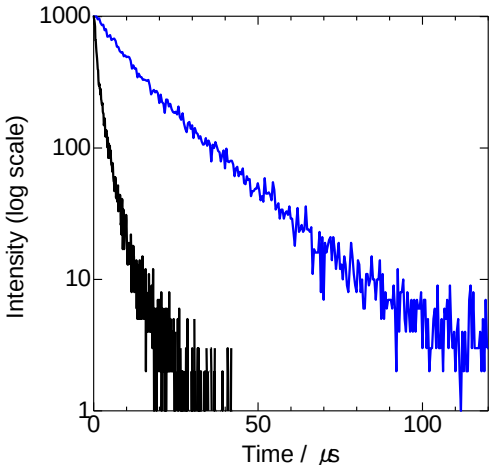

Figure 13. Emission decay curves of ionic liquid **1** at 298 K (black line) and 77 K (blue line).

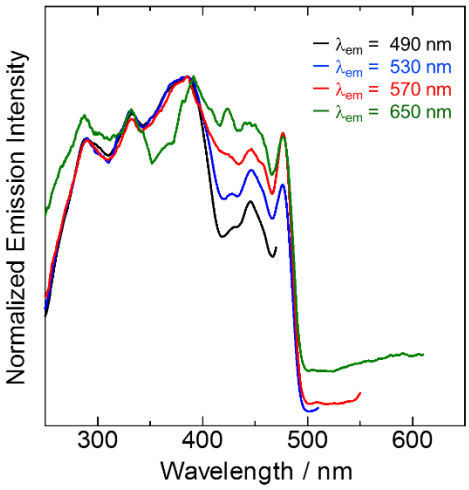

Figure 14. Excitation spectra of **1** detected at different emission wavelengths at 77 K. Neat of **1** was measured with a quartz tube under N_2 atmosphere.

Two different mechanisms have been suggested for dual emission from electronically coupled systems.[24] One is a thermal equilibrium model, which is based on the Boltzmann population between two emission states in thermal equilibrium. In this model, the emission intensity of the lower energy band increases at low temperatures. The other mechanism is a competing system of emission and energy transfer processes with an energy barrier. The dual emission behavior for **1** could be assigned to the latter case because the emission intensity ratio of the lower energy band increased with increasing temperature. The shape of the spectrum of **1** changed when the excitation wavelength was

longer than 490 nm, as mentioned above (Figure 8). The fact that the emission intensity from the monomeric species at 530 nm decreased at excitations with longer wavelengths also indicates that the back-energy transfer from the aggregated species to the monomer did not occur. The energy transfer should play a key role in temperature-dependent dual emission. Overall, the phosphorescent cyclometalated Pt(II) complex would be advantageous to dual emission of the ionic liquid because of the competitive quenching by energy transfer and other nonradiative decay and relatively slow radiative rate constants (k_r, Table 5).

2-4. Conclusion

In conclusion, succeeded in the synthesis of the first ionic liquid based on a Pt(II) complex. This ionic liquid exhibited dual emission from both the monomeric and aggregated excited states, and these dual-emissive properties gave rise to distinct thermochromic luminescence. Because of the co-existence of monomeric and aggregated forms in disordered liquid and glass phases, the energy transfer from the monomeric excited states to the aggregated states led to dual emission. To our knowledge, this is also the first report of a well-defined dual-emissive ionic liquid. Such dual-emissive phosphorescent ionic liquids could potentially be used as luminescent materials for simple light-emitting and/or -sensing devices. Further studies concerning Pt(II)-based ionic liquids are important.

2-5. References

1 (*a*) J. P. Hallett and T. Welton, *Chem. Rev*. 2011, **111**, 3508; (*b*) P. Wasserscheid and W. Keim, *Angew. Chem. Int. Ed.*, 2000, **39**, 3772; (*c*) M. Armand, F. Endres, D. R. MacFarlane, H. Ohno and B. Scrosati, *Nat. Mat.* 2009, **8**, 621; (*d*) S.-G. Lee, *Chem. Commun*., 2006, 1049.

2 (*a*) M. Okuhata, Y. Funasako, K. Takahashi and T. Mochida, *Chem. Commun*., 2013, **49**, 7662; (*b*) A. Branso, L. C. Branco and F. Pina, *Chem. Commun*., 2011, **47**, 2300; (*c*) M. Steichen, N. R. Brooks, L. V. Meervelt, J. Fransaerc and K. Binnemans, *Dalton Trans*., 2014, **43**, 12329; (*d*) N. R. Brooks, S. Schaltin, K. V. Hecke, L. V. Meervelt, K. Binnemans and J. Fransear, *Chem. Eur. J.* 2011, **17**, 5054; (*e*) Y. Funasako, T. Mochida, K. Takahashi, T. Sakurai and H. Ohta, *Chem. Eur. J.*, 2012, **18**, 11929.

3 (*a*) S. Tang, A. Babai and A.-V. Mudring, *Angew. Chem. Int. Ed*., 2008, **47**, 7631; (*b*) A. Getsis, S. Tang and A.-V. Mudring, *Eur. J. Inorg. Chem*., 2010, 2172.

4 S. Pitula and A.-V. Mudring, *Chem. Eur. J*. 2010, **16**, 3355.

5 S. Gago, L. Cabrita, J. C. Lima, L. C. Branco and F. Pina, *Dalton Trans.*, 2013, **42**, 6213.

6 E. T. Spielberg, E. Edengeiser, B. Mallick, M. Havenith and A.-V. Mudring, *Chem. Eur. J.* 2014, **20**, 5338.

7 (*a*) A. Tokarev, J. Larionova, Y. Guari, J. M. López-de-Luzuriaga, M. Monge, P. Dieudonné and C. Blanc, *Dalton Trans*., 2010, **39**, 10574; (*b*) Y. Yoshida, J. Fujii, G. Saito, T. Hiramatsu and N. Sato, *J. Mater. Chem*., 2006, **16**, 724.

8 Z.-P. Wang, J.-Y. Wang, J.-R. Li, M.-L. Feng, G.-D. Zou and X.-Y. Huang, *Chem. Commun.*, 2015, **51**, 3094.

9 (*a*) M. Kato, *Bull. Chem. Soc. Jpn*., 2007, **8**, 287; (*b*) B. Ma, P. I. Djurovich and M. E. Thompson, *Coord. Chem. Rev*., 2005, **249**, 1501; (*c*) K. M.-C. G Wong and V. W.-W. Yam, *Acc. Chem. Res.*, 2011, **44**, 424; (*d*) A. Kobayashi and M. Kato, *Eur. J. Inorg. Chem.*, 2014, **27**, 4469.

10 (*a*) B. W. D'Andrade, J. Brooks, V. Adamovich, M. E. Thompson and S. R. Forrest, *Adv. Mater.*, 2002, **14**, 1032; (*b*) J. Kalonowski, M. Cocchi, D. Virgili, V. Fattori and J. A. G. Williams, *Adv. Mater*., 2007, **19**, 4000; (*c*) J. Kalinowski, M. Cocchi, L. Murphy, J. A. G. Williams and V. Fattori, *Chem. Phys.*, 2010, **378**, 47; (*d*) L. Murphy, P. Brulatti, V. Fattori, M. Cocchi and J. A. G. Williams, *Chem. Commun*., 2012, **48**, 5817; (*e*) G. Zhou, Q. Wang, X. Wang, C.-L. Ho, W.-Y. Wong, D. Ma, L. Wang and Z. Lin, *J. Mater. Chem.*, 2010, **20**, 7472.

11 R. Costa, E. Ortí, H. J. Bolink, F. Monti, G. Accorsi and N. Armaroli, *Angew. Chem. Int. Ed*., 2012, **51**, 8178.

12 (a) W. R. Dawson and M. W. Windsor, *J. Phys. Chem*., 1968, **72**, 325; (b) W. H. Melhuish, *J. Phys. Chem*., 1961, **65**, 229.

13 CrystalClear, Molecular Structure Corporation, Oren, UT, 2001.

14 SIR-2004: M. G. Burla, R. Caliandro, M. Camalli, B. Carrozzini, G. L. Cascarano, L. DeCaro, C. Giacovazzo, G. Polidori and R. Spagna, *J. Appl. Crystallogr*., 2005, **38**, 381.

15 SIR-2011: M. C. Burla, R. Caliandro, M. Camalli, B. Carrozzini, G. L. Cascarano, C. Giacovazzo, M. Mallamo, A. Mazzone, G. Polidori and R. Spagna, *J. Appl. Crystallogr*., 2012, **45**, 357.

16 SHELXL97: G. M. Sheldrick, Acta Crystallogr., Sect. A: Fundam. Crystallogr., 2008, **64**, 112.

17 *CrystalStructure 4.0*, Rigaku Corporation, Tokyo196-8666, Japan, 2000-2010.

18 C. C. Weber, A. F. Masters and T. Maschmeyer, *Angew. Chem. Int. Ed*., 2012, **51**, 11483.

19 H. Uesugi, T. Tsukuda, K. Takao and T. Tsubomura, *Dalton Trans*., 2013, **42**, 7396.

20 (*a*) J. Forniés, S. Fuertes, J. A. López, A. Martín and V. Sicilia, *Inorg. Chem*., 2008, **47**, 7166; (*b*) A. F. Rausch, U. V. Monkowius, M. Zabel and H. Yersin, *Inorg. Chem*., 2010, **49**, 7818; (*c*) J. Brooks, Y. Babayan, S. Lamansky, P. I. Djurovich, I. Tsyba, R. Bau and M. E. Thompson, *Inorg. Chem*., 2002, **41**, 3055.

21 (*a*) G. L. Closs, P. Piotrowiak, J. M. MacInnis and G. R. Fleming, *J. Am. Chem. Soc.*, 1988, **110**, 2652; (*b*) G. L. Closs, M. D. Johnson, J. R. Miller and P. Piotrowiak, *J. Am. Chem. Soc.*, 1989, **111**, 3751.

22 J. R. Lakowicz, Principles of Fluorescence Spectroscopy, Springer, New York, 2006, pp. 141–142.

23 M. Han, Y. Tian, Z. Yuan, L. Zhu and B. Ma, *Angew. Chem. Int. Ed*., 2014, **53**, 10908.

24 E. J. McLaurin, L. R. Bradshaw and D. R. Gamelin, *Chem. Mater*., 2013, **25**, 1283.

Chapter 3

Phosphorescence Properties of Anionic Platinum(II) Complexes Bearing N-heterocyclic Carbenes in the Solid State: Temperature Dependence and Regioselective π-extension

3-1 Introduction

Phosphorescent transition-metal complexes, such as platinum(II), iridium(III), and ruthenium(II) ions with polypyridine ligands, have been intensively investigated owing to their characteristic emission properties for potential applications in biological imaging,[1] photosensitizers,[2] chemical sensing,[3] and emitters for organic light-emitting diodes (OLEDs).[4] The phosphorescence properties of these noble metal complexes are attributed to the spin-orbit coupling of the metal ion, which causes an efficient intersystem crossing from the excited singlet states to the triplet states.[5] Several strategies have been commonly employed to construct phosphorescent metal complexes with high luminescent efficiencies, several strategies have been commonly employed; including the use of strong ligand fields to suppress nonradiative deactivation via d-d excited states, the construction of robust structures to suppress vibrational deactivation in the emissive excited state, and the design of molecules with large transition dipole moments.

In coordinatively unsaturated Pt(II) complexes, intermolecular interactions with solvent molecules and counter ions should be taken into consideration as another deactivation process resulting in reduced luminescence. In contrast, the self-assembly property of Pt(II) complexes is an advantageous for unique luminescence based on the metal–metal electronic interactions. Utilizing the above characteristics, various Pt(II) complexes have been developed to afford strong and stimulus-responsive chromic luminescence. For example, cyclometalated Pt(II) complexes chelated by carbanions and other coordinating atoms provide promising phosphorescence materials, where not only monomer phosphorescence, but also excimer and/or dimer phosphorescence can be used in OLED applications[6] and chemical sensors.[3a,7] Cyclometalated Pt(II) complexes, [Pt(C^N)(O^O)] (C^N = 2-phenylpyridinate and its analogues, O^O = acetylacetonate and its derivatives) exhibit strong luminescence, which has been assigned to the phosphorescence from the lowest ligand-centred triplet (^{3}LC) states perturbed by higher-lying metal-to-ligand charge transfer singlet and triplet (^{1,3}MLCT) states.[8]

The efficient phosphorescence of these complexes is attributed to the strong σ donor ability of the carbanion of the cyclometalating ligands, which forms a strong ligand field with a large d-orbital splitting. Therefore, non-radiative decay pathways through d–d excited states (metal-centred, ^{1,3}MC) can be suppressed in the cyclometalated Pt(II) complexes.

In the past decade, *N*-heterocyclic carbene (NHC) ligands have been attracted much research attention in the fabrication of novel cyclometalating ligands for strong phosphorescent materials.[9] NHC ligands are relatively easy to synthesize and provide stronger ligand fields than the aforementioned C^N ligands, such as 2-phenylpyridine. Furthermore, the emission properties can be controlled through the combination of carbene and aryl groups. In 2010, Strassner and co-workers reported the synthesis of blue luminescent cyclometalated Pt(II)-NHC complexes bearing β-

diketonato ligands, and their application to OLEDs.[10] Since then, various phosphorescent Pt(II)-NHC complexes have been reported.[11-12] However, detailed studies of excited states and photophysical properties of the Pt(II)-NHC complexes have not been investigated broadly.

The phosphorescence properties of transition metal complexes have been investigated using variable temperature spectroscopy.[13-14] At temperatures below 100 K, the phosphorescence properties of luminescent Ru(II) and Ir(III) complexes, which have typically the ^{3}MLCT emission states, exhibit remarkable changes due to the changes in the thermal population of the triplet sublevels having a quite large zero-field splitting (ZFS) at around 100 cm^{-1} compared to those of organic compounds (< 0.1 cm^{-1}).[15] At around ambient temperature, the emission properties of metal complexes are affected by several excited states, such as the metal-centred state that causes thermally activated non-radiative decay, leading to low emission efficiency. The $[Ru(bpy)_3]^{2+}$ (bpy = 2,2′-bipyridine) complex and its derivatives have triplet metal-centred states (^{3}MC) located around 3000–4000 cm^{-1} higher than the ^{3}MLCT lowest excited state, giving rise to non-radiative decay at room temperature.[16] Furthermore, in cyclometalated Ir(III) complexes, suppression of the deactivation process via thermal population of ^{3}MC is essential for achieving intense blue phosphorescence.[17] Green emissive Ir(III) complex, $[Ir(ppy)_3]$ (Hppy = 2-phenylpyridine) is known to exhibit a high emission quantum yield approaching 100 %,[18] whereas the blue emissive $[Ir(ppz)_3]$ (Hppz = phenylpyrazole) exhibits quite a low emission quantum yield ($\Phi < 0.01$) because the blue emissive complex has access to the MC state.[19] Therefore, control of the excited states through ligand design is required to develop efficient blue phosphors.

In the excited states of Pt(II) complexes with square-planar geometry, additional deactivation processes can occur in fluid solutions. The luminescence of such coordinatively unsaturated complexes is quenched by solvent molecules and counter ions. Square-planar Pt(II) complexes often form excimers and exciplexes, which affect the emission color and intensity.[20] In contrast, stacking based on the Pt–Pt interactions and/or π–π interactions among square-planar Pt(II) complexes generates characteristic emission states, such as a metal-metal-to-ligand charge transfer state (^{3}MMLCT).[3a,7,21] Therefore, the photophysical properties of Pt(II) complexes are diverse, which is advantageous for fabrication of stimulus-responsive systems. On the other hand, sophisticated systems containing discrete and stable Pt(II) complexes are required to elucidate the essential luminescence properties of Pt(II) complexes.

Herein, four anionic platinum complexes have been prepared as tetra(*n*-butyl) ammonium salts, *n*-$Bu_4N[Pt(CN)_2(L)]$ (H_2L^+ = 1-methyl-3-phenyl-1H-imidazolium (**1**), 1-methyl-3-phenyl-1H-benzimidazolium (**2**), 1-methyl-3-(naphthalen-2-yl)-1H-imidazolium (**3**), and 1-methyl-3-(naphthalen-1-yl)-1H-imidazolium (**4**)) (Scheme 1), and their luminescence properties are reported. These anionic Pt(II)-NHC complexes are coordinated by four carbon atoms that can form strong ligand fields. The *n*-Bu_4N^+ cation can provide an isolated environment for the anionic complexes.[22-25] The rigid packing structure without direct intermolecular interactions between Pt(II)-NHC complexes

shows blue-to-orange emissions. The thermally activated deactivation process via upper non-emissive states, and zero-field splitting properties were investigated by the emission lifetime analysis over a wide temperature range (4–300 K). Ground- and excited-state quantum chemical studies were also performed to rationalize the origin of the emission and clarify the regioselective effects of π extension on emission color tunability.

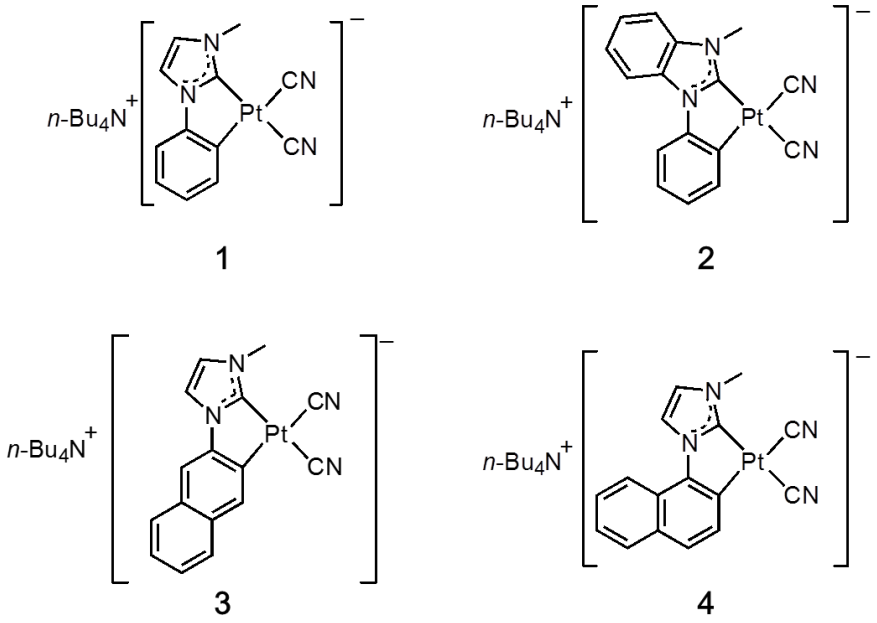

Scheme 1. Structural formula of **1**–**4**.

3-2 Experimental

3-2-1Materials.

Caution! *Although no difficulties were experienced by us, most of the chemicals used in this study are potentially harmful, particularly $AgClO_4$, which is explosive, and KCN, which is poisonous, and should be used in small quantities and handled with care in a fume hood.* All reagents were purchased from Wako Pure Chemical Industries. All solvents were purchased from Kanto Chemical Co., Inc. These chemicals were used without any further purifications. All precursors $[Pt_2(\mu\text{-}Cl)_2(mpi)_2]$ (H_2mpi^+ = 1-methyl-3-phenyl-1*H*-imidazolium), $[Pt_2(\mu\text{-}Cl)_2(mpb)_2]$ (H_2mpb^+ = 1-methyl-3-phenyl-1*H*-benzimidazolium), $[Pt_2(\mu\text{-}Cl)_2(2mni)_2]$ (H_22mni^+ = 1-methyl-3-(naphtharene-2-yl)-1*H*-imidazolium), and $[Pt_2(\mu\text{-}Cl)_2(1mni)_2]$ (H_21mni^+ = 1-methyl-3-(naphtharene-1-yl)-1*H*-imidazolium) were prepared using the literature method.[12]

3-2-2 Synthesis

n-$Bu_4N[Pt(CN)_2(mpi)]$ (1)

$AgClO_4$ (165 mg, 0.80 mmol) and $[Pt_2(\mu\text{-}Cl)_2(mpi)_2]$ (316 mg, 0.41 mmol) were dissolved in acetonitrile (35 mL). After stirring for 4 h in the dark, the mixture was filtered through celite. The yellow filtrate was evaporated to dryness and the resulting yellow solid was suspended in methanol (50 mL), and KCN (104 mg, 1.6 mmol) was added, and the suspension was stirred for 2 h. The reaction mixture was filtered, and the solution was evaporated to dryness. The resulting yellow solid was suspended in H_2O (50 mL) and n-Bu_4NCl (222 mg, 0.80 mmol) was added. The precipitated solid was then collected by filtration. After recrystallization from methanol/Et_2O, colorless crystals were obtained.

Yield, 46 mg (0.06 mmol, 8%). ^1H NMR (CD_3CN, 270 MHz): δ = 8.06 (tdd, J = 27.0, 7.0, 1.6 Hz, 1H), 7.44 (d, J = 2.0 Hz, 1H), 7.13 (dt, J = 7.5, 1.8 Hz, 1H), 7.05–6.91 (m, 3H), 4.09 (s, 3H), 3.10–3.04 (m, 8H), 1.68–1.53 (m, 8H), 1.36 (sext, J = 7.3 Hz, 8H), 0.96 (t, J = 0.96 Hz, 12H). Anal. Calcd. for $C_{28}H_{45}N_5Pt$: C, 52.00; H, 7.01; N, 10.83%. Found: C, 51.73; H, 6.94; N, 10.81%.

n-$Bu_4N[Pt(CN)_2(mpb)]$ (2)

$AgClO_4$ (51 mg, 0.25 mmol) and $[Pt_2(\mu\text{-}Cl)_2(mpb)_2]$ (108 mg, 0.12 mmol) were dissolved in acetonitrile (20 mL). After stirring for 4 h in the dark, the mixture was filtered through celite. The yellow filtrate was evaporated to dryness and the resulting yellow solid was suspended in methanol (100 mL), KCN (32 mg, 0.49 mmol) was added, and the suspension was stirred for 2 h. The reaction mixture was filtered and the solution was evaporated to dryness. The resulting yellow solid was suspended in H_2O (50 mL) and n-Bu_4NCl (69 mg, 0.25 mmol) was added. The precipitated solid was then collected by filtration. After recrystallization from methanol/Et_2O, pale yellow crystals were

obtained.

Yield, 81 mg (0.11 mmol, 44%). ^{1}H NMR (CD_3CN, 270 MHz): δ = 8.22 (tdd, J = 28.9, 6.9, 1.6 Hz, 1H), 8.12 (dd, J = 6.5, 2.1 Hz, 1H), 7.73 (d, J = 8.1 Hz, 1H), 7.62 (dd, J = 6.9, 2.4 Hz, 1H), 7.46–7.41 (m, 2H), 7.15 (td, J = 7.6, 1.6 Hz, 1H), 7.02 (td, J = 7.4, 1.2 Hz, 1H), 4.34 (s, 3H), 3.10–3.04 (m, 8H), 1.65–1.53 (m, 8H), 1.35 (sext, J = 7.8 Hz, 8H), 0.96 (t, J = 7.2 Hz, 12H). Anal. Calcd. for $C_{32}H_{47}N_5Pt \cdot 0.5CH_3OH$: C, 54.76; H, 6.93; N, 9.82%. Found: C, 54.50; H, 6.94; N, 9.88%.

n-Bu_4N[$Pt(CN)_2$(2mni)] (3)

$AgClO_4$ (75 mg, 0.36 mmol) and [$Pt_2(\mu\text{-}Cl)_2(2mni)_2$] (163 mg, 0.19 mmol) were dissolved in acetonitrile (60 mL). After stirring for 4 h in the dark condition, the mixture was filtered through celite. The yellow filtrate was evaporated to dryness and the resulting yellow solid was suspended in methanol (30 mL), KCN (47 mg, 0.72 mmol) was added, and the suspension was stirred for 2 h. The reaction mixture was filtered and the solution was evaporated to dryness. The resulting yellow solid was suspended in H_2O (30 mL) and n-Bu_4NBr (132 mg, 0.41 mmol) was added. The precipitated solid was then collected by filtration. After recrystallization from methanol/Et_2O, pale yellow crystals were obtained.

Yield, 172 mg (0.247 mmol, 69%). ^{1}H NMR (CD_3CN, 270 MHz): δ = 8.49 (t, J = 28.6 Hz, 1H), 7.77–7.69 (m, 2H), 7.62 (d, J = 1.9 Hz, 1H), 7.57 (t, J = 5.0 Hz, 1H), 7.34–7.30 (m, 2H), 7.10 (d, J = 1.9 Hz, 1H), 4.12 (s, 3H), 3.09–3.03 (m, 8H), 1.63-1.51 (m, 8H), 1.34 (sext, J = 7.5 Hz, 8H), 0.95 (t, J = 7.3 Hz, 12H). Anal. Calcd for $C_{32}H_{47}N_5Pt$: C, 55.16; H, 6.80; N, 10.05%. Found: C, 55.02; H, 6.80; N, 9.96%.

n-Bu_4N[$Pt(CN)_2$(1mni)] (4)

$AgClO_4$ (118 mg, 0.57 mmol) and [$Pt_2(\mu\text{-}Cl)_2(1mni)_2$] (254 mg, 0.29 mmol) were dissolved in acetonitrile (100 mL). After stirring for 8 h in the dark, the mixture was filtered through celite. The yellow filtrate was evaporated to dryness and the yellow solid was suspended in methanol (50 mL), KCN (74 mg, 1.1 mmol) was added, and the suspension was stirred for 2 h. The reaction mixture was filtered and the solution was evaporated to dryness. The resulting yellow solid was suspended in H_2O (50 mL) and n-Bu_4NBr (200 mg, 0.62 mmol) was added. The precipitated solid was then collected by filtration. After recrystallization from methanol/Et_2O, pale yellow crystals were obtained.

Yield, 249 mg (0.358 mmol, 63%). ^{1}H NMR (CD_3CN, 270 MHz): δ = 8.43 (td, J = 27.0, 8.0 Hz, 1H), 8.26 (d, J = 8.5 Hz, 1H), 8.11–8.08 (m, 1H), 7.83 (d, J = 8.2 Hz, 1H), 7.52 (d, J = 8.2 Hz, 1H), 7.46 (ddd, J = 7.1, 6.8, 1.5 Hz, 1H), 7.34 (ddd, J = 7.0, 6.8, 1.2 Hz, 1H), 7.15–7.10 (m, 1H), 4.16 (s, 3H), 3.09–3.03 (m, 8H), 1.64-1.52 (m, 8H), 1.35 (sext, J = 7.5 Hz, 8H), 0.95 (t, J = 7.3 Hz, 12H). Anal. Calcd for $C_{32}H_{47}N_5Pt \cdot CH_3OH$: C, 54.38; H, 7.05; N, 9.61%. Found: C, 54.00; H, 6.80; N, 9.88%.

3-2-3 Luminescence measurements

Luminescence spectra were measured using a JASCO FP-6600 spectrofluorometer at room temperature and 77 K. Slit widths of the excitation and emission light were 5 or 6 nm. Luminescence quantum yields were recorded using a Hamamatsu Photonics C9920-02 absolute photoluminescence quantum yield measurement system equipped with an integrating sphere apparatus and CW Xenon light source (150 W). A Hamamatsu Photonics A10095-03 non-luminescent quartz sample holder was used for absolute photoluminescence quantum yield measurements. The instrument accuracy was confirmed by measuring the quantum yield of anthracene in ethanol solution (Φ = 0.27).[26] Emission lifetime measurements were recorded using streak cameras, namely, Hamamatsu C4334 at 337 nm (nitrogen laser, KEN-X) excitation and Hamamatsu C4334 system at 355 nm (Nd:YAG laser, LOTIS TII) excitation. Liquid N_2 or liquid He cryosystems (Optistat-DN or Optistat-CF with ITC-503 temperature controller, Oxford Instruments) or a liquid He cryostat (Optistat-DN optical Dewar and ITC-503 temperature controller, Oxford Instruments) were used for the temperature control. Temperature-dependent data of the emission lifetimes were fitted by Origin2017 software using Boltzmann-type equations.

3-2-4 Single crystal X-ray diffraction measurements

All single crystal X-ray diffraction measurements were performed using a Rigaku AFC-7R diffractometer with a Mercury CCD area detector and graphite monochromatized Mo K_α radiation (λ = 0.71069 Å) at 200 K (complexes **1** and **3**) and 150 K (complexes **2** and **4**), respectively. Each single-crystal was mounted on a MicroMount using liquid paraffin. These crystals were cooled using a N_2-flow-type temperature controller. Diffraction data were collected and processed using the Crystal-Clear software.[27] Structures were solved by direct methods (SHELXS2013[28] for **1**; SIR2011[29] for **2, 3**, and **4**). Structural refinements were conducted by the full-matrix least-squares method using SHELXL2013.[28] Non-hydrogen atoms were refined anisotropically, and all hydrogen atoms were refined using the rigid model. All calculations were performed using the CrystalStructure crystallographic software package[30] except for refinement. Crystallographic data of **1**–**4** are summarized in Table 2.

3-2-5 Other measurements

^{1}H NMR spectroscopy was performed using a JEOL EX-270 NMR spectrophotometer. Elemental analyses were carried out at the analysis center of Hokkaido University. Absorption spectra were measured using a Shimadzu UV-2500PC Spectrophotometer under a N_2 atmosphere using quartz cells with an optical-path length of 1 cm.

3-2-6 Computational methods

DFT and TD-DFT calculations for the complexes were performed using the Gaussian 09 program.[31] The B3LYP[32] functional was used for ground state structure optimizations. The M06-2X[33] functional was employed for vertical excitation energy calculations and lowest singlet and triplet states optimizations. The SDD basis set and associated effective core potentials were used for Pt,[34] and the 6-31G(d,p) basis sets were used for other atoms.[35] An isovalue of 0.02 was used for Kohn–Sham orbital pictures and spin density plots.

3-3 Results and discussion

3-3-1 Crystal structures

The structures of complex anions of **1**–**4** determined by single crystal X-ray analysis are shown in Figure 1. For all complexes, platinum ions adopted the four-coordinated square-planar geometry typical of divalent platinum complexes showing high flatness (sum of the angles = 360.0° (**1** and **2**), 359.9° (**3**), 360.1° (**4**)). The four coordination sites are occupied by two carbon atoms of cyanide anions, one aryl carbanion, and one carbene carbon atom, to form anionic Pt(II)-C_4 complexes. Selected bond lengths and angles of the complexes are listed in Table 1. The platinum carbene bonds (Pt–C3, 2.004(4)–2.008(7) Å) were slightly shorter than those of platinum with cyclometalated carbon of the aryl ring (Pt–C4, 2.045(6)–2.054(3) Å). This tendency was also found in related complexes. Both of the Pt-carbene and Pt-aryl bond lengths of these complexes were slightly longer than those of Pt(II)-NHC acetylacetonato complexes ([Pt(acac)(L)] (H_2L^+ = 1-(dibenzofuranyl)-3-methylimidazolium, Hacac = acetylacetone), Pt–C(aryl) = 1.960, Pt–C(carbene) = 1.937 Å)[10] due to the *trans* influence caused by the stronger σ donor ability of cyanide ligands compared to that of the oxygen donor atoms of the acetylacetonato ligands. The bond lengths between platinum and cyanide carbon atoms coordinated *trans* to the carbenes (Pt–C1, 1.995(5)–2.027(8) Å) were slightly shorter than that of the other cyanide ligands (Pt–C2, 2.03(1)–2.031(6) Å). These differences were due to the π acceptor ability of the carbene atoms, despite the strong σ donor abilities of both of aryl carbon and carbene atoms. Consequently, these four anionic complexes had extremely strong ligand fields due to the σ donor ability of the four Pt–C bonds and π acceptor abilities of cyanide and carbene ligands.

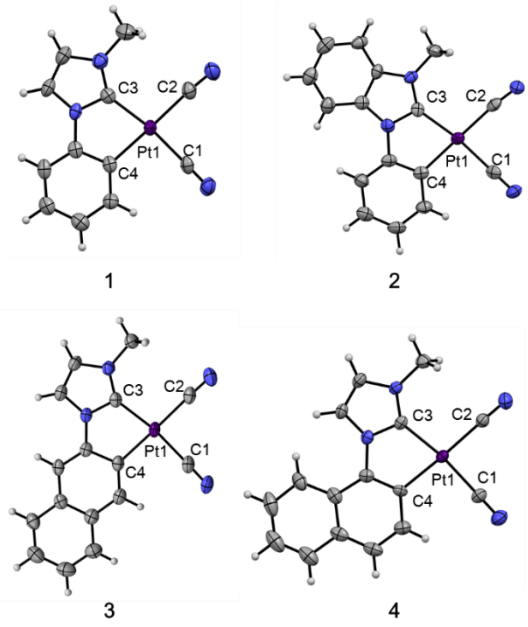

Figure 1. Molecular structures of the Pt(II) complex anions for **1**–**4**. The thermal ellipsoids are displayed at the 50% probability level for non-hydrogen atoms.

Table 1. Selected bond lengths (Å) and angles (°) for **1**–**4**.

	1	**2**	**3**	**4**
Pt1–C1	1.995(5)	2.003(7)	1.995(3)	2.027(8)
Pt1–C2	2.028(5)	2.025(10)	2.022(3)	2.031(6)
Pt1–C3	2.004(4)	2.008(7)	2.016(3)	2.005(6)
Pt1–C4	2.054(3)	2.052(8)	2.049(3)	2.045(6)
C1–Pt1–C2	88.5(2)	86.4(3)	89.9(1)	89.2(3)
C3–Pt1–C4	79.0(1)	79.0(3)	80.1(1)	78.5(2)
C2–Pt1–C3	99.6(2)	101.3(3)	98.4(1)	98.9(2)
C1–Pt1–C4	92.9(2)	93.3(3)	91.5(1)	93.5(3)
C1–Pt1–C3	171.8(2)	172.3(3)	171.5(1)	171.9(3)
C2–Pt1–C4	178.0(2)	176.7(3)	178.5(1)	177.3(2)

In the packing structures of **1**–**4**, *n*-tetrabutylammonium cations were arranged between adjacent platinum complex anions to form alternative stacking structures (Figure 2–5 for **1**–**4**, respectively). Therefore, no π–π interactions between the NHC ligands nor Pt–Pt interactions were present in these crystals. The shortest distances between Pt atoms (8.51 Å (**1**), 8.67 Å (**2**), 8.64 Å (**3**), and 9.18 Å (**4**), respectively) were much longer than 3.5 Å, which is twice the van der Waals radius of the Pt atom.[26] These crystals provided a suitable discrete environment for the Pt(II) complexes as in the case of other tetra(*n*-butyl)ammonium salts.[22-25] In fact, we previously reported two completely different crystal structures for $[Pt(CN)_2(ptpy)]^-$ (ptpy = *p*-tolylpyridinate): The tetra(*n*-butyl)ammonium salt adopted a separated structure similar to those of complexes **1**–**4**, while the potassium salt took a dimeric structure with a short Pt–Pt contact.[23]

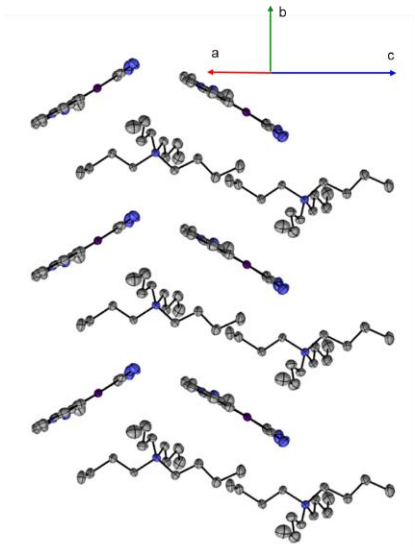

Figure 2. Packing structure of **1**. Hydrogen atoms are omitted for clarity.

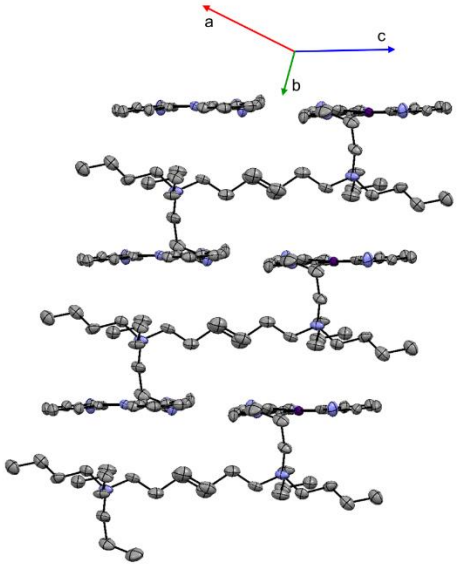

Figure 3. Packing structure of complex **2**. Hydrogen atoms and solvent molecules were omitted for clarity. Atom color represents Pt (purple), N (blue), and C (gray), respectively.

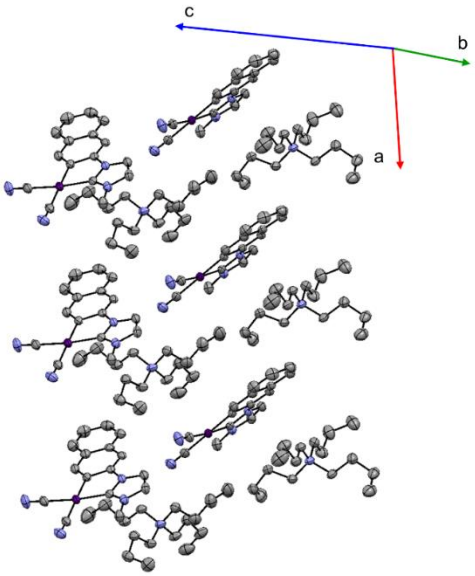

Figure 4. Packing structure of complex **3**. Hydrogen atoms were omitted for clarity. Atom color represents Pt (purple), N (blue), and C (gray), respectively.

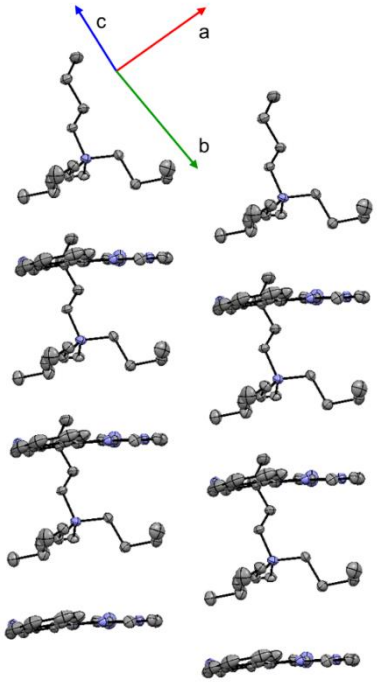

Figure 5. Packing structure of complex **4**. Hydrogen atoms and solvent molecules were omitted for clarity. Atom color represents Pt (purple), N (blue), and C (gray), respectively.

Table 2. Crystal Data for complexes **1**–**4**

	1	**2**·CH_3OH	**3**	**4**·H_2O
Formula	$C_{28}H_{45}N_5Pt$	$C_{33}H_{51}N_5OPt$	$C_{32}H_{47}N_5Pt$	$C_{32}H_{49}N_5OPt$
Formula Weight	646.79	728.89	696.85	714.86
Crystal system	monoclinic	monoclinic	monoclinic	Monoclinic
Space group	$P2_1/c$	$P2_1/n$	$P2_1/n$	Cc
a (Å)	19.244(4)	19.851(5)	8.988(1)	11.361(5)
b (Å)	8.507(2)	8.671(2)	20.266(3)	14.415(6)
c (Å)	17.517(3)	20.623(5)	17.404(2)	19.602(8)
α (°)	90	90	90	90
β (°)	96.009(2)	116.377(3)	99.042(2)	99.495(5)
γ (°)	90	90	90	90
V (Å^3)	2852.0(9)	3180(1)	3130.9(7)	3166(2)
T (K)	200	150	200	150
Z	4	4	4	4
D_{calc} (g cm^{-3})	1.506	1.522	1.478	1.500
F(000)	1304.00	1480.00	1408.00	1448.00
measured refl.	22258	23636	24692	23642
unique refl.	6495	7166	7137	7178
GOF on F^2	1.001	1.058	1.064	0.978
R_{int}	0.0463	0.0596	0.0258	0.0363
R_1[a]	0.0366	0.0485	0.0272	0.0228
wR_2[b](all data)	0.0844	0.1286	0.0658	0.0430

[a] $R_1 = \Sigma||F_o| - |F_c||/\Sigma|F_o|$. [b] $wR_2 = [\Sigma w(F_o^2 - F_c^2)/\Sigma w(F_o)^2]^{1/2}$, $w = [\sigma_c^2(F_o^2) + (xP)^2 + yP]^{-1}$, $P = (F_o^2 - 2F_c^2)/3$.

3-3-2 Absorption and emission properties

The UV-vis absorption spectra of **1**–**4** in fluid solution (acetonitrile, 0.5 × 10^{-4} M) at ambient temperature are presented in Figure 6. They exhibited ligand-centered $^1\pi\pi^*$ (or ^{1}LC) transition bands of the NHC ligands at shorter wavelengths shorter than 300 nm ($\varepsilon > 10000\ M^{-1}cm^{-1}$). Absorptions at longer wavelength regions 300–400 nm ($\varepsilon < 10000\ M^{-1}cm^{-1}$) were assigned to the spin-allowed metal-to-ligand charge transfer (^{1}MLCT) bands, which were absent in absorption spectra of the free ligands (Figure 7). Reflecting the π-extended effect, the absorption spectra of complexes **2**–**4** were red-shifted compared to that of complex **1**. For complex **4**, in particular, a discriminable absorption band assignable to the ^{1}MLCT transition was observed in the 350–400 nm region, suggesting that the π extension was effective at the 5,6-position of the phenyl ring of the original NHC ligand.

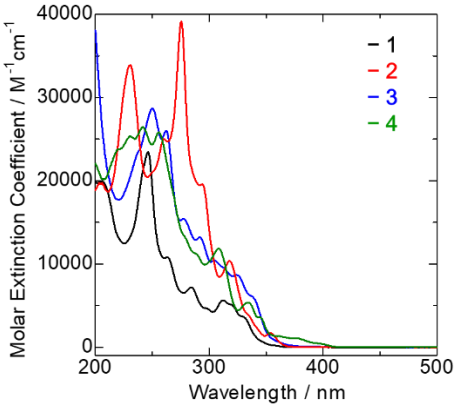

Figure 6. UV-vis spectra of **1** (black), **2** (red), **3** (blue), and **4** (green) in acetonitrile (0.5 × 10^{-4} M) at RT.

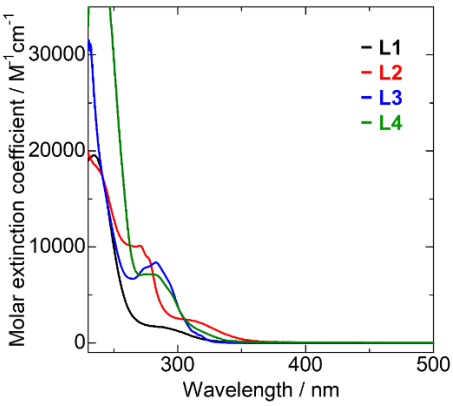

Figure 7. UV-vis absorption spectra of the ligands in CH_2Cl_2 (concentration = 1.0 × 10^{-5} M) at room temperature: L1 = 1-methyl-3-phenyl-1*H*-benzimidazolium (black line), L2 = 1-methyl-3-phenyl-1*H*-benzimidazolium (red line), L3 = 1-methyl-3-(naphtharene-2-yl)-1*H*-imidazolium (blue line), and L4

= 1-methyl-3-(naphtharene-1-yl)-1*H*-imidazolium (green line).

Figure 8 shows the emission spectra of **1**–**4** in the solid samples. All the emission spectra displayed structured profiles with maxima of the first vibrational satellite band at 430 (**1**), 452 (**2**), 530 (**3**), and 558 (**4**) nm, respectively, and vibronic bands corresponding to ground state modes of the NHC ligands (band spacing, 1300–1500 cm^{-1})[37] at room temperature. Compared to the spectrum of **1**, the emission maximum of complex **2** was slightly shifted (by 22 nm) to a longer wavelength than that of complex **1**, while significantly longer wavelength shifts were observed for **3** and **4** (100 and 128 nm shifts, respectively). The CIE coordinates for these emission spectra are shown in Figure 9, indicating the luminescence with different colors, from deep blue (0.15, 0.10) for **1**, and light blue (0.15, 0.19) for **2** to yellow (0.43, 0.57) for **3** and yellow-orange (0.53, 0.47) for **4**, respectively.

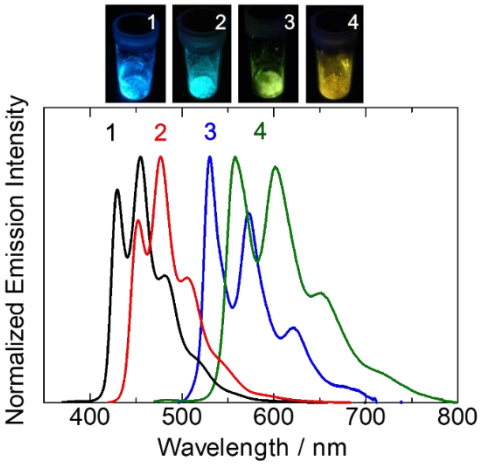

Figure 8. Emission spectra of **1**–**4** at 298 K in the solid states (λ_{ex} = 350 nm) with images of the luminescence.

Table 3. Photophysical data of **1**–**4** in the solid state.

Complex	T (K)	λ_{em} (nm)	Φ	τ (μs)	k_r (s^{-1})	k_{nr} (s^{-1})
1	298	430, 455, 481	0.69(3)	5.3	1.3×10^5	5.8×10^4
	77	436, 454, 483	0.95(3)	8.4	1.1×10^5	6.0×10^3
2	298	452, 477, 505	0.34(3)	2.5	1.3×10^5	2.5×10^5
	77	450, 476, 507	0.89(3)	8.5	1.0×10^5	1.3×10^4
3	298	530, 572, 621	0.72(3)	69	1.0×10^4	4.1×10^3
	77	525, 570, 620	0.73(3)	77	9.4×10^3	3.5×10^3
4	298	558, 601, 651	0.24(3)	24	9.2×10^3	2.9×10^4
	77	560, 608, 661	0.22(3)	25	7.7×10^3	2.7×10^4

Photophysical data, including emission lifetimes and quantum yields of **1**–**4** in the solid state at 298 and 77 K, are summarised in Table 3. Based on the structured spectral profiles and the lifetimes in the order of microseconds, the emission of these complexes was assigned to phosphorescence from the triplet ligand-centred (^{3}LC) excited state with some mixing of higher-lying singlet and triplet metal-to-ligand charge transfer (^{1,3}MLCT) states. High photoluminescence quantum yields were obtained for **1** and **3** (0.69 and 0.72, respectively), even at room temperature, while complexes **2** and **4** exhibited moderate values (0.34 and 0.24, respectively). The calculated radiative rate constants (k_r) were in the order of 10^5 for complexes **1** and **2**, which suggested that efficient spin-orbit coupling (SOC) occurred in high energy excited states for the blue emissive compounds (>20,000 cm^{-1}). Compared with **1** and **2**, smaller radiative rate constants were obtained for complexes **3** (1.0×10^4) and **4** (9.2×10^3), suggesting that the SOC efficiency was lower because of larger energy separation between triplet states and singlet states. The nonradiative rate constants did not decrease linearly in ln(k_{nr}) with increasing emission energy, indicating that the luminescence properties of these complexes were not governed by the energy gap law (Figure 10). The larger nonradiative rate constants of blue emissive complexes **1** and **2** compared to that of complex **3** suggested that there might be thermal access to higher lying nonradiative states. The emission quantum yields reached to almost practically limited values (0.95 for **1** and 0.89 or **2**) at 77 K, which was attributed to suppressed nonradiative deactivation ($k_{nr} = 6.0 \times 10^3$ s^{-1} (**1**) and 1.3×10^4 s^{-1} (**2**) at 77 K).

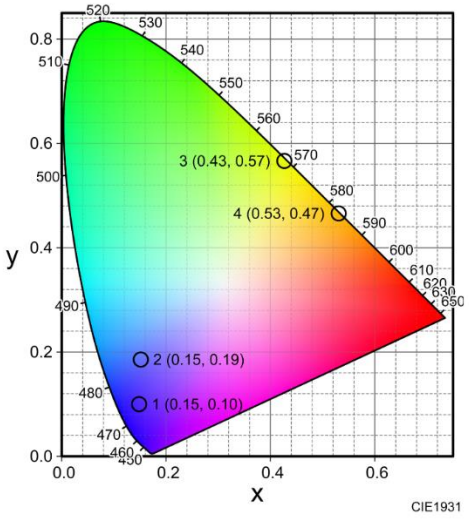

Figure 9. CIE coordinates for emission spectra of complexes **1**-**4** at room temperature.

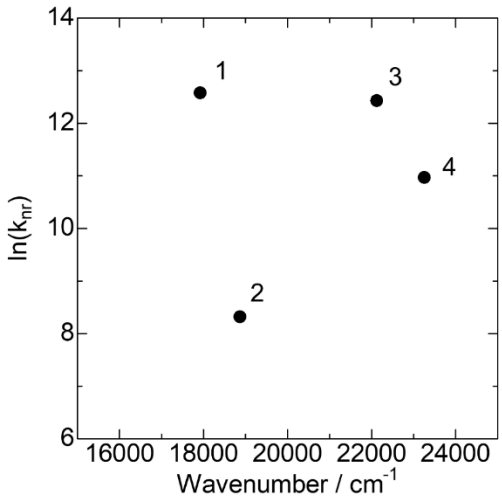

Figure 10. Plot of the observed value of ln (k_{nr}) vs. the emission maximum (cm^{-1}). Both values are for room-temperature in solid states. The non-linear relationship indicates the direct nonradiative decay path from emissive triplet excited states to ground states is not dominant for the emission properties for complexes **1**-**4**.

3-3-3 Temperature dependence of emission lifetimes

To obtain detailed information on the emission states, the temperature dependence of the phosphorescence lifetimes was investigated from ambient temperature (298 K) to very low temperature (4 K). Figure 11 shows the plots of emission lifetimes against temperature for **1**–**4**, which clearly show the different features of the four complexes.

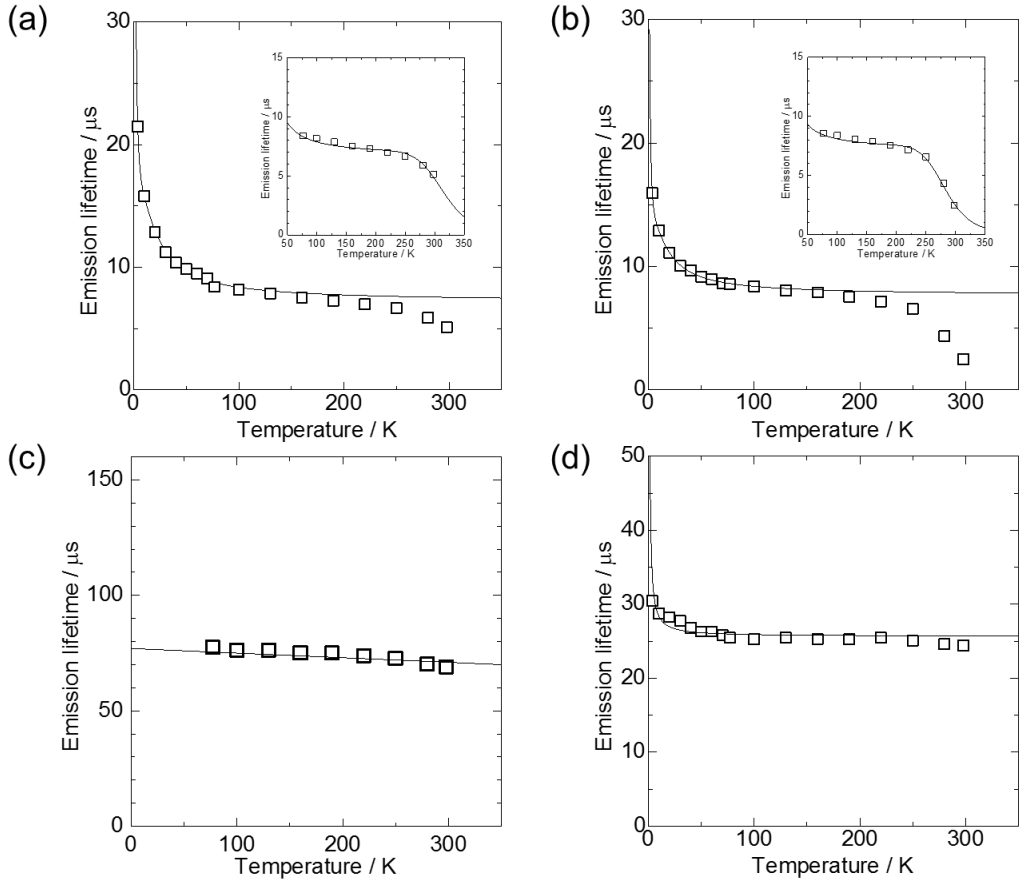

Figure 11. Temperature dependence of emission lifetime for complexes **1** (a), **2** (b), **3** (c), and **4** (d). The solid thin lines show the fitting results based on Eq (2) using the data in the temperature regions of 4–77 K, while those of insets in (a) and (b) are the fitting curves in the temperature regions of 77–298 K based on the Eq (1).

For the blue luminescent complexes **1** and **2**, the lifetimes increased clearly with decreasing temperature from 298 K to 200 K, and when further decreasing the temperatures to 4 K, a remarkable

increase was observed. This was ascribed to changes in the thermal population of several low-lying electronic excited states. In the relatively high-temperature region, the change would be due to the thermal activation to upper nonradiative states.[38] Accordingly, the temperature dependence of emission lifetimes between 298 K and 77 K were analysed by using the Boltzmann model equation (1) containing two temperature-dependent terms, where τ = experimental emission lifetime at temperature T, k_0 = radiative rate constant at the very low temperature, k_1 = radiative rate constant at ambient temperature, k_2 = rate constant of transition to higher-lying non-radiative excited state, E_1 and E_2 = activation energies, and k_B = Boltzmann constant. In the temperature region, a fixed value of k_0 = 1.0×10^4 s^{-1} was used for this fitting process, based on other cyclometalated Pt(II) complexes (k_0 = $1–5 \times 10^4$ s^{-1}).[4a,39] In this situation, E_1 would roughly correspond to the energy difference between highest and lowest triplet sublevels. The fitting results are shown in the insets of Figure 11 and the values are listed in Table 4. The estimated activation energies required to populate the higher-lying non-radiative states were 2900 and 2600 cm^{-1} for **1** and **2**, respectively. These values indicated that thermally activated non-radiative decay was effectively suppressed for **1** and **2**, but not to the extent of complete suppression at ambient temperature. The rate constants from the nonradiative states (k_2) are very large (1.6 and 1.5×10^{11} s^{-1} for **1** and **2**, respectively), suggesting the internal conversion to the metal-centred (^{3}MC) states in the Pt(II) complexes.[40] Notably, the ligand field strength for these *N*-heterocyclic carbene complexes was not enough to create blue phosphors with quantum yields of almost the theoretical limit (Φ = 1.0). The smaller activation energy (E_2) for **2** than that of **1** caused the lower emission quantum yield at 298 K of the blue emissive compound.

$$\tau = \frac{1}{k_{obs}} = \frac{1+\exp\left(\frac{-E_1}{k_B T}\right)+\exp\left(\frac{-E_2}{k_B T}\right)}{k_0+k_1\exp\left(\frac{-E_1}{k_B T}\right)+k_2\exp\left(\frac{-E_2}{k_B T}\right)} \qquad (1)$$

Table 4. Fitting parameters based on the analysis of lifetimes (298–77 K) using Eq. (1).

	k_0 (s^{-1})	k_1 (s^{-1})	E_1 (cm^{-1})	k_2 (s^{-1})	E_2 (cm^{-1})
1	1.0×10^4	2.9×10^5	23	1.6×10^{11}	2920
2	1.0×10^4	2.7×10^5	18	1.5×10^{11}	2618

Next, the emission lifetime data in the lower temperature region (4–77 K) were further analysed for **1** and **2** using equation (2), which is essentially the same as equation (1).

$$\tau = \frac{1}{k_{\mathrm{obs}}} = \frac{1+\exp\left(\frac{-\Delta E_{\mathrm{I-II}}}{k_{\mathrm{B}} T}\right)+\exp\left(\frac{-\Delta E_{\mathrm{I-III}}}{k_{\mathrm{B}} T}\right)}{k_{\mathrm{I}}+k_{\mathrm{II}}\exp\left(\frac{-\Delta E_{\mathrm{I-II}}}{k_{\mathrm{B}} T}\right)+k_{\mathrm{III}}\exp\left(\frac{-\Delta E_{\mathrm{I-III}}}{k_{\mathrm{B}} T}\right)} \qquad (2)$$

where k_n (n = I, II, and III) is the rate constant of individual sub-levels of the triplet state (T_1), and $\Delta E_{\mathrm{I\text{-}II}}$ and $\Delta E_{\mathrm{I\text{-}III}}$ correspond to energy separations between the sub-levels. Energy diagrams of the obtained

triplet spin sublevels are shown in Figure 12(a) and (b). The $\Delta E_{\text{I-III}}$ values around 30 cm^{-1} indicated the major contribution of the ^{3}MLCT character to the emission states (*vide infra*).

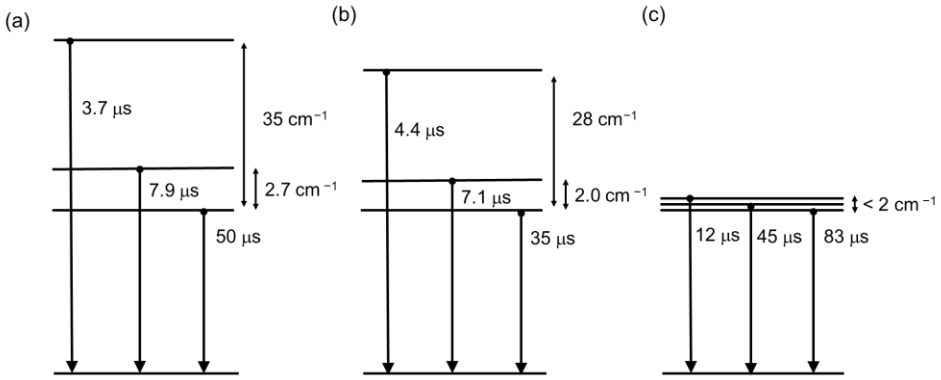

Figure 12. Energy diagrams of the triplet spin sublevels for **1** (a), **2** (b), and **4** (c).

In contrast to **1** and **2**, the lifetimes of complexes **3** and **4** were insensitive to temperature (Figure 11(c) and (d)), exhibiting relatively long emission lifetimes at room temperature (70 and 20 μs for **3** and **4**, respectively) with no distinct increase observed even at very low temperature (4 K). The emission features of **3** and **4** suggested their emission states were considerably pure ^{3}LC states. A rough estimation based on the lifetime data of complex **4** provided a very small ZFS of less than 2 cm^{-1} (Figure 12(c)). Unfortunately, a similar analysis could not be applied to **3** because the emission spectrum exhibited a remarkable blue shift below 60 K.

3-3-4 Computational studies

Density functional theory (DFT) and time-dependent DFT (TD-DFT) were used to study the ground state and lowest singlet and triplets excited states of four complexes (Tables 6–10). Starting from the ground state optimized structures, vertical excitation energies were calculated by using TD-DFT, with the key excitation and Kohn–Sham orbitals depicted in Figure 14–17. The Kohn–Sham orbitals in the frontier region of the complexes **1**–**4** were shown in Figure 13, including the highest occupied molecular orbitals (HOMOs) and lowest unoccupied molecular orbitals (LUMOs) of the singlet ground states. The HOMOs of the four complexes were mainly localized on Pt, with some partial delocalization on the ligands. Therefore, the calculated first excitation, HOMO → LUMO, had both ^{1}MLCT and ^{1}LC characters. In the case of complexes **1** and **2**, the LUMOs were delocalized on Pt($6p_z$) and ligand. On the other hand, the LUMOs of complexes **3** and **4** were mainly delocalized on naphthyl moiety of the NHC ligands, whereas the (LUMO+1)s were mainly localized on Pt with partial delocalization on the naphthyl ring of the NHC ligand. This switching of orbitals was due to the extended phenyl ring of the complexes **3** and **4**. However, the calculated first excitation, HOMO → LUMO, was the forbidden transition. The highest allowed transition was the Pt(d_z^2) → LUMO ^{1}MLCT transition (Tables 6–9), which supported the absorption bands appearing at around 300–400 nm for these complexes (Figure 6).

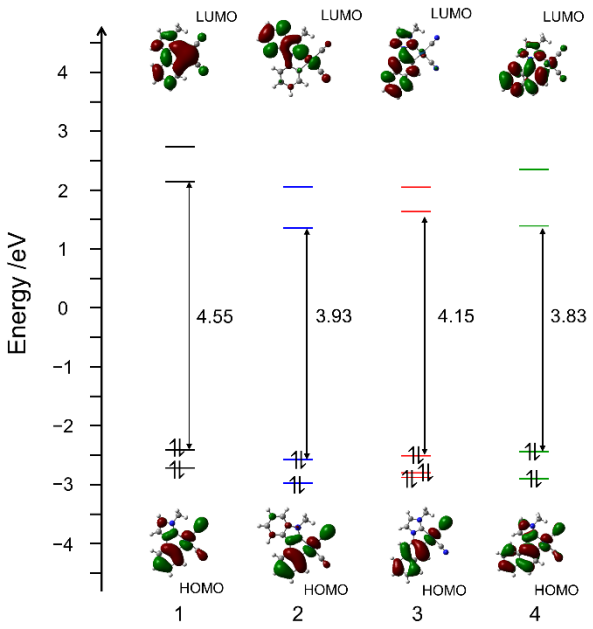

Figure 13. Energy level diagrams for **1**–**4** including surface drawings of HOMOs and LUMOs of the singlet states.

Table 5. Calculated bond lengths and angles for the complexes **1**–**4** and comparison with observed value from crystal structures.

bond (Å) or angle (°)		**1**	**2**	**3**	**4**
Pt(1)–C(1)	Calculated	2.01	2.01	2.01	2.01
	Crystal	1.995(5)	2.003(7)	1.995(3)	2.027(8)
Pt(1)–C(2)	Calculated	2.04	2.05	2.04	2.04
	Crystal	2.028(5)	2.025(10)	2.022(3)	2.031(6)
Pt(1)–C(3)	Calculated	2.04	2.02	2.03	2.03
	Crystal	2.004(4)	2.008(7)	2.016(3)	2.005(6)
Pt(1)–C(4)	Calculated	2.07	2.06	2.07	2.06
	Crystal	2.054(3)	2.052(8)	2.049(3)	2.045(6)
C(1)–Pt(1)–C(2)	Calculated	91.5	90.1	91.3	90.9
	Crystal	88.5(2)	86.4(3)	89.9(1)	89.2(3)
C(3)–Pt(1)–C(4)	Calculated	79.3	79.3	79.5	78.7
	Crystal	79.0(1)	79.0(3)	80.1(1)	78.5(2)
C(2)–Pt(1)–C(3)	Calculated	97.3	98.6	97.4	98.1
	Crystal	99.6(2)	101.3(3)	98.4(1)	98.9(2)
C(1)–Pt(1)–C(4)	Calculated	91.9	92.1	91.8	92.4
	Crystal	92.9(2)	93.3(3)	91.5(1)	93.5(3)
C(1)–Pt(1)–C(3)	Calculated	171.2	171.3	171.3	170.7
	Crystal	171.8(2)	172.3(3)	171.5(1)	171.9(3)
C(2)–Pt(1)–C(4)	Calculated	176.6	177.8	176.9	176.0
	Crystal	178.0(2)	176.7(3)	178.5(1)	177.3(2)

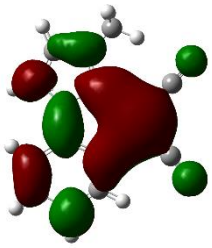	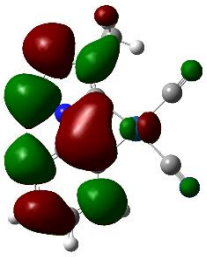	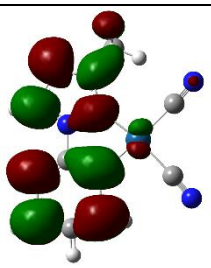	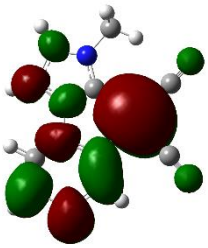
LUMO 2.14 eV 14/5/47/34	LUMO+1 2.74 eV 3/1/62/34	LUMO+2 3.43 eV 1/0/50/48	LUMO+3 3.99 eV 29/2/17/52
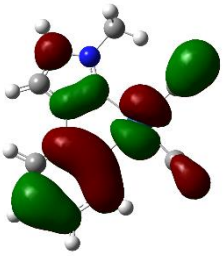	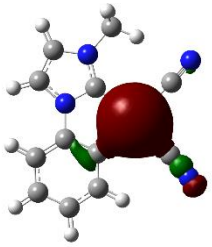	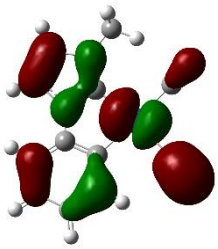	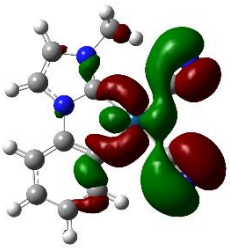
HOMO −2.41 eV 53/11/8/28	HOMO−1 −2.72 eV 95/2/1/2	HOMO−2 −2.77 eV 57/20/15/8	HOMO−3 −2.93 45/42/5/8

Figure 14. Selected molecular orbitals for the ground state of complex **1** calculated by DFT method at the B3LYP level (isovalue = 0.02), combined with the energy (eV) and compositions of orbitals (Pt/CN/azole/aryl, %). The green and red color represent different phases, respectively.

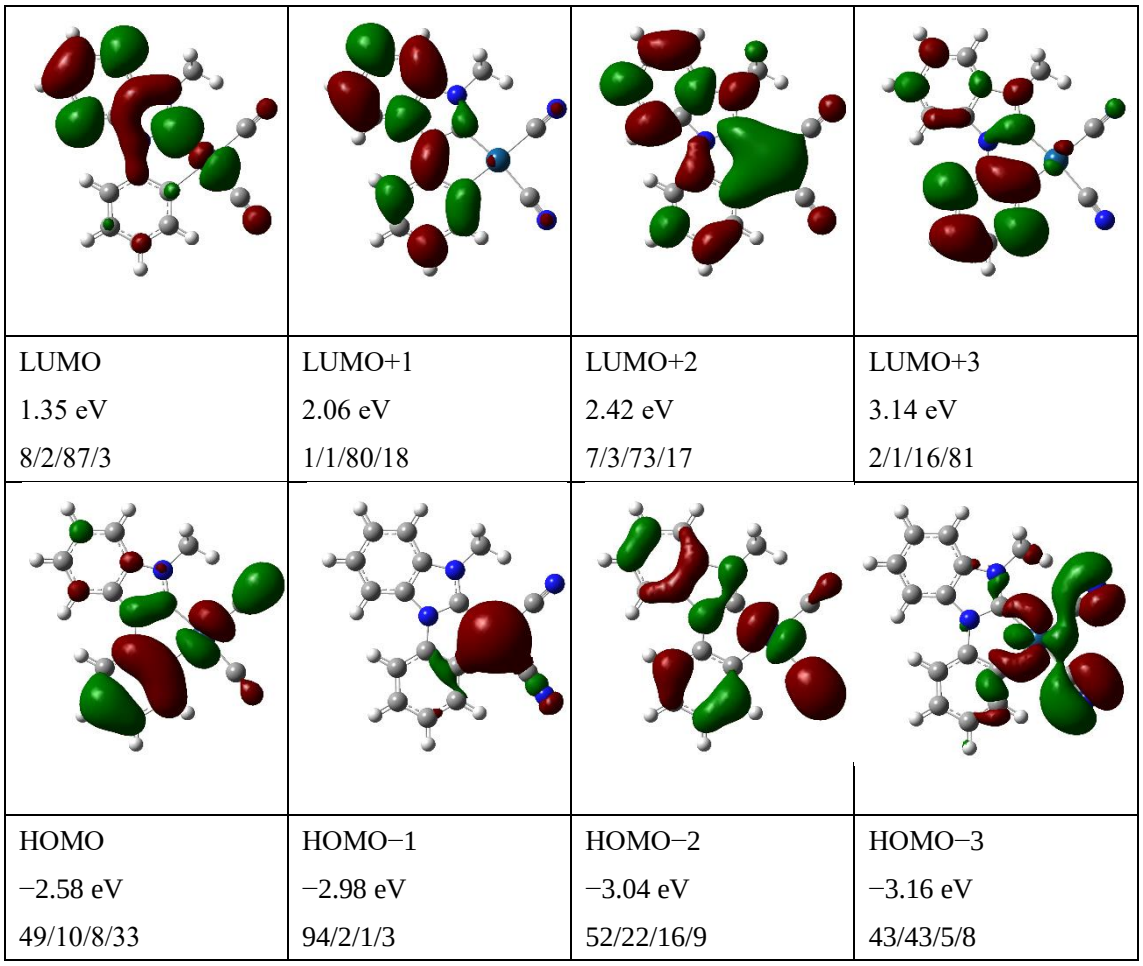

Figure 15. Selected molecular orbitals for the ground state of complex **2** calculated by DFT method at the B3LYP level (isovalue = 0.02), combined with the energy (eV) and compositions of orbitals (Pt/CN/azole/aryl, %). The green and red color represent different phases, respectively.

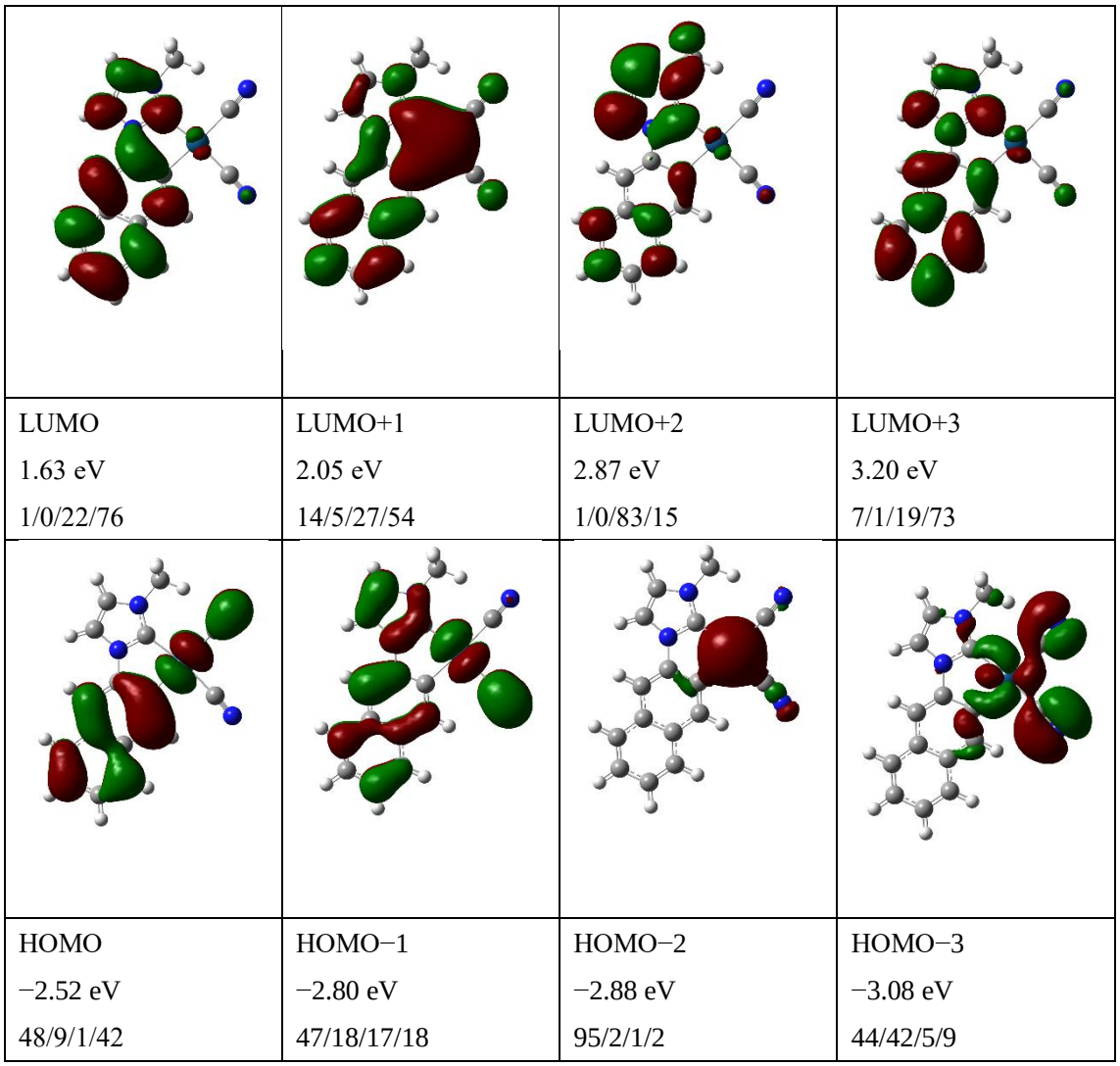

Figure 16. Selected molecular orbitals for the ground state of complex **3** calculated by DFT method at the B3LYP level (isovalue = 0.02), combined with the energy (eV) and compositions of orbitals (Pt/CN/azole/aryl, %). The green and red color represent different phases, respectively.

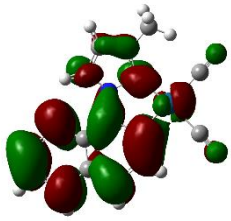	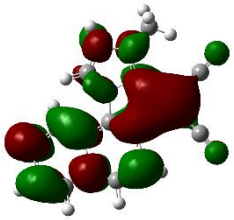	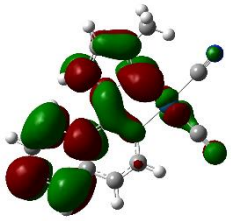	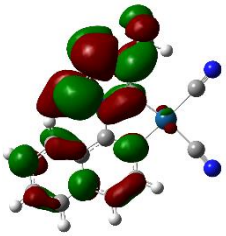
LUMO 1.39 eV 6/2/16/76	LUMO+1 2.35 eV 7/3/22/68	LUMO+2 2.58 eV 5/2/34/59	LUMO+3 3.03 eV 1/0/73/26
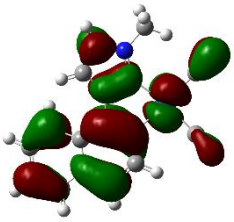	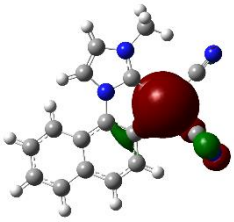	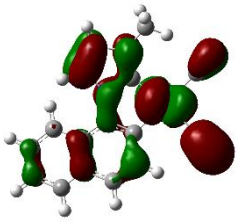	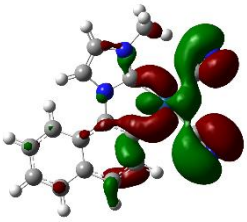
HOMO −2.44 eV 38/7/13/42	HOMO−1 −2.90 eV 94/3/1/2	HOMO−2 −2.96 eV 58/19/15/8	HOMO−3 −3.10 eV 43/40/5/11

Figure 17. Selected molecular orbitals for the ground state of complex **4** calculated by DFT method at the B3LYP level (isovalue = 0.02), combined with the energy (eV) and compositions of orbitals (Pt/CN/azole/aryl, %). The green and red color represent different phases, respectively.

The HOMO–LUMO gap of **1** was larger than those of **2**–**4**. It is suspected that π-extension of the NHC ligand affected the LUMO energy. The LUMO of complex **1** was mainly localised on Pt, which is among the characteristic properties of the Pt-NHC complexes, where electron density on the heavy Pt atom can enhance the efficient spin–orbit coupling promoting efficient phosphorescence (*vide infra).* Through the π-extension, LUMOs were delocalized on the extended part of the NHC ligands of complexes **2**–**4**. The LUMO energy of **4** was stabilised compared to that of **3** due to the π extension of complex **1**. To consider the π-extension effect, the simple molecular orbital theory reported by Uno and co-workers would be useful.[41] As shown in Figure 18, the energy levels of the π orbitals can be stabilized by the π extension at the position with the same π-phase carbons. Therefore, the LUMO of complex **1** was most stabilized by the benzannulation at the 5,6-position of the phenyl ring, while the LUMO+1 of complex **1** had the same π-phase aromatic carbons at the 4,5-position of the phenyl ring, resulting in the stabilization of the level for complex **3** (Figure 18). These calculations clearly showed the regioselectivity to the π-extension effects for the Pt-NHC complexes.

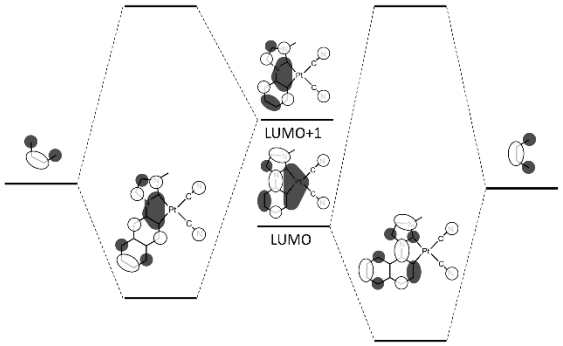

3 **1** **4**

Figure 18. Schematic diagram showing the effects of π-extension forming complexes **3** and **4** from complex **1** (centre).

To obtain insight into the phosphorescence properties, the lowest excited triplet states of **1**–**4** were optimized by using TD-DFT (Table 10-22). Calculated emission wavelengths (443, 454, 546, and 651 nm for **1**–**4**, respectively) obtained from the excitation energies exhibited a tendency corresponding to the emission spectral red-shifts in the order **1** < **2** <**3** < **4**, in good agreement with the experimental results (Figure 19 and Table 3). For complexes **1**–**3**, the values were in good agreement with the experimental values; however, the calculated emission wavelength (651 nm) for complex **4** was different to the experimental value (558 nm). This was due to the fact that lowest triplet excited state optimized structure of **4** having a slightly bent structure (Figure 19 and 20), specifically the C15-C8-C9-N4 angle was 15.5° vs. 6(1)° for the X-ray structure (Figure 20b). Then, optimization the lowest triplet excited state was calculated with angle C15-C8-C9-N4 frozen to 0.0° and. The calculated emission value of this constrained structure (620 nm) showed better agreement with the observed value. In our computational models, steric effects of the surrounding complexes were not taken into account, and this effect was only present for complex **4**. The results indicate that the effective crystal space also play a role to suppress the deformation of the molecule in a free space.

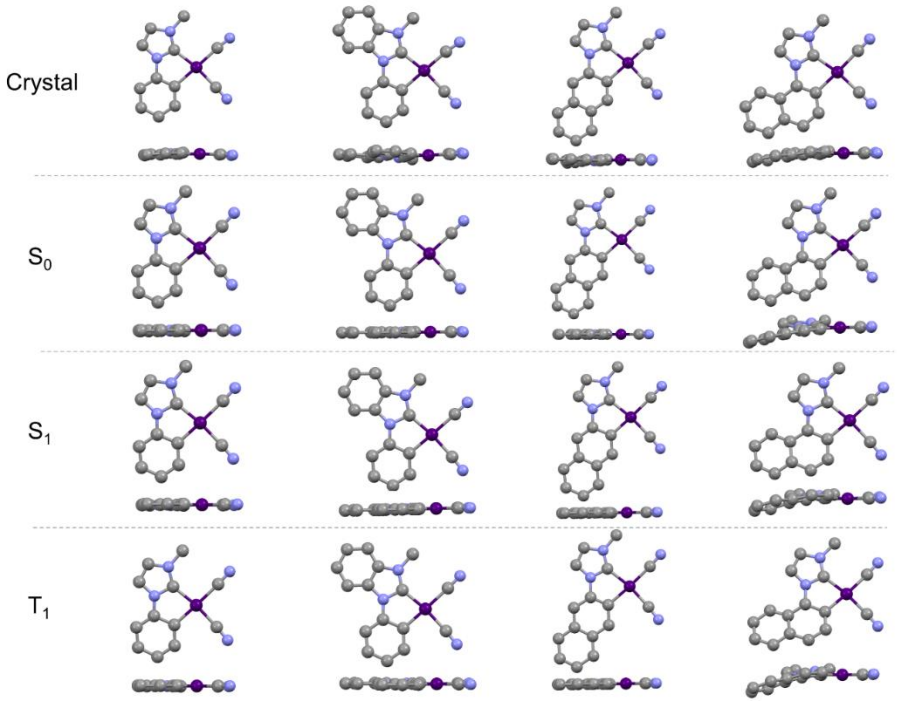

Figure 19. Crystal, ground state (S_0), excited singlet state (S_1), excited triplet state (T_1) optimized structure of complexes **1**–**4** viewed from top and side. The hydrogen atoms were omitted for clarity. The atom color represents Pt (purple), C (gray), and N (blue), respectively

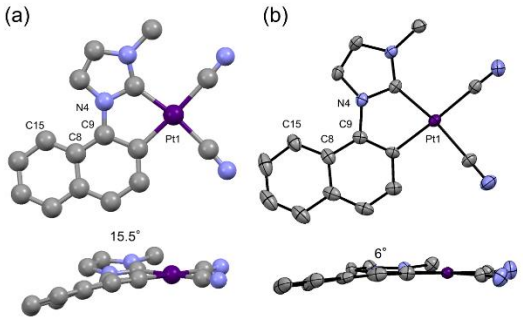

Figure 20. Atom numbers and torsion angles of (a) calculated optimized structure of excited triplet state and (b) crystal structure of **4**.

Table 6. selected excited singlet states of TD-DFT calculations for complex **1**.

Excited states	Energy / eV(nm)	Oscillator strengths	Major contributions (%)
1	3.67 (338.1)	0.01	HOMO-LUMO (97)
2	3.94 (314.7)	0.02	HOMO−1-LUMO (98)
3	4.16 (298.1)	0.00	HOMO−3-LUMO (97)
4	4.25 (292.0)	0.12	HOMO−2-LUMO (93)
5	4.49 (276.1)	0.05	HOMO−6-LUMO (3)
			HOMO−4-LUMO (5)
			HOMO-LUMO+1 (88)

Table 7. selected excited singlet states of TD-DFT calculations for complex **2**.

Excited states	Energy / eV(nm)	Oscillator strengths	Major contributions (%)
1	3.18 (389.4)	0.00	HOMO-LUMO (96)
2	3.50 (354.7)	0.01	HOMO−1-LUMO (96)
3	3.76 (329.4)	0.00	HOMO−3-LUMO (93)
			HOMO−3-LUMO+2 (3)
4	3.87 (320.7)	0.10	HOMO−2-LUMO (77)
			HOMO-LUMO+1 (18)
5	4.03 (307.5)	0.09	HOMO−4-LUMO (31)
			HOMO−2-LUMO (10)
			HOMO-LUMO+1 (51)

Table 8. selected excited singlet states of TD-DFT calculations for complex **3**.

Excited states	Energy / eV(nm)	Oscillator strength	Major contributions (%)
1	3.11 (354.7)	0.01	HOMO−1-LUMO (4)
			HOMO-LUMO (75)
			HOMO-LUMO+1 (15)
2	3.76 (329.9)	0.00	HOMO−2-LUMO (91)
			HOMO−2-LUMO+1 (6)
3	3.80 (326.1)	0.03	HOMO−1-LUMO (51)
			HOMO−1-LUMO+1 (6)
			HOMO-LUMO (11)
			HOMO-LUMO+2 (24)
4	3.98 (311.3)	0.15	HOMO−4-LUMO (10)
			HOMO−1-LUMO (35)
			HOMO−1-LUMO+1 (15)
			HOMO-LUMO+1 (31)
5	4.04 (306.6)	0.00	HOMO−4-LUMO (85)
			HOMO−4-LUMO+1 (12)

Table 9. selected excited singlet states of TD-DFT calculations for complex **4**.

Excited states	Energy / eV(nm)	Oscillator strength	Major contributions (%)
1	3.19 (388.8)	0.01	HOMO->LUMO (94)
2	3.52 (352.4)	0.00	HOMO−1->LUMO (96)
3	3.76 (329.2)	0.01	HOMO−3->LUMO (84)
			HOMO−3->LUMO+1 (2)
			HOMO−2->LUMO (9)
4	3.77 (329.2)	0.08	HOMO−3->LUMO (9)
			HOMO−2->LUMO (81)
			HOMO->LUMO+1 (3)
			HOMO->LUMO+2 (2)
5	3.99 (310.9)	0.02	HOMO−4->LUMO (65)
			HOMO−2->LUMO (3)
			HOMO->LUMO+1 (24)

Table 10. Calculated Excited Triplet Energy Levels and Orbital Transition Analyses of complexes **1**–**4**.

Complexes	energy / eV(nm)	major contributions (%)
1	2.80 (442.6)	HOMO->LUMO (90)
		HOMO->LUMO+4 (4)
2	2.73 (453.6)	HOMO->LUMO (66)
		HOMO->LUMO+4 (16)
		HOMO->LUMO+6 (8)
		HOMO->LUMO+9 (2)
3	2.27 (546.2)	HOMO->LUMO (87)
		HOMO−1->LUMO (3)
		HOMO−2->LUMO (3)
4	1.90 (651.7)	HOMO->LUMO (94)

Table 11. Cartesian coordinates for optimized ground state structure of complex **1** by theoretical calculation.

atoms	X	y	Z
Pt	0.5926190	-0.6723460	-0.0001090
N	3.8026810	-0.7276070	-0.0009260
N	1.1843700	2.4857940	0.0003010
N	-0.8727530	1.8314910	-0.0001360
N	0.3022800	-3.8345950	0.0014520
C	0.4575940	-2.6741920	0.0007420
C	0.4165160	1.3607640	-0.0004140
C	-1.4691180	-0.4650910	0.0000710
C	-2.4756610	-1.4433590	0.0000780
C	-3.8350920	-1.1067080	-0.0001550
C	-4.2380340	0.2299520	-0.0004190
C	-3.2710720	1.2390320	-0.0003810
C	-1.9279870	0.8689120	-0.0001260
C	-0.9060580	3.2129810	0.0004470
C	0.3884220	3.6265440	0.0009120
C	2.6425430	2.5301940	0.0002210
C	2.6306600	-0.7563130	-0.0006490
H	-2.1806960	-2.4884540	0.0002030
H	-4.5859150	-1.8945510	-0.0001910
H	-5.2933360	0.4919800	-0.0006280
H	-3.5734470	2.2840290	-0.0004840
H	-1.8226710	3.7794420	0.0004740
H	0.8118880	4.6186970	0.0016540
H	2.9961130	3.0593170	0.8913030
H	3.0352970	1.5131280	0.0012850
H	2.9961660	3.0575110	-0.8919340

Table 12. Cartesian coordinates for optimized ground state structure of complex **2** by theoretical calculation

atoms	X	y	Z
Pt	1.3856170	-0.4682230	0.0001780
N	-1.3117000	0.6216280	-0.0006350
N	-1.5975010	-1.5514000	-0.0015280
N	1.9974510	-3.6258800	-0.0019090
N	4.4803500	0.2619730	0.0040240
C	0.8839450	1.5335100	0.0005160
C	1.7297040	2.6524310	0.0007310
C	1.2281590	3.9588680	-0.0007890
C	-0.1475060	4.1840990	-0.0030590
C	-1.0279780	3.0984490	-0.0032440
C	-0.5016040	1.8062720	-0.0009340
C	-2.6900590	0.4179630	0.0002930
C	-3.8112950	1.2547040	0.0027400
C	-5.0752470	0.6600000	0.0032910
C	-5.2358860	-0.7325650	0.0016630
C	-4.1244880	-1.5768580	-0.0001710
C	-2.8651920	-0.9825360	-0.0006380
C	-0.6354830	-0.5853410	-0.0012180
C	-1.3842950	-2.9925920	-0.0020560
C	1.8073270	-2.4694460	-0.0011140
C	3.3525800	-0.0509270	0.0025750
H	2.8027950	2.4883010	0.0019120
H	1.9151300	4.8027200	-0.0005290
H	-0.5453230	5.1960040	-0.0048090
H	-2.0936040	3.2863620	-0.0060540
H	-3.7260870	2.3318710	0.0047790
H	-5.9539060	1.2988270	0.0051660
H	-6.2343870	-1.1598340	0.0020670
H	-4.2339770	-2.6562030	-0.0010700
H	-1.8448340	-3.4317140	-0.8935550
H	-0.3154710	-3.2030210	-0.0021860
H	-1.8447590	-3.4323180	0.8891920

Table 13. Cartesian coordinates for optimized ground state structure of complex **3** by theoretical calculation

atoms	X	y	Z
Pt	-1.2292640	-0.7297470	0.0000220
N	-0.5031870	-3.8209160	-0.0006740
N	-4.3980370	-1.2395020	0.0005610
N	-2.2571690	2.3089400	-0.0002920
N	-0.1274270	1.9559080	0.0000690
C	-0.8190960	-2.6938160	-0.0001970
C	-3.2340860	-1.1010340	0.0002700
C	-1.3385380	1.3045170	0.0000040
C	0.7822040	-0.2448920	0.0000020
C	1.8973300	-1.0634210	-0.0000220
C	3.2282250	-0.5554090	0.0000220
C	3.4466750	0.8625690	0.0000660
C	2.3126510	1.7174530	0.0000660
C	1.0546200	1.1622040	0.0000430
C	-0.2921670	3.3294670	-0.0001960
C	-1.6313670	3.5518750	-0.0003580
C	4.3630370	-1.4112320	0.0000170
C	5.6447510	-0.9028170	0.0000600
C	5.8552340	0.4976350	0.0001180
C	4.7771910	1.3576420	0.0001190
C	-3.7074780	2.1475410	0.0000550
H	1.7573890	-2.1411930	-0.0000910
H	2.4675580	2.7943110	0.0000170
H	0.5337680	4.0212150	-0.0001390
H	-2.1924960	4.4731570	-0.0005220
H	4.1960920	-2.4857570	-0.0000080
H	6.4987230	-1.5758440	0.0000430
H	6.8684420	0.8922710	0.0001560
H	4.9341480	2.4349420	0.0001960
H	-4.1311790	2.6205210	0.8919630
H	-4.1315910	2.6207400	-0.8914910
H	-3.9526480	1.0852130	0.0000790

Table 14. Cartesian coordinates for optimized ground state structure of complex **4** by theoretical calculation

atoms	x	y	Z
Pt	-1.4338590	-0.5084930	0.0363220
N	-2.0469050	-3.6227770	-0.1224650
N	-4.5192530	0.2850580	0.4311920
N	-1.1540970	2.6608100	-0.1358110
N	0.6722730	1.4933060	-0.0772280
C	-1.8708800	-2.4674710	-0.0528680
C	-3.4050270	-0.0478960	0.2848290
C	-0.6987260	1.3869310	0.0032510
C	0.5931650	-0.8631870	-0.1298540
C	1.2425450	-2.1229010	-0.2459390
C	2.6136500	-2.2333810	-0.2858660
C	3.4446690	-1.0963190	-0.1190630
C	2.8392670	0.2019980	0.0478790
C	1.4171730	0.2623850	-0.0597930
C	1.0430840	2.8071220	-0.3281390
C	-0.1002540	3.5388060	-0.3497210
C	4.8583000	-1.2165040	-0.0755750
C	5.6699340	-0.1323170	0.1740480
C	5.0792510	1.1268790	0.4246470
C	3.7105170	1.2864420	0.3658170
C	-2.5497130	3.0851420	-0.1105850
H	0.6222490	-3.0107010	-0.3171500
H	3.0865260	-3.2055450	-0.4131230
H	2.0552010	3.1135900	-0.5149970
H	-0.2555010	4.5955110	-0.5004420
H	5.2907250	-2.2032990	-0.2275830
H	6.7502480	-0.2462350	0.2088800
H	5.7063410	1.9766560	0.6836230
H	3.2982620	2.2503900	0.6335900
H	-2.6955360	3.8204740	0.6873760
H	-2.8144310	3.5414970	-1.0699990
H	-3.1889820	2.2209880	0.0684690

Table 15. Cartesian coordinates for optimized excited singlet state structure of complex **1** by theoretical calculation

atom	x	y	z
Pt	-0.5443280	-0.6695240	0.0000420
N	-0.1806230	-3.8339380	-0.0002200
N	-3.7644740	-0.9004450	0.0008650
N	-1.2730810	2.4464870	0.0000580
N	0.8438810	1.8523840	-0.0001430
C	-0.3597690	-2.6894770	-0.0001180
C	-2.6057210	-0.8569160	0.0005730
C	-0.4794160	1.3171210	-0.0000200
C	1.4152440	-0.4254000	-0.0001530
C	2.4467080	-1.3978660	-0.0002250
C	3.7800510	-1.0465200	-0.0003150
C	4.1659750	0.3202190	-0.0003310
C	3.2263750	1.3250760	-0.0002710
C	1.8651550	0.9683190	-0.0001960
C	0.8052510	3.2445010	-0.0001340
C	-0.5081490	3.5843320	-0.0000090
C	-2.7225160	2.4563630	0.0001550
H	2.1557980	-2.4417830	-0.0002060
H	4.5452460	-1.8138210	-0.0003610
H	5.2199800	0.5764750	-0.0003890
H	3.5279710	2.3663490	-0.0002840
H	1.6876260	3.8579310	-0.0002270
H	-0.9620110	4.5621660	0.0000330
H	-3.0933300	2.9670140	0.8923540
H	-3.0934690	2.9667000	-0.8921670
H	-3.0852680	1.4318960	0.0003530

Table 16. Cartesian coordinates for optimized excited triplet state structure of complex **1** by theoretical calculation

atom	x	y	z
Pt	-0.5780860	-0.6606050	0.0000130
N	-0.3166930	-3.8235520	-0.0000390
N	-3.7961960	-0.7321620	0.0001790
N	-1.1723540	2.4853570	0.0001000
N	0.9089220	1.8223340	-0.0000020
C	-0.4619760	-2.6742890	-0.0000280
C	-2.6363620	-0.7540720	0.0001060
C	-0.4210600	1.3415580	0.0000370
C	1.4027560	-0.5022430	-0.0000800
C	2.4133830	-1.4840650	-0.0001210
C	3.7566320	-1.1640530	-0.0001680
C	4.1922170	0.2216040	-0.0001910
C	3.2885740	1.2413840	-0.0001520
C	1.9067240	0.9102710	-0.0000700
C	0.9243530	3.2158040	0.0000380
C	-0.3763300	3.6036030	0.0000920
C	-2.6248670	2.5399010	0.0001250
H	2.1034270	-2.5230340	-0.0001200
H	4.5063880	-1.9456920	-0.0002000
H	5.2538510	0.4423430	-0.0002540
H	3.6135130	2.2760850	-0.0001890
H	1.8309300	3.7923880	0.0000130
H	-0.8006660	4.5941660	0.0001320
H	-2.9738350	3.0640630	0.8922620
H	-2.9738890	3.0638100	-0.8921400
H	-3.0190310	1.5268300	0.0002690

Table 17. Cartesian coordinates for optimized excited singlet state structure of complex **2** by theoretical calculation

atoms	x	y	z
Pt	-1.3753300	-0.4569610	0.0000570
N	-4.4769050	0.2648920	0.0007540
N	-2.0194720	-3.6185650	-0.0013920
N	1.6271740	-1.5426410	0.0001580
N	1.3101730	0.6436890	0.0001730
C	-3.3609050	-0.0466290	0.0005270
C	-1.8134010	-2.4773920	-0.0008480
C	0.6126630	-0.6132770	0.0002840
C	-0.9014620	1.4551580	-0.0001150
C	-1.7756740	2.5746360	-0.0004300
C	-1.3002370	3.8652900	-0.0002640
C	0.0934340	4.1122980	0.0001840
C	1.0048430	3.0782510	0.0003840
C	0.5267310	1.7570460	0.0001130
C	2.6941690	0.4469420	0.0000160
C	2.8646730	-0.9563410	0.0000290
C	4.1322940	-1.5396650	-0.0000460
C	5.2353560	-0.6771340	-0.0002030
C	5.0777860	0.7006190	-0.0002800
C	3.7949120	1.2886040	-0.0001680
C	1.4623800	-2.9797440	0.0003760
H	-2.8417660	2.3830340	-0.0007090
H	-1.9894060	4.7016550	-0.0004200
H	0.4550460	5.1345950	0.0003770
H	2.0597830	3.2974780	0.0007790
H	4.2529950	-2.6149820	-0.0000100
H	6.2338020	-1.0993920	-0.0002730
H	5.9489310	1.3435190	-0.0004220
H	3.7090610	2.3627860	-0.0002520
H	1.9355860	-3.4030310	0.8911470
H	0.4041940	-3.2230500	0.0005230
H	1.9353460	-3.4032830	-0.8904000

Table 18. Cartesian coordinates for optimized excited triplet state structure of complex **2** by theoretical calculation

atoms	x	y	z
Pt	-1.3783900	-0.4573790	-0.0000570
N	-4.4755290	0.2675940	-0.0001050
N	-2.0051190	-3.6193200	-0.0001590
N	1.6195400	-1.5449830	0.0000020
N	1.3085240	0.6482780	0.0001100
C	-3.3596050	-0.0447870	-0.0000900
C	-1.8104640	-2.4755920	-0.0001200
C	0.6148270	-0.6021500	0.0000560
C	-0.9122820	1.4617100	0.0000250
C	-1.7702470	2.5914360	-0.0000160
C	-1.2873910	3.8776700	0.0001400
C	0.1283610	4.1256500	0.0003850
C	1.0285650	3.0947160	0.0004040
C	0.5387070	1.7663470	0.0001640
C	2.6946520	0.4370160	0.0000460
C	2.8573420	-0.9659610	-0.0000030
C	4.1234410	-1.5512940	-0.0000510
C	5.2256440	-0.6998730	-0.0000770
C	5.0738350	0.6855330	-0.0000600
C	3.8017220	1.2722950	0.0000000
C	1.4374330	-2.9821830	-0.0000150
H	-2.8385540	2.4104170	-0.0001520
H	-1.9696690	4.7193940	0.0001150
H	0.4902740	5.1476220	0.0005770
H	2.0850390	3.3104410	0.0006400
H	4.2386810	-2.6275640	-0.0000730
H	6.2222690	-1.1260540	-0.0001180
H	5.9481430	1.3238440	-0.0000960
H	3.7173290	2.3469840	-0.0000110
H	1.9030090	-3.4115180	0.8914340
H	0.3756590	-3.2106970	-0.0000560
H	1.9030760	-3.4114970	-0.8914370

Table 19. Cartesian coordinates for optimized excited singlet state structure of complex **3** by theoretical calculation

atoms	x	y	z
Pt	-1.1731200	-0.7267690	0.0012150
N	-0.3663550	-3.8027840	0.0033200
N	-4.3249850	-1.4199950	-0.0091660
N	-2.3329710	2.2708570	-0.0002640
N	-0.1739600	1.9710400	-0.0002760
C	-0.7042370	-2.6946740	0.0025930
C	-3.1853020	-1.2040600	-0.0053000
C	-1.3870490	1.2779780	0.0003460
C	0.7340220	-0.1974230	0.0000600
C	1.8666500	-1.0283010	-0.0006750
C	3.1827170	-0.5177900	-0.0006210
C	3.3814200	0.9176850	-0.0002520
C	2.2656750	1.7798290	0.0000110
C	0.9862990	1.2452420	-0.0002400
C	-0.3926670	3.3431030	-0.0008830
C	-1.7426010	3.5084450	-0.0008700
C	4.3041620	-1.3779200	-0.0009450
C	5.5928290	-0.8824310	-0.0009480
C	5.7855570	0.5197150	-0.0006030
C	4.7181980	1.3922610	-0.0002730
C	-3.7708490	2.0685220	0.0007910
H	1.7191620	-2.1032450	-0.0009980
H	2.4318350	2.8520350	0.0004030
H	0.4044070	4.0642410	-0.0014710
H	-2.3292140	4.4122650	-0.0012620
H	4.1227380	-2.4478510	-0.0011610
H	6.4445920	-1.5504750	-0.0011620
H	6.7951140	0.9173860	-0.0005800
H	4.8918920	2.4633890	-0.0000180
H	-4.2080510	2.5194530	0.8942190
H	-4.2096930	2.5233170	-0.8898460
H	-3.9804240	1.0025550	-0.0013050

Table 20. Cartesian coordinates for optimized excited triplet state structure of complex **3** by theoretical calculation

atoms	x	y	z
Pt	-1.2247320	-0.7335030	0.0000090
N	-0.4053920	-3.7875710	0.0005010
N	-4.3763590	-1.2982940	-0.0001960
N	-2.2893810	2.2956930	-0.0000210
N	-0.1726850	1.9509980	0.0000360
C	-0.7614540	-2.6846770	0.0003300
C	-3.2263490	-1.1443950	-0.0000930
C	-1.3728070	1.3026100	0.0000650
C	0.7444490	-0.2081740	-0.0000380
C	1.9267110	-1.0569650	-0.0000830
C	3.2390880	-0.5437350	-0.0001030
C	3.4420910	0.8831790	-0.0000830
C	2.2974400	1.7213650	-0.0000400
C	1.0002660	1.1430200	-0.0000310
C	-0.3359670	3.3164850	0.0000330
C	-1.6744610	3.5363840	0.0000330
C	4.3722260	-1.3847470	-0.0001440
C	5.6998580	-0.8445210	-0.0001660
C	5.8865760	0.5053500	-0.0001440
C	4.7469510	1.3878100	-0.0001010
C	-3.7355580	2.1227580	0.0001120
H	1.7816390	-2.1317440	-0.0001090
H	2.4363760	2.7975620	-0.0000030
H	0.4878070	4.0079690	0.0000140
H	-2.2398520	4.4524450	0.0000170
H	4.2230300	-2.4580330	-0.0001570
H	6.5479100	-1.5193690	-0.0001990
H	6.8848420	0.9270380	-0.0001580
H	4.9002920	2.4614930	-0.0000840
H	-4.1566440	2.5884420	0.8925780
H	-4.1570000	2.5906810	-0.8910100
H	-3.9669160	1.0604910	-0.0011130

Table 21. Cartesian coordinates for optimized excited singlet state structure of complex **4** by theoretical calculation

atoms	x	y	z
Pt	-1.4070710	-0.4957120	0.0681410
N	-2.0983670	-3.6089880	0.0635210
N	-4.5096010	0.3725680	0.1447910
N	-1.1429620	2.6234040	-0.1480790
N	0.7066360	1.4599160	-0.0789420
C	-1.8900560	-2.4693610	0.0775230
C	-3.4054840	0.0186840	0.1235270
C	-0.6969000	1.3484550	-0.0165480
C	0.5358110	-0.8837310	-0.1080760
C	1.1743320	-2.1139460	-0.3342380
C	2.5495840	-2.2036590	-0.4204280
C	3.4081650	-1.0840440	-0.1937790
C	2.8350860	0.2028970	0.0777230
C	1.4139390	0.2850260	-0.0402550
C	1.0661050	2.7919630	-0.2624220
C	-0.0934400	3.4969120	-0.3048290
C	4.8078110	-1.2155940	-0.1897770
C	5.6366080	-0.1380710	0.1255740
C	5.0818730	1.0890080	0.4676700
C	3.6923940	1.2574260	0.4498970
C	-2.5486480	3.0017730	-0.1419460
H	0.5627360	-3.0039170	-0.4206760
H	3.0183350	-3.1675470	-0.5937400
H	2.0749980	3.1176530	-0.4225180
H	-0.2519730	4.5539390	-0.4383000
H	5.2375430	-2.1836880	-0.4235500
H	6.7131630	-0.2675180	0.1232660
H	5.7187580	1.9165980	0.7569810
H	3.2814550	2.1945870	0.7966420
H	-2.6080450	4.0859020	-0.2342840
H	-3.0685910	2.5180460	-0.9674890
H	-3.0198720	2.6707630	0.7819710

Table 22. Cartesian coordinates for optimized excited triplet state structure of complex **4** by theoretical calculation

atoms	x	y	z
Pt	-1.4300740	-0.4971680	0.0558050
N	-2.1287300	-3.5962730	0.0503930
N	-4.4786530	0.4544680	0.3725200
N	-1.1098760	2.6177460	-0.1875600
N	0.7094700	1.4482080	-0.1137330
C	-1.9221030	-2.4562030	0.0676670
C	-3.3933350	0.0600310	0.2616800
C	-0.6714940	1.3508650	-0.0453650
C	0.5338740	-0.9297780	-0.1571800
C	1.1739370	-2.1204530	-0.3987350
C	2.5845110	-2.2001660	-0.4837630
C	3.4390490	-1.0889990	-0.2005930
C	2.8447590	0.1894130	0.0945550
C	1.4289690	0.2567260	-0.0646360
C	1.0900140	2.7663980	-0.3330690
C	-0.0533520	3.4896000	-0.3724790
C	4.8286540	-1.2080840	-0.1624320
C	5.6539710	-0.1139800	0.2110520
C	5.0874190	1.0812090	0.5682520
C	3.6737590	1.2348210	0.5236380
C	-2.5159120	3.0073190	-0.1830660
H	0.5828710	-3.0234010	-0.4988500
H	3.0572610	-3.1576810	-0.6775210
H	2.1071050	3.0664500	-0.4966390
H	-0.2058360	4.5444840	-0.5243010
H	5.2785960	-2.1621470	-0.4132130
H	6.7309310	-0.2379230	0.2268200
H	5.7038790	1.9139060	0.8855060
H	3.2424990	2.1567180	0.8879530
H	-2.5674590	4.0850300	-0.3353880
H	-3.0480280	2.4821470	-0.9737140
H	-2.9778170	2.7301450	0.7620750

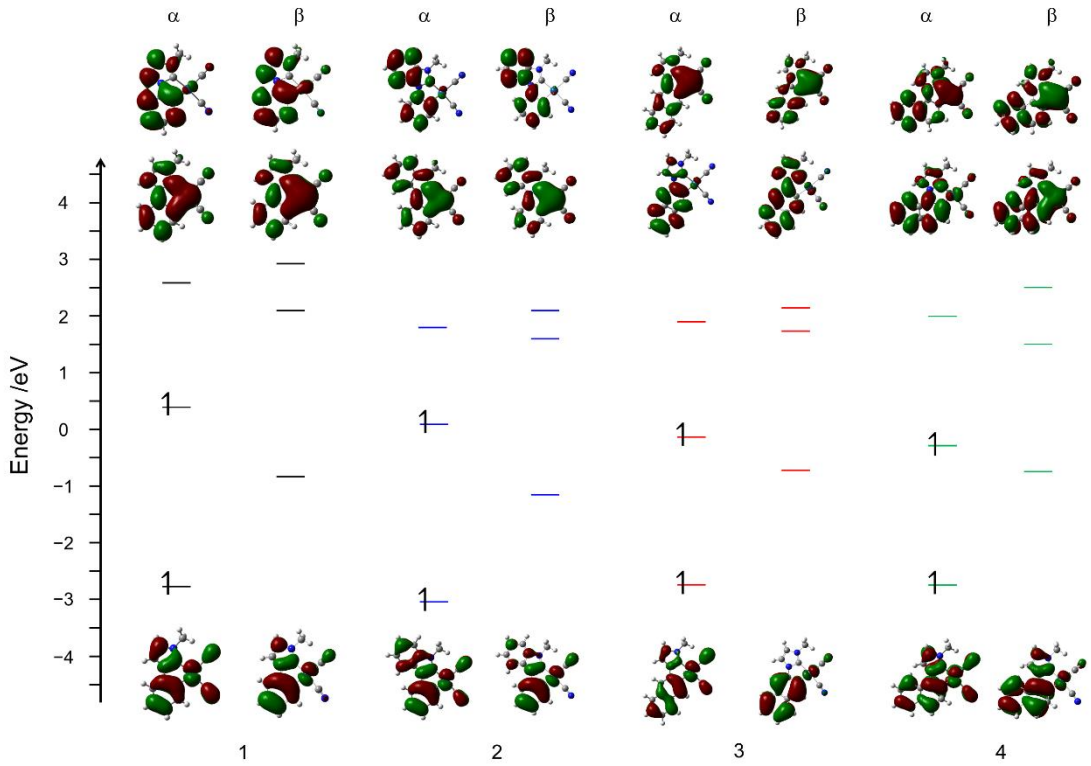

Figure 21. Kohn–Sham orbitals in the frontier region of the T_1 structures. Singly occupied molecular orbitals (SOMOs) are marked in red boxes (UB3LYP single-point energies starting from the TD-DFT optimized triplet states structures).

In order to rationalise the nature of the emission, the spin density distributions of the T_1 structures were checked using UB3LYP single-point energy calculations. Calculated spin density plots are shown in Figure 22, and the Kohn-Sham orbitals in the frontier region are shown in Figure 21. For complexes **3** and **4**, spin density was mainly delocalised in the NHC ligand, implying the ^{3}LC state mixed to some extent with the ^{3}MLCT state. In contrast, the spin density for **1** and **2** was delocalised over the metal and the NHC ligand, suggesting the larger contribution of the ^{3}MLCT character. Similar conclusions can be made by looking at the SOMOs of complexes **1**–**4** (Figure 21). Clearly, the contribution of metal orbitals was much larger in complexes **1** and **2** than in complexes **3** and **4**.

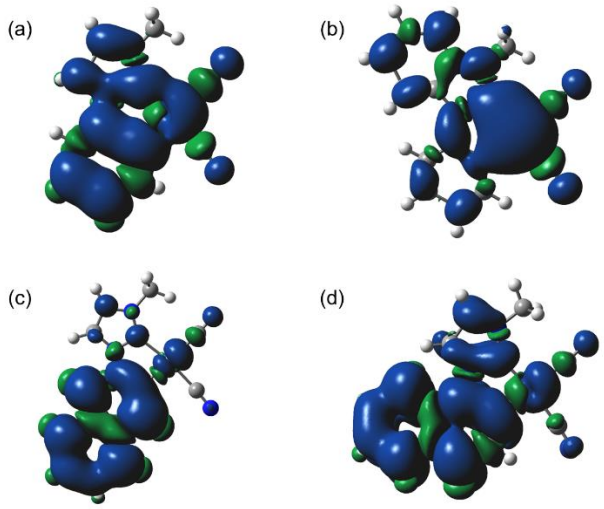

Figure 22. Spin density plots for triplet states of **1** (a), **2** (b), **3** (c) and **4** (d)

3-3-5 Effects of spin-orbit coupling

Spin-orbit interactions play a key role in the phosphorescence of metal complexes. To obtain insight into the detailed phosphorescence properties of metal complexes, it is essential to consider the zero-field splitting parameters of the triplet states controlled by the spin–orbit coupling (SOC). Strong SOC affords the phosphorescence pathways and the lowest excited triplet states perturbed by several excited states, including metal characters, such as MLCT or LMCT, that exhibit a large ZFS energy (ΔE(ZFS)), which corresponds to the $\Delta E_{\text{I-III}}$ value in Eq. (2).[42] As has been well investigated, the ^{3}MLCT states of $[Ru(bpy)_3]^{2+}$,[43] and $[Ir(ppy)_3]$[44] and their analogues have large ΔE(ZFS) values of 60–170 cm^{-1},[45] while the ligand centred (^{3}LC) states of $[Rh(bpy)_3]^{3+}$ have a very small ΔE(ZFS) (< 0.1 cm^{-1}) and long lifetimes in the order of milliseconds. Yersin and coworkers reported that ΔE(ZFS) values for square-planar mononuclear Pt(II) complexes are in the middle region between the two as mixed states of ^{3}LC and ^{3}MLCT.[4a] They also proposed a relationship between radiative rate constants at room temperature and ΔE(ZFS) based on SOC, expressing the energy levels of the ^{3}MLCT sub-levels.

Blue emissive complexes **1** and **2** had ΔE(ZFS) of 35 and 28 cm^{-1}, respectively, which suggested that the lowest triplet states were mixed with higher lying singlet states via spin-orbit coupling of the heavy atom effect of the Pt atom. Compared to these complexes, a blue emissive Pt(II) complex bearing substituted phenylpyridinate, *n*-$Bu_4N[Pt(CN)_2$(4,6-dFppy)] (4,6-HdFppy = 2,4-difluorophenylpyridine), exhibited quite different phosphorescence properties despite showing a similar emission spectrum with a maximum of 459 nm and high quantum yield (Φ = 0.6) in the solid state.[25] For the complex, the calculated radiative rate constant based on the Eq. (2) was small (3.2×10^4 s^{-1}) and the ΔE(ZFS) was less than 2 cm^{-1}, indicating the clear character of ^{3}LC ($^3\pi\pi^*$) emission

with only a small MLCT admixture. Therefore, the blue emissive Pt-NHC complexes **1** and **2** were characteristic of their efficient spin–orbit coupling, which could be attributed to the $6p_z$ orbital of the LUMO of the complexes, as mentioned as the part of the theoretical calculations. The reported highly emissive Pt(II)-NHC complexes also show contributions from the electron density of the Pt-$6p_z$ orbital of LUMO or LUMO+1.[46] As the electron density localized on Pt-$6p_z$ contributes to the efficient spin–orbit coupling, the Pt-NHC complexes had larger k_r values than those of Ir(III)-NHC complexes that are not able to acquire the mixing effect of the $6p_z$ orbital due to the octahedral coordination geometry.

3-4 Conclusion

In this chapter, the novel anionic Pt(II)-NHC complexes were synthesized and characterized. The n-Bu4N+ cations realised an isolated environment of the anionic square-planar complexes and the rigid structures without any intermolecular interactions that brought about highly efficient emission (Φ = 0.24–0.72) of the mononuclear complexes with different luminescence colors in the solid state at room temperature. The regioselective π-extension of the ligands effectively to controlled the emission colors, as explained by the molecular orbital theory concerning orbital overlap due to regioselective π-extension. Based on the temperature dependence of the luminescence lifetimes between 298 and 77 K, the deactivation effect via thermal population to the metal-centred state was recognised for blue-emissive Pt-NHC complexes, regardless of their strong ligand fields. Lifetime measurements at low temperatures (4–77 K) showed different emission state properties for complexes 1–4. Compared to the blue emitting Pt-ppy derivatives, larger spin–orbit coupling was observed for Pt-NHC complexes 1 and 2, which was ascribed to the effect of mixing Pt-based molecular orbitals, as suggested by DFT and TD-DFT calculations. This efficient spin–orbit coupling realised efficient blue phosphorescence with distinct MLCT characters in complexes 1 and 2. In contrast, the complexes 3 and 4 exhibited purer ligand centred (^{3}LC) phosphorescence, which was in agreement with the very small ZFS energy of less than 2 cm^{-1}.

Compared to neutral complexes, ionic complexes have diverse factors for functionalization that are advantageous for tuning emission properties, controlling solubility in organic and aqueous solvents, and an application in light-emitting electrochemical cells (LECs)[47] by combining various counter ions. In particular, the bulky tetrabutylammonium cation provided a good environment as a counter cation for anionic Pt(II) complexes, supporting strong phosphorescence, despite these complexes being weakly emissive in fluid solutions.[25] Therefore, this strategy would be applicable to achieving further progress in functional phosphorescence materials.

References

1 (*a*) Q. Zhao, C. Huang and F. Li, *Chem. Soc. Rev*., 2011, **40**, 2508–2524; (*b*) K. K.-W. Lo and S. P.-Y. Li, *RSC Adv.*, 2014, **4**, 10560–10585.

2 (*a*) Y.-J. Yuan, Z.-T. Yu, D.-Q. Chen and Z.-G. Zou, *Chem. Soc. Rev*., 2017, 46, 603–631; (*b*) P. D. Frischmann, K. Mahata and F. Würthner, *Chem. Soc. Rev*., 2013, **42**, 1847–1870.

3 (*a*) O. S. Wenger, *Chem. Rev*., 2013, **113**, 3686−3733; (*b*) Anna J. McConnell, Christopher S. Wood, Prakash P. Neelakandan, and Jonathan R. Nitschke, *Chem. Rev*. 2015, **115**, 7729−7793.

4 (*a*) H. Yersin, A. F. Rausch, R. Czerwieniec, T. Hofbeck, T. Fischer, *Coord. Chem. Rev*., 2011, **255**, 2622–2652; (*b*) Y. Chi and P.-T. Chou, *Chem. Soc. Rev.*, 2010, **39**, 638–655.

5 G. Baryshnikov, B. Minaev and H. Ågren, *Chem. Rev*., 2017, **117**, 6500−6537.

6 J. Kalinowski, V. Fattori, M. Cocchi, J. A. G. Williams, *Coord. Chem. Rev*., 2011, **255**, 2401–2425.

7 (*a*) M. Kato, *Bull. Chem. Soc. Jpn*., 2007, **80**, 287–294; (*b*) A. Kobayashi and M. Kato, *Eur. J. Inorg. Chem*., 2014, 4469–4483.

8 J. Brooks, Y. Babayan, S. Lamansky, P. I. Djurovich, I. Tsyba, R. Bau and M. E. Thompson, *Inorg. Chem*. 2002, **41**, 3055–3066.

9 R. Visbal and M. Concepción Gimeno, *Chem. Soc. Rev*., 2014, **43**, 3551–3574.

10 Y. Unger, D. Meyer, O. Molt, C. Schildknecht, I. Münster, G. Wagenblast and T. Strassner, *Angew. Chem. Int. Ed*. 2010, **49**, 10214–10216.

11 T. Strassner, *Acc. Chem. Res*., 2016, **49**, 3551 2680–2689.

12 S. Fuertes, H. García, M. Perálvarez, W. Hertog, J. Carreras and V. Sicilia, *Chem. Eur. J*., 2015, **21**, 1620-1631.

13 (*a*) G. D. Hager, R. J. Watts and G. A. Crosby, *J. Am. Chem. Soc.*, 1975, **97**, 7031-7037; (*b*) W. H. Elfring, G. A. Crosby, *J. Am. Chem. Soc.*, 1981, **103**, 2683–2687; (*c*) M. Kato, S. Yamauchi, and N. Hirota, *J. Phys. Chem.*, 1989, **93**, 3422–3425; (*d*) M. Kato, S. Yamauchi, and N. Hirota, *Chem. Phys. Lett*., 1989, **157**, 543-546.

14 (*a*) Y.-S. Yeh, Y.-M. Cheng, P.-T. Chou, G.-H. Lee, C.-H. Yang, Y. Chi, C.-F. Shu and C.-H. Wang, *ChemPhysChem*, 2006, **7**, 2294–2297; (*b*) C.-H. Yang, S.-W. Li and Y. Chi, *Inorg. Chem*., 2005, **44**, 7770–7780.

15 M. Montalti, A. Credi, L. Prodi, M. T. Gandolfi, Handbook of photochemistry, 3rd ed., CRC press; US, 2006.

16 J. Van Houten and R. J. Watts, *J. Am. Chem. Soc.*, 1976, **98**, 4853–4858.

17 T. Sajoto, P. I. Djurovich, A. B. Tamayo, Jonas Oxgaard, William A. Goddard, and Mark E. Thompson, *J. Am. Chem. Soc.*, 2009, **131**, 9813-9822

18 (*a*) K. Goushi, Y. Kawamura, H. Sasabe and C. Adachi, *Jap. J. App. Phys.*, 2004, **43**, L937–L939; (*b*) T. Hofbeck and H. Yersin, *Inorg. Chem*., 2010, **49**, 9290–9299.

19 T. Sajoto, P. I. Djurovich, A. Tamayo, M. Yousufuddin, R. Bau, and M. E. Thompson, *Inorg. Chem*., 2005, **44**, 7992-8003.

20 B. Ma, P. I. Djurovich, M. E. Thompson, *Coord. Chem. Rev.*, 2005, **249**, 1501–1510.

21 (*a*) A. Aliprandi, D. Genovese, M. Mauro and L. De Cola, *Chem. Lett.*, 2015, **44**, 1152–1169; (*b*) K. M.-C. Wong and V. W.-W. Yam, *Acc. Chem. Res.*, 2011, **44**, 424–434.

22 J. Forniés, S. Fuertes, J. A. López, A. Martín and V. Sicilia, *Inorg. Chem*., 2008, **47**, 7166-7176.

23 T. Ogawa, M. Yoshida, H. Ohara, A. Kobayashi and M. Kato, *Chem. Commun.*, 2015, **51**, 13377-13380.

24 J. R. Berenguer, E. Lalinde and J. Torroba, *Inorg. Chem*., 2007, **46**, 9919-9930.

25 A. F. Rausch, U. V. Monkowius, M. Zabel and H. Yersin, *Inorg. Chem*., 2010, **49**, 7818-7825.

26 (*a*) W. R. Dawson and M. W. Windsor, *J. Phys. Chem.*, 1968, **72**, 3251–3260; (*b*) W. H. Melhuish, *J. Phys. Chem.*, 1961, **65**, 229–235.

27 CrystalClear: Data Collection and Processing Software, Rigaku Corporation (1998-2014). Tokyo 196-8666, Japan.

28 SHELXS2013: G. M. Sheldrick, *Acta Crystallogr.*, 2008, **A64**, 112–122.

29 SIR2011: M. C. Burla, R. Caliandro, M. Camalli, B. Carrozzini, G. L. Cascarano, C. Giacovazzo, M. Mallamo, A. Mazzone, G. Polidori, and R. Spagna, *J. Appl. Cryst.* 2012, **45**, 357–361.

30 *CrystalStructure 4.0*, Rigaku Corporation, Tokyo196-8666, Japan, 2000–2010.

31 M. J. Frisch, G. W. Trucks, H. B. Schlegel, G. E. Scuseria, M. A. Robb, J. R. Cheeseman, G. Scalmani, V. Barone, B. Mennucci, G. A. Petersson, H. Nakatsuji, M. Caricato, X. Li, H. P. Hratchian, A. F. Izmaylov, J. Bloino, G. Zheng, J. L. Sonnenberg, M. Hada, M. Ehara, K. Toyota, R. Fukuda, J. Hasegawa, M. Ishida, T. Nakajima, Y. Honda, O. Kitao, H. Nakai, T. Vreven, J. A. Montgomery, Jr., J. E. Peralta, F. Ogliaro, M. Bearpark, J. J. Heyd, E. Brothers, K. N. Kudin, V. N. Staroverov, R. Kobayashi, J. Normand, K. Raghavachari, A. Rendell, J. C. Burant, S. S. Iyengar, J. Tomasi, M. Cossi, N. Rega, J. M. Millam, M. Klene, J. E. Knox, J. B. Cross, V. Bakken, C. Adamo, J. Jaramillo, R. Gomperts, R. E. Stratmann, O. Yazyev, A. J. Austin, R. Cammi, C. Pomelli, J. W. Ochterski, R. L. Martin, K. Morokuma, V. G. Zakrzewski, G. A. Voth, P. Salvador, J. J. Dannenberg, S. Dapprich, A. D. Daniels, Ö. Farkas, J. B. Foresman, J. V. Ortiz, J. Cioslowski, and D. J. Fox, GAUSSIAN 09 (Revision E.01), Gaussian, Inc., Wallingford, CT, 2009.

32 (*a*) C. Lee, W. Yang, and R. G. Parr, *Phys. Rev. B: Condens. Matter Mater. Phys.*, 1988, **37**, 785–789. (*b*) A. D. Becke, *J. Chem. Phys.*, 1993, **98**, 5648−5652.

33 Y. Zhao, N. E. Schultz, and D. G. Truhlar, *J. Chem. Theory Comput.*, 2006, **2**, 364–382.

34 (*a*) P. Fuentealba, H. Preuss, H. Stoll, and L. Vonszentpaly, *Chem. Phys. Lett.*, 1982, **89**, 418–422; (*b*) T. H. Dunning Jr., P. J. Hay, *Modern Theoretical Chemistry*; Plenum: New York, *1977*, **3**, 1–28.

35 (*a*) R. Ditchfield, W. J. Hehre, and J. A. Pople, *J. Chem. Phys.*, 1971, **54**, 724–728; (*b*) W. J. Hehre, R. Ditchfield, and J. A. Pople, *J. Chem. Phys.*, 1972, **56**, 2257–2261; (*c*) P. C. Hariharan and J. A. Pople, *Theor. Chem. Acc*., 1973, **28**, 213–222; (*d*) P. C. Hariharan and J. A. Pople, Mol. Phys., 1974, **27**, 209-214; (e) R. C. Binning Jr. and L. A. Curtiss, *J. Comp. Chem.*, 1990, **11**, 1206–1216.

36 A. Bondi, *J. Phys. Chem*., 1964, **68**, 441-451.

37 (*a*) A. Tronnier, A. Pöthig, S. Metz, G. Wagenblast, I. Münster and T. Strassner, *Inorg. Chem*., 2014, **53**, 6346-6356; (*b*) A. Tronnier, G. Wagenblast, I. Mìnster and T. Strassner, *Chem. Eur. J*., 2015, **21**, 12881–12884; (*c*) A. Tronnier, N. Nischan, S. Metz, G. Wagenblast, I. Münster and T. Strassner, *Eur. J. Inorg. Chem.* 2014, 256–264; (*d*) A. Tronnier, S. Metz, G. Wagenblast, I. Münster and T. Strassner, *Dalton Trans.*, 2014, **43**, 3297–3305.

38 (*a*) G. H. Aallen, B. P. Sullivan, and T. J. Meyer, *J. Chem. Soc. Chem. Comm*., 1981, 793–795; (*b*) E. M. Kober, J. L. Marshall, W. J. Dressick, B. P. Sullivan, J. V. Caspar and T. J. Meyer, *Inorg. Chem.* 1985, **24**, 2755–2763.

39 (*a*) A Bossi, A. F. Rausch, M. J. Leitl, R. Czerwieniec, M. T. Whited, P. I. Djurovich, H. Yersin, and M. E. Thompson, *Inorg. Chem.*, 2013, **52**, 12403-12415; (*b*) A. F. Rausch, L. Murphy, J. A. G. Williams and H. Yersin, *Inorg. Chem*., 2012, **51**, 312-319; (*c*) A. F. Rausch, M. E. Thompson and H. Yersin., *Chem. Phys. Lett.*, 2009, **468**, 46-51; (*d*) A. M. Prokhorov, T. Hofbeck, R. Czerwieniec and A. F. Suleymanova, *J. Am. Chem. Soc.*, 2014, **136**, 9637−9642.

40 (*a*) C. B. Blanton, Z. Murtaza, R. J. Shaver, and D. P. Rillema, *Inorg. Chem*., 1992, **31**, 3230-3235; (*b*) F. Barigelletti, J. D. Sandrini, M. Maestri, V. Balzani, A. von Zelewsky, L. Chassot, P. Jolliet and U. Maeder, *Inorg. Chem*., 1988, **27**, 3644−3647.

41 (*a*) B. Uno, K. Kano, T. Konse, T. Kubota, S. Matsuzaki, A. Kuboyama, *Chem. Pharm. Bull*., 1985, **33**, 5155–5166; (*b*) K. Hanson, P. I. Djurovich, F. Zahariev, M. S. Gordon, and M. E. Thompson, *J. Am. Chem. Soc.*, 2010, **132**, 16247−16255; (*c*) S. Koseki, Y. Kagita, S. Matsumoto, T. Asada, S. Yagi, H. Nakazumi and T. Matsushita, *J. Phys. Chem. C*, 2014, **118**, 15412−15421.

42 (*a*) R.W. Harrigan and G.A. Crosby, *J. Chem. Phys.*, 1973, **59**, 3468−3476; (*b*) J. Strasser, H. H. H. Homeier and H. Yersin, *Chem. Phys.*, 2000, **255**, 301–316; (*c*) D. R. Striplin and G. A. Crosby, *Chem. Phys. Lett*., 1994, **221**, 426−430.

43 D. W. Thompson, A. Ito and T. J. Meyer, *Pure Appl. Chem.*, 2013, **85**, 1257–1305.

44 (a) W. J. Finkenzeller, H. Yersin, *Chem. Phys. Lett.*, 2003, **377**, 299–305; (b) T. Hofbeck and H. Yersin, I*norg. Chem.* 2010, **49**, 9290–9299.

45 (*a*) S.P. McGlynn, T. Azumi and M. Kinoshita, Molecular Spectroscopy of the Triplet State, Prentice-Hall, Eaglewood Cliff, 1969; (*b*) S. Ikeda, S. Yamamoto, K. Nozaki, T. Ikeyama, T. Azumi, J. A. Burt, G. A. Crosby, *J. Phys. Chem.*, 1991, **95**, 8538-8541.

46 J.-L. Liao, Y. Chi, J.-Y. Wang, Z.-N. Chen, Z.-H. Tsai, W.-Y. Hung, M.-R. Tseng and G.-H. Lee, *Inorg. Chem*., 2016, **55**, 6394–6404.

47 R. Costa, E. Ortí, H. J. Bolink, F. Monti, G. Accorsi and N. Armaroli, *Angew. Chem., Int. Ed*., 2012, **51**, 8178–618211.

Chapter 4.
Luminescent ionic liquids based on cyclometalated platinum(II) complexes exhibiting thermochromic behavior in different color regions

4-1 Introduction

Ionic liquid materials have attracted much attention because of their physicochemical properties such as wide liquid range, large electrochemical window, and electric conductivity, for use as alternative solvents.[1] electrochemical applications,[2] energy generation, and energy storage.[3] On the other hand, luminescence properties of ionic liquids have been less likely to be developed, although they have appropriate properties such as optically transparent, non-volatile, and deformability. To add luminescence properties to ionic liquids, one promising approach is utilization of ionic metal complexes as cation or anion of ionic liquids. It allows us design diverse luminescent ionic liquids based on luminescence properties of metal complexes.[4] In chapter 2, the introduction of a stimuli-responsive Pt(II) complex into an ionic liquid material was demonstrated.[5] Square planar Pt(II) complexes exhibit chromic absorption and emission behavior depending on the existence and extent of π-π and/or Pt-Pt interactions in ground state[6] and excimer formation.[7] The resulting room temperature ionic liquid $[C_2mim][Pt(CN)_2(ptpy)]$ (C_2mim = 1-methyl-3-ethylimidazolium ion, Hptpy = 2-p-tolylpyridine (**4**)) emitted both monomer and dimer emission after photo-excitation, and the ratio of monomer and dimer emission depends on the temperature.

To study universality of photophysical properties of Pt(II) ionic liquid, several analogue compounds should be studied. In this chapter, two ionic liquid complexes $[C_4mim][Pt(CN)_2(L)]$ (C_4mim = 1-methyl-3-butyl-imidazolium ion, H_2L_1 = 1-methyl-3-phenylimidazolium (**1**), HL_2 = benzo[*h*]quinoline (**2**) (Scheme 1)) were reported. These two liquid Pt(II) complexes have similar thermal properties and thermochromic luminescence properties.

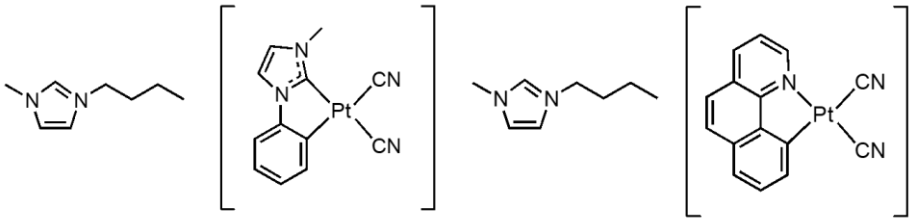

$[C_4mim][Pt(CN)_2(mpi)]$ (**1**) $[C_4mim][Pt(CN)_2(bzq)]$ (**2**)

Scheme 1. Structural formula of Pt(II) complexes **1** and **2**.

4-2 Experimental

4-2-1 Physical measurements

^{1}H NMR spectroscopy was performed using a JEOL EX-270 NMR spectrophotometer. Elemental analyses were carried out at the analysis center in Hokkaido University. Thermogravimetry-differential thermal analysis (TG-DTA) measurements were recorded using a Rigaku Thermoplus EVO TG-DTA 8120 with Al sample pans under a N_2 flow. Differential scanning calorimetry (DSC) measurements were performed using a METTLER DSC 1 under a N_2 flow.

4-2-2 Luminescence measurements

All luminescence measurements of neat **1** and **2** were performed under N_2 atmosphere. Luminescence spectra were measured using a JASCO FR-6600 spectrofluorometer at room temperature and 77 K. Slit widths of the excitation and emission light were 5 or 6 nm. Variable temperature luminescence spectra were measured by a photonic multichannel analyzer Hamamatsu PMA12. Luminescence quantum yields were recorded on a Hamamatsu Photonics C9920-02 absolute photoluminescence quantum yield measurement system equipped with an integrating sphere apparatus and 150 W CW Xenon light source. Hamamatsu Photonics A10095-03 non-luminescent quartz sample holder was used for absolute photoluminescence quantum yield measurements. The accuracy of the instrument was confirmed by the measurement of quantum yield of anthracene in ethanol solution (Φ = 0.27).[8] Emission life time measurements were recorded using a Hamamatsu Photonics, C4334 system equipped with a streak camera as a Photo detector and a nitrogen laser for the 337 nm excitation. Liquid N_2 cryostat (Optistat-DN optical Dewar and ITC-503 temperature controller, Oxford Instruments) was used for the temperature control.

4-2-3 Single crystal X-ray diffraction measurements

All single crystal X-ray diffraction measurements were performed using a Rigaku AFC-7R diffractometer with a Mercury CCD area detector and graphite monochromatized Mo Kα radiation (λ = 0.71069 Å) at 200 K. Each single-crystal was mounted on a MicroMount using liquid paraffin. These crystals were cooled using a N_2-flow type temperature controller. Diffraction data were collected and processed using the Crystal-Clear software.[9] The structures were solved by direct methods (SHELXS-2013).[10] Structural refinements were conducted by the full-matrix least-squares method using SHELXL-2014.[11] Non-hydrogen atoms were refined anisotropically, and all hydrogen atoms were refined using the rigid model. All calculations were performed using the CrystalStructure crystallographic software package[12] except for refinement. The crystallographic data of a potassium salt of $[Pt(CN)_2(mpi)]^-$, **3** are summarized in Table 1.

Table 1. Crystal Data for complexes K[Pt(CN)$_2$(mpi)] (**3**)

	K[Pt(CN)$_2$(mpi)] (**3**)
Formula	$C_{12}H_9KN_4Pt$
Formula Weight	443.42
Crystal system	Triclinic
Space group	*P*-1
a (Å)	8.400(1)
b (Å)	16.506(3)
c (Å)	20.116(4)
α (°)	109.731(2)
β (°)	94.688(2)
γ (°)	90.344(*)
V (Å^3)	2615.0(8)
T (K)	200
Z	8
D_{calc} (g cm^{-3})	2.252
F(000)	1648.00
measured refl.	21080
unique refl.	11795
GOF on F^2	0.965
R_{int}	0.0346
R_1[a]	0.0468
wR_2[b] (all data)	0.1391

[a] $R_1 = \Sigma||F_o| - |F_c||/\Sigma|F_o|$. [b] $wR_2 = [\Sigma w(F_o^2 - F_c^2)/\Sigma w(F_o)^2]^{1/2}$, $w = [\sigma_c^2(F_o^2) + (xP)^2 + yP]^{-1}$, $P = (F_o^2 - 2F_c^2)/3$.

4-2-4. Materials

Potassium tetrachloridoplatinate(II) ($K_2[PtCl_4]$) was purchased from Tanaka Holdings Co., Inc. All other reagents were purchased from Wako Pure Chemical Industries. All solvents were purchased from Kanto Chemical Co., Inc. All of solvents for the measurements were distilled by standard methods and stored under a N_2 atmosphere.

1-methyl-3-butylimidazolium Bromide ([C_4mim][Br]) was synthesized by the literature method.[13] K[Pt(CN)$_2$(bzq)][14] and [Pt$_2$(μ-Cl)$_2$(mpi)$_2$][15] was synthesized according to the reported method. All of the solvents for syntheses were used without further purification.

Computational methods

Gaussian16 program was used to perform DFT and TD-DFT calculations.[16] The ground state structures (S_0) were fully optimized with the M06L[17] functional. Vibrational frequency calculations confirmed that optimized S_0 states were minima (i.e. no imaginary frequencies). In the case of the dimer systems of **1** and **2**, N atoms of the –CN groups were frozen at their positions in the crystallographic structures to avoid structure deformation upon structure optimization. Starting from the S_0, the lowest optimized triplet state (T_1) were calculated using the M06-2X[18] functional. Vibrational frequency calculations were performed using the TDDFT method on the optimized T1 state structures to confirm that they are minima. For DFT or TDDFT calculations, the SDD basis set and associated effective core potentials were applied for Pt,[19] and the 6-31+G(d) basis sets were employed for remaining atoms.[20]

4-2-5. Synthesis

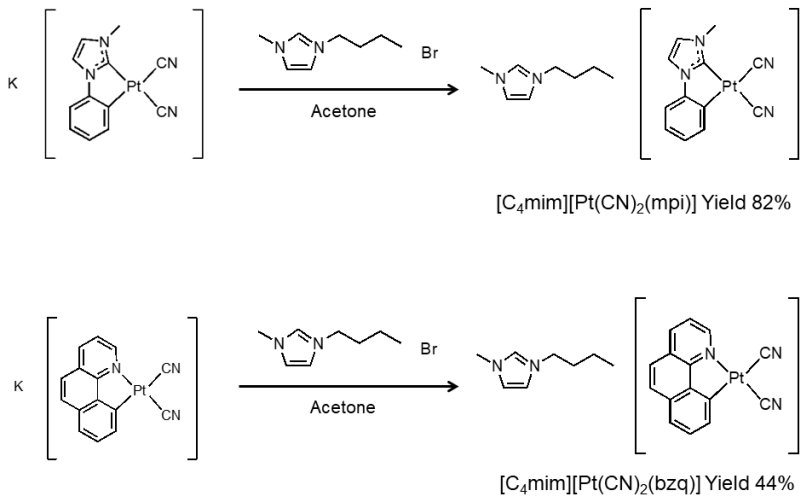

Scheme 2. Synthetic scheme of ionic liquid Pt(II) complexes.

K[Pt(CN)$_2$(mpi)] (3)

To the suspension of [Pt$_2$ (μ-Cl)$_2$(mpi)$_2$] (340 mg, 0.44 mmol) in acetonitrile (30 mL), $AgClO_4$ (181 mg, 0.88 mmol) was added. After stirred for 8 h in dark condition, the mixture was filtered through celite. The resulting yellow solution was evaporated to dryness. Then, yellow solid was suspended in methanol (50 mL), and KCN (114 mg, 176 mmol) was added. After stirring for 2 h at room temperature, the reaction mixture was filtered through celite and evaporated to dryness. After recrystallization from MeOH/Et_2O, pale yellow powder was obtained. By the crystallization from slow evaporation of MeOH solution, yellow crystals suitable for the single X-ray crystallography were yielded.

Yield, 224 mg (0.51 mmol, 57%). ^{1}H NMR (Acetonitrile-d_3, 270 MHz): δ = 8.04 (td, J = 25, 6.8 Hz, 1H), 7.43 (d, J = 2.3 Hz, 1H), 7.12 (t, J = 7.5 Hz, 1H), 7.05-6.90 (m, 3H), 4.07 (s, 3H).

[C_4mim][Pt(CN)$_2$(mpi)] (1)

K[Pt(CN)$_2$(mpi)] (89 mg, 0.20 mmol) and [C_4mim][Br] (43 mg, 0.20 mmol) were dissolved in acetone (50 mL) and stirred for 1h at room temperature. The white suspension was filtrated, and then the colorless solution was evaporated and dried under reduced pressure at 60°C for 12h. The colorless liquid was yielded. Yield, 89 mg (0.16 mmol, 80%). ^{1}H NMR (Acetone-d_6, 270 MHz): δ = 9.29 (s, 1H), 8.24 (td, J = 27, 6.8 Hz, 1H), 7.79 (d, J = 12.5 Hz, 2H), 7.64 (s, 1H), 7.21-7.12 (m, 2H), 6.99-6.83 (m, 2H), 4.40 (t, J = 7.3 Hz, 2H), 4.12 (s, 3H), 4.10 (s, 3H), 1.93 (q, J = 6.8 Hz, 2H), 1.39 (sextet, J = 7.3 Hz, 2H), 0.93 (t, J = 7.3 Hz, 3H). Anal: Calc. for $C_{20}H_{27}N_6Pt\cdot1.5H_2O$: C, 42.10; H, 4.77; N, 14.73%. Found: C, 42.36; H, 4.71; N, 14.91%.

[C_4mim][Pt(CN)$_2$(bzq)] (2)

K[Pt(CN)$_2$(bzq)] (93 mg, 0.20 mmol) and [C_4mim][Br] (43 mg, 0.20 mmol) were dissolved in acetone (50 mL) and stirred for 1h at room temperature. The yellow suspension was filtrated, and then the solution was evaluated to dryness. The yellow substance was dissolved in dichloromethane and solution was washed with water until no bromine ions were detected in $AgNO_3$ test. The organic layer was evaporated and dried under reduced pressure at 60°C for 12h. The yellow viscous liquid was yielded. Yield, 50 mg (0.088 mmol, 44%). ^{1}H NMR (Acetone-d_6, 270 MHz): δ = 9.67 (td, J = 16.0 Hz, 4.8 Hz 1H), 9.18 (s, 1H), 8.59 (d, J = 6.8 Hz, 1H), 8.34 (td, J = 22, 7.0 Hz, 1H), 7.83 (d, J = 8.9 Hz, 1H), 7.78 (d, J = 12.6 Hz, 2H), 7.71-7.62 (m, 2H), 7.58 (t, J = 6.8 Hz, 1H), 7.53 (t, J = 6.8 Hz, 1H), 4.38 (t, J = 7.3 Hz, 2H), 4.10 (s, 3H), 1.92 (q, J = 7.3 Hz, 2H), 1.35 (sextet, J = 7.3 Hz, 2H), 0.91 (t, J = 7.3 Hz, 3H). Anal: Calc. for $C_{23}H_{23}N_5Pt\cdot0.6H_2O$: C, 48.01; H, 4.24; N, 12.17%. Found: C, 48.06; H, 4.19; N, 11.89%.

4-3. Results and discussion

4-3-1. Phase transition behavior of Pt(II) ionic liquid

Synthesized liquid **1** and **2** were also hygroscopic likewise [C_2mim][Pt(CN)$_2$(ptpy)] reported in chapter 2. To elucidate thermal properties of unhydrated **1** and **2**, the samples were dried under reduced pressure and stored in nitrogen atmosphere before measurements. Thermal properties of ionic liquid **1** and **2** were determined by thermogravimetry (TG) and differential scanning calorimetry (DSC). The TG curves of **1** and **2** were shown in Figure 1, the degradation points of **1** and **2** were estimated to be around 160°C and 170°C, respectively. Three ionic liquid Pt(II) complexes have similar decomposition points, and these values are enough stable to dry in an oil bath (60°C).

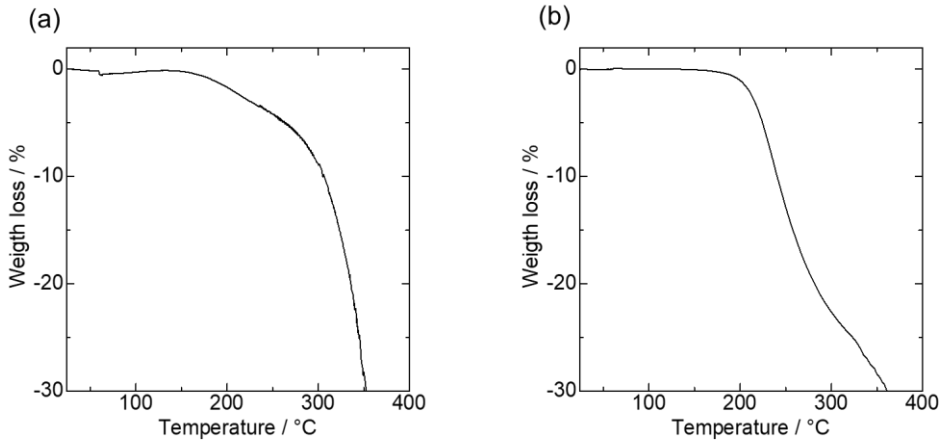

Figurer 1. TG curves of **1** (a) and **2**. The measurements were carried out under Ar atmosphere with scan rate of 5 K min^{-1}.

The DSC curves of **1** and **2** were presented in Figure 2. In the first cooling and second heating processes after heated to 100°C, the baseline change was observed in both **1** and **2**. Other discriminable thermal events such as endo- and exothermic peaks were not observed in both complexes. As shown in Figure 3, the glass transition points were estimated to be −41 (**1**) and −13°C (**2**). Therefore, two ionic liquids are classified into room temperature ionic liquids, and the liquid phase transform to glass state. No crystalline phase was observed in these measurement conditions.

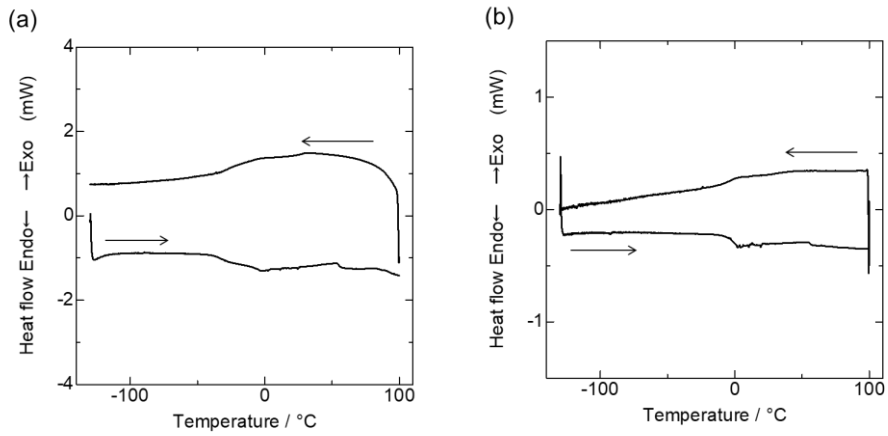

Figure 2. DSC curves of (a) **1** and (b) **2**, (first cooling scan and second heating scan, scan rate = 5 K min^{-1}).

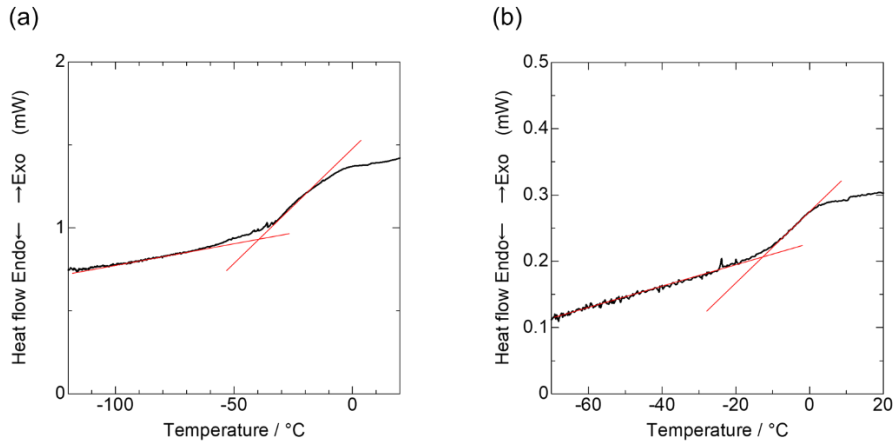

Figure 3. Glass transition point determination for (a) **1** and (b) **2**, using first cooling scan of DSC curves (scan rate = 5 K min^{-1}).

4-3-2. Photoluminescence properties of Pt(II) ionic liquids

Ionic liquid **1** and **2** exhibit broad structure less emission with emission maxima at 505 (**1**) and 618 (**2**) nm as shown in Figure 4. The dimer structures were also found in the corresponding Pt(II) complex anion with potassium ion. For complex anion $[Pt(CN)_2(mpi)]^-$ the crystal structure with potassium cation was successfully analyzed (Table 1). In the crystal structure, two crystallographically independent Pt-Pt distances (3.526 and 3.475 Å) was formed around 3.5 Å which is twice of Van der Waals radius of Pt (Figure 5). In the crystalline state, $K[Pt(CN)_2(mpi)]$ shows broad emission spectrum with emission maximum at 502 nm. Therefore, broad emission of crystalline **3** and liquid **1** were assigned to ^{3}MMLCT phosphorescence. For the complex **2**, the corresponding crystalline complex with potassium ($K[Pt(CN)_2(bzq)]$) was reported by Sicilia and co-workers.[14] The ^{3}MMLCT was observed at 636 nm in the solid state at room temperature, which suggests that the broad emission of complex **2** in liquid state is assignable to ^{3}MMLCT phosphorescence. There is no detectable peak assigned to monomer species in emission spectra of **1** and **2** at room temperature.

The emission spectra of **1** and **2** at 77 K were also presented in Figure 4. Both complexes exhibit vibronic structured spectra with three emission maxima in each spectrum. The corresponding monomer ligand center emission were listed in Table 3, each two shorter wavelength maxima show good agreement with corresponding monomer emission maxima. The slight broad longer wavelength peaks can be assigned to ^{3}MMLCT which was observed at room temperature. It was clearly observed that not only in the case of $[C_2mim][Pt(CN)_2(ptpy)]$ but also both newly synthesized ionic liquid Pt(II) complexes exhibit temperature dependent chromic behavior.

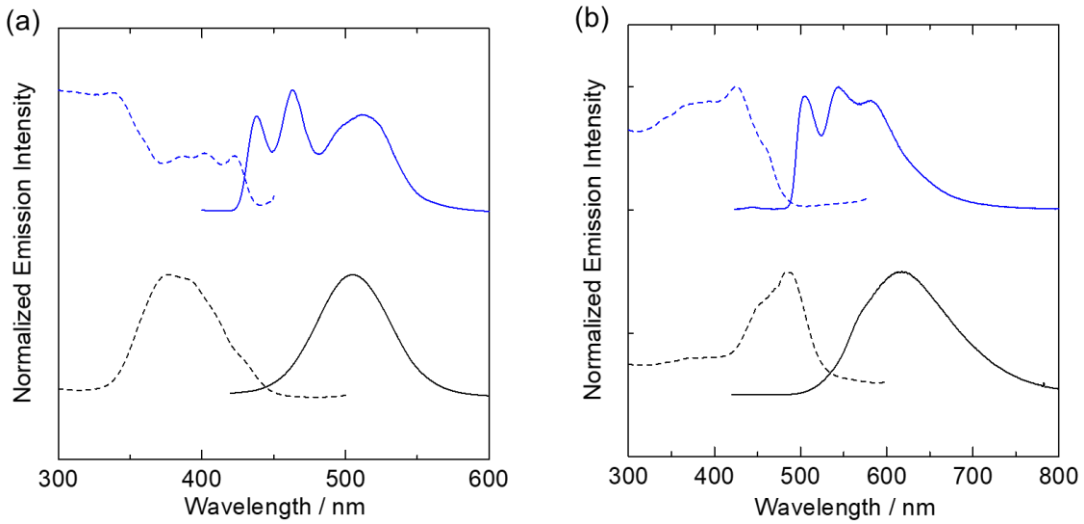

Figure 4. Emission (solid lines) and excitation (dotted lines) spectra of neat **1** (a) (λ_{ex} = 350 nm, λ_{em} = 520 nm) and **2** (b) (λ_{ex} = 350 nm, λ_{em} = 620 nm) at 298 (black) and 77 K (blue) under N_2 atmosphere.

Table 2. Emission data of **1** and **2** in neat liquid or glass state.

Complex	Temperature	$\lambda_{(max)em}$	$\lambda_{(max)ex}$	Φ
1	298 K	505 nm	376 nm	0.12
	77 K	438, 463, 511 nm	340 nm	0.94
2	298 K	618 nm	495 nm	0.10
	77 K	506, 546, 585 nm	420 nm	0.59

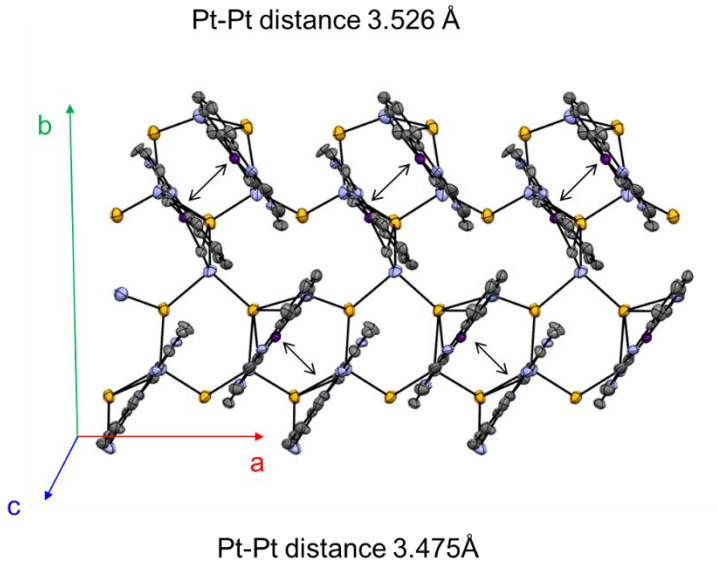

Figure 5. ORTEP drawings showing the dimer structure of potassium salt (**3**). Displacement parameters are drawn at the 50% probability level. Hydrogen atoms are omitted for clarity. Color code: Pt, purple; C, grey; N, blue; K, orange.

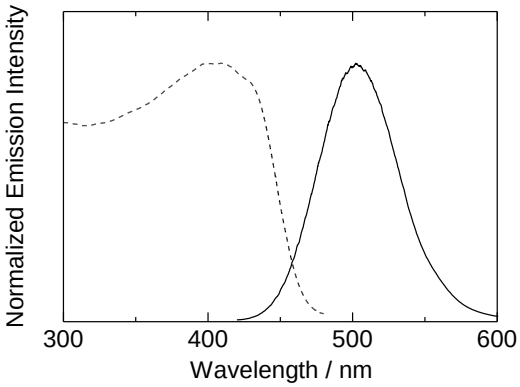

Figure 6. Emission (solid line) and excitation (dotted line) spectra of **3** in the solid state at room temperature (λ_{ex} = 350, λ_{em} = 500 nm).

Table 3. Emission spectral data of corresponding crystalline complexes of monomer and dimer structures

Complex anion	$[Pt(CN)_2(mpi)]^-$		$[Pt(CN)_2(bzq)]^-$	
Cation	n-Bu_4N^+	K^+	n-Bu_4N^+	K^+
λ_{max} / nm	430, 455, 481	502	480, 515, 553	636
assinment	^{3}LC	^{3}MMLCT	^{3}LC	^{3}MMLCT

4-3-4. Temperature dependence emission behaviours

Temperature dependent emission spectra were measured (Figure 7). With decreasing temperature, the emission intensity at shorter wavelength regions gradually increased. However, the spectral change at around the glass-phase transition point (−41°C c.a. 232 K for **1** and −13°C c.a. 260 K) was not distinct, which indicates that the fluidity or translational motion were not important factors for the dual emission. The monomer emission intensity increased below 160 K (**1**) and 100 K (**2**). Spectrum shape of complex **1** at 77 K is almost consistent to that of monomer. On the other hand, distinct ^{3}MMLCT emission remained in spectrum of **2** at 77 K. These deference might be attributed to the ligands π system, the complex anion $[Pt(CN)_2(bzq)]^-$ has higher tendency to form aggregates.[14]

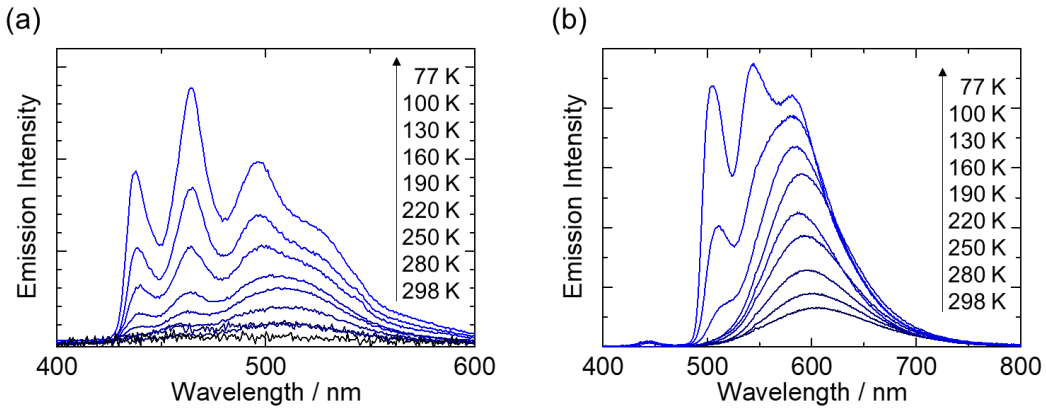

Figure 7. Emission spectra of (a) **1** and (b) **2** at different temperatures. λex = 337 nm. The relative emission intensities were adjusted for clarity.

4-3-3. Time-resolved emission behaviours

For further insight, time-resolved emission behaviours were investigated. As shown in Figure 8, the emission decay curves were analysed by bi-exponential fitting (Table 4-5). The long lifetime components at 77 K are similar to emission lifetimes of corresponding monomer in the solid state (8.4 μs for n-Bu_4[$Pt(CN)_2$(mpi)] and 173 μs for n-Bu_4[$Pt(CN)_2$(bzq)][14]). Therefore, long lifetime components can be assigned to lifetimes of monomer species. The remarkable lifetime increases around 160-130 K suggest the monomer excited states are not quenched by several non-radiative processes, such as excimer formation, energy transfer, and/or direct deactivation to the ground states via coordination geometry distortion below such temperature. Unfortunately, these non-radiative processes are all temperature dependence.[21] Therefore, it is quite difficult to completely assign a dominant process of this thermochromic behaviour. Furthermore, excimer formation and geometry distortion also depend on the rigidity of materials. However, the emission change around glass transition point is negligible. Therefore, energy transfer from monomer to dimer might be plausible dominant key of this thermochromic emission behaviour.

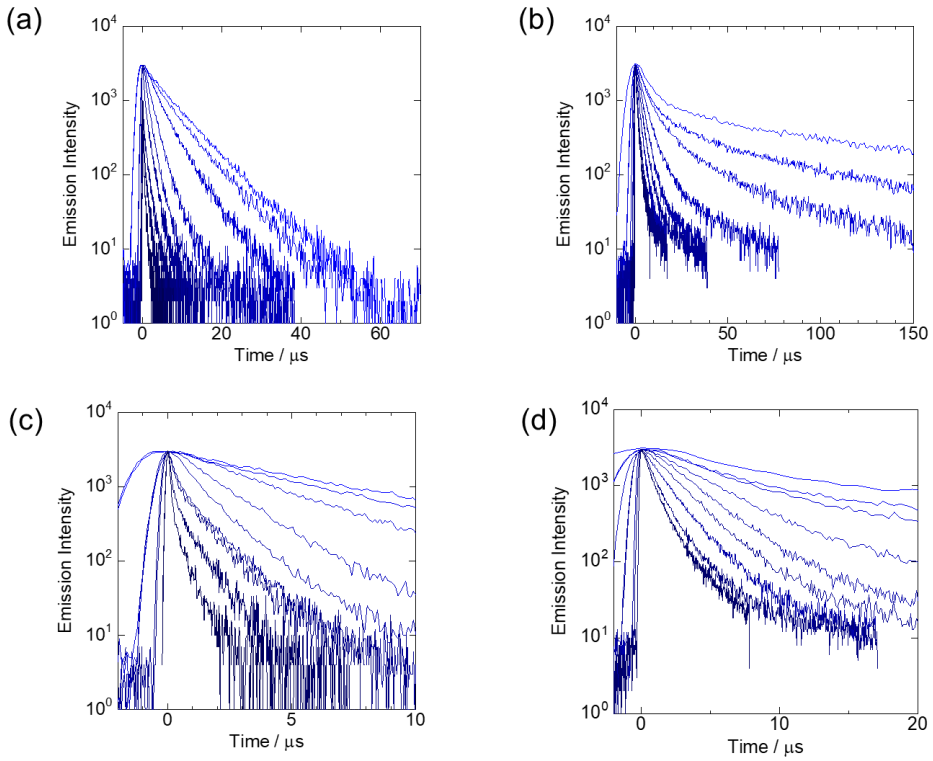

Figure 8. Temperature dependence of emission lifetime for (a) **1** and (b) **2**, and their enlarged figure of short range (c) **1** and (d) **2**. (at 77, 100, 130, 160, 190, 220, 250, 280, and 298 K)

Table 4. data of temperature dependence of emission lifetime measurements of **1**

Temperature	A_1[a]	τ_1[b] (μs)	A_2[a]	τ_2[b] (μs)
77	0.43	5.0	0.56	8.6
100	0.48	3.9	0.52	7.7
130	0.72	2.8	0.36	5.8
160	1.04	1.8	0.08	4.5
190	1.05	1.0	0.16	2.5
220	0.66	0.33	0.36	1.4
250	0.73	0.25	0.38	1.2
280	0.97	0.13	0.24	0.85
298	1.13	0.10	0.13	0.57

[a] Pre-exponential factors. [b] Emission lifetimes; Emission decays were analyzed with bi-exponential fitting: $I = A_1\exp(-t/\tau_1) + A_2\exp(-t/\tau_2)$.

Table 5. data of temperature dependence of emission lifetimesfor **2**

Temperature	A_1[a]	τ_1[b] (μs)	A_2[a]	τ_2[b] (μs)
77	0.87	10.1	0.20	147.0
100	0.88	6.6	0.17	68.3
130	0.96	6.6	0.10	43.8
160	1.09	4.3	0.04	25.0
190	1.17	3.1	0.02	21.7
220	1.16	2.4	0.02	19.4
250	1.01	1.7	0.04	7.2
280	1.00	1.1	0.04	5.6
298	0.93	0.75	0.15	2.4

[a] Pre-exponential factors. [b] Emission lifetimes; Emission decays were analyzed with bi-exponential fitting: $I = A_1\exp(-t/\tau_1) + A_2\exp(-t/\tau_2)$.

4-3-4. Computational studies

The ground and lowest triplet excited states of **4** and **1** were calculated by using density functional theory (DFT) and time-dependent DFT (TD-DFT) methods (Tables 6-13). Total spin density plot of the optimized lowest triplet state (T_1) of the monomer complex for **4** suggests that the two unpaired electrons delocalized mainly on the ptpy ligand, and therefore the T_1 state of monomer species for **4** has the ^{3}LC character (Figure 9). In the case of the monomer complex for **1**, total spin density of the optimized T_1 state is delocalized both on the Pt ion and the mpi ligand, which is more like a mixed ^{3}LC and ^{3}MLCT (Figure 10). Optimized dimer structures (Pt···Pt = 3.37 Å for 3 and 3.60 Å for 1) (Figures 11 and 12) are qualitatively in agreement with the crystal structures. According to TD-DFT calculations on the dimer systems, emission from T_1 occurs at 567 nm for **4** and at 472 nm for **1** and can be assigned to the ^{3}MMLCT origin, while emission from T_1 occurs at 529 nm for monomer of **1** and at 444 nm for monomer of **1** (Table 14). The calculated values support the experimental results, where the emission at the shorter-wavelength region appearing mainly at low temperature is originated from the monomer species. On the other hand, the emission at longer-wavelength region appearing at room temperature comes from the dimer species.

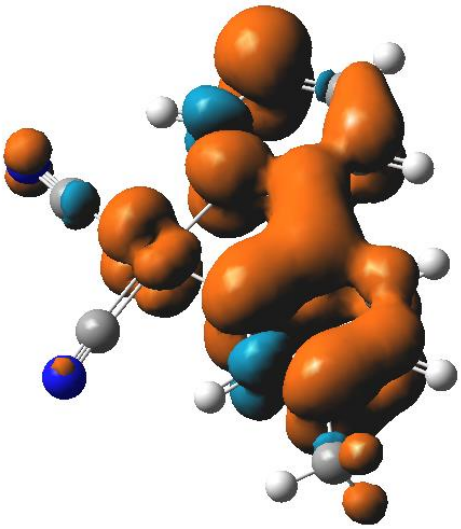

Figure 9. Spin density of monomer **4** ($[Pt(CN)_2(ptpy)]^-$) of the S=1 state mainly delocalized on the ptpy ligand, suggesting that the two-unpaired electron are on the ptpy ligand. Therefore, S=1 state can be assigned to ^{3}**LC**.

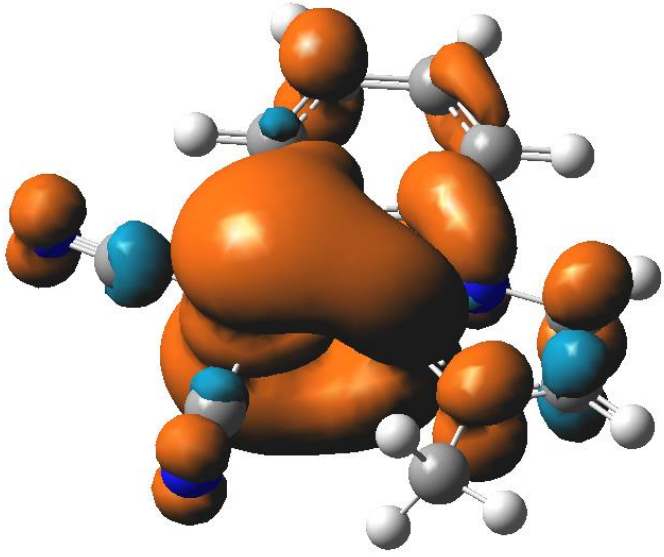

Figure 10. Spin density of monomer **1** ($[Pt(CN)_2(mpi)]^-$) of the S=1 state is delocalized on both Pt ion and mpi ligand, suggesting that the two-unpaired electron are on Pt ion and mpi ligand. Therefore, S=1 may show both ^{3}**LC** and ^{3}**MLCT** mixed character.

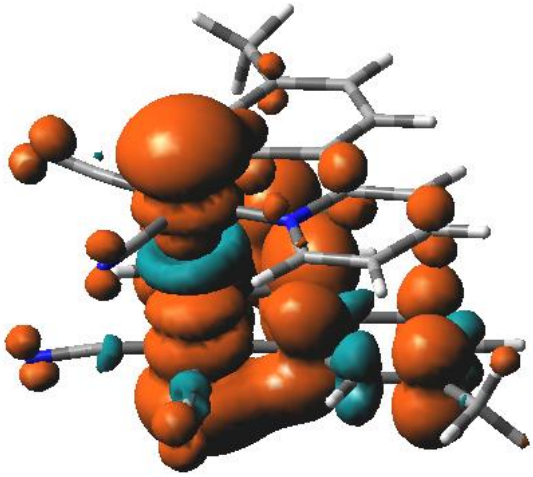

Figure 11. Spin density of dimer **4** ($[Pt(CN)_2(ptpy)]^-$) of the S=1 state is delocalized on both Pt ions a ptpy ligand, suggesting that the two-unpaired electron are on the Pt ions and a ptpy ligand. Therefore, S=1 state can be assigned to **^{3}MMLCT**.

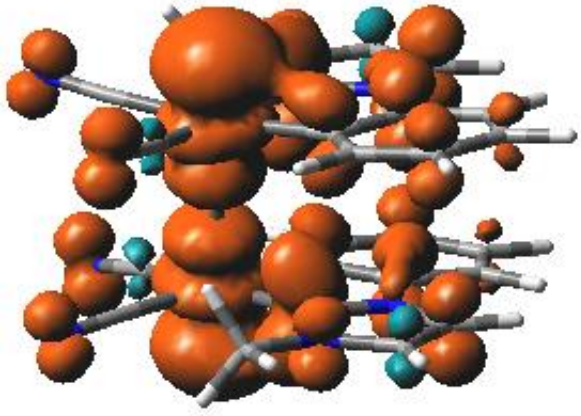

Figure 12. Spin density of dimer **1** ($[Pt(CN)_2(mpi)]^-$) of the S=1 state is delocalized on both Pt ions a both mpi ligands, suggesting that the two-unpaired electron are on the Pt ions and mpi ligands. Therefore, S=1 state can be assigned to **^{3}MMLCT**.

Table 6. Cartesian coordinates of the optimized ground state monomer structure of **4** ($[Pt(CN)_2(ptpy)]^-$).

Pt	2.545369	-0.72595	3.449749
N	0.381916	1.115905	4.752314
N	1.030105	-1.52104	0.724712
N	4.205151	-1.92257	2.827966
C	4.274058	-2.6173	1.681707
C	5.383237	-3.37689	1.336249
C	6.46267	-3.41377	2.218706
C	6.393171	-2.697	3.403284
C	5.250151	-1.94418	3.708929
C	5.056183	-1.15323	4.915588
C	6.0303	-1.06531	5.924171
C	5.801042	-0.29904	7.05567
C	4.589305	0.397512	7.203424
C	3.628904	0.302333	6.194341
C	3.817866	-0.46148	5.03147
C	4.33947	1.226386	8.42866
C	1.168561	0.414962	4.224597
C	1.487437	-1.16433	1.751141
H	3.394208	-2.53982	1.04305
H	5.392661	-3.92294	0.396091
H	7.352447	-3.99777	1.984421
H	7.224797	-2.71358	4.104172
H	6.978696	-1.59814	5.82958
H	6.562519	-0.2352	7.835408
H	2.689106	0.84504	6.312468
H	4.371759	0.618708	9.344034
H	5.097541	2.013083	8.54918
H	3.358629	1.712472	8.386905

Table 7. Cartesian coordinates of the excited triplet state monomer structure of **4** ($[Pt(CN)_2(ptpy)]^-$).

Pt	2.613655	-0.655	3.43042
N	0.477853	1.24511	4.664617
N	1.038042	-1.30837	0.689701
N	4.196094	-1.90116	2.80412
C	4.281876	-2.58837	1.671273
C	5.376897	-3.39076	1.345717
C	6.460562	-3.48352	2.266738
C	6.394094	-2.78412	3.440472
C	5.253161	-1.97076	3.740357
C	5.06748	-1.21269	4.900936
C	6.022644	-1.14542	5.977815
C	5.7557	-0.37915	7.074194
C	4.537606	0.378134	7.201077
C	3.606412	0.324326	6.170983
C	3.795841	-0.43606	5.006929
C	4.313499	1.199618	8.438446
C	1.253443	0.529268	4.170407
C	1.536062	-1.01812	1.704181
H	3.433251	-2.4876	0.999513
H	5.384929	-3.9265	0.403683
H	7.325049	-4.10009	2.039463
H	7.206496	-2.83877	4.157697
H	6.9543	-1.70081	5.923047
H	6.481801	-0.33253	7.885225
H	2.684487	0.894268	6.260878
H	5.097871	1.958404	8.563653
H	3.349453	1.713314	8.395326
H	4.326201	0.575235	9.342115

Table 8. Cartesian coordinates of the optimized ground state monomer structure of **1** ($[Pt(CN)_2(mpi)]^-$).

Pt	5.536674	-3.45997	5.402163
N	7.129699	-0.96563	4.146945
N	6.095646	-2.29246	2.801263
N	6.686796	-2.13633	8.097177
N	4.028824	-5.86153	6.853604
C	5.296465	-3.41446	2.452508
C	3.746048	-5.6159	1.944611
H	3.128403	-6.49384	1.748947
C	4.183967	-4.83084	0.878162
H	3.916053	-5.08467	-0.14731
C	4.881082	-4.17298	3.56508
C	7.677581	-0.32895	5.328071
H	8.771998	-0.31573	5.270175
H	7.309905	0.701058	5.39979
H	7.369195	-0.88619	6.21643
C	4.603326	-4.95541	6.368387
C	4.089945	-5.28989	3.260089
H	3.737183	-5.91681	4.079506
C	7.337256	-0.49066	2.861986
H	7.92728	0.395794	2.671987
C	6.240753	-2.66128	7.140103
C	4.973822	-3.70869	1.132134
H	5.324396	-3.08399	0.3085
C	6.683972	-1.32918	2.014396
H	6.592741	-1.31697	0.937417
C	6.357821	-2.08955	4.135522

Table 9. Cartesian coordinates of the optimized excited triplet state monomer structure of **1** ($[Pt(CN)_2(mpi)]^-$).

Pt	5.514582	-3.43138	5.342572
N	7.151303	-0.98965	4.138228
N	6.109269	-2.31634	2.740082
N	6.669028	-2.08171	8.035171
N	3.983233	-5.76076	6.888801
C	5.337277	-3.37482	2.409669
C	3.729474	-5.60842	1.999869
H	3.103339	-6.47385	1.804806
C	4.202302	-4.82173	0.879372
H	3.922041	-5.1133	-0.12958
C	4.876394	-4.15252	3.601884
C	7.665824	-0.39142	5.358702
H	8.263222	0.481557	5.085894
H	6.839957	-0.10031	6.010147
H	8.274571	-1.11564	5.902904
C	4.559062	-4.89124	6.36736
C	4.066759	-5.26722	3.300112
H	3.703585	-5.86828	4.12931
C	7.385273	-0.52662	2.869223
H	7.992092	0.34934	2.691969
C	6.230126	-2.60254	7.087342
C	4.992797	-3.72258	1.072492
H	5.347884	-3.13231	0.231674
C	6.745314	-1.33768	1.978022
H	6.691862	-1.29991	0.902756
C	6.360261	-2.10572	4.118869

Table 10. Cartesian coordinates of the optimized ground state dimer structure of **4** ($[Pt(CN)_2(ptpy)]^-$).

Pt	2.735372	-0.63795	3.384538
Pt	4.025582	1.845521	1.513732
N	0.365932	1.019675	4.555776
N	3.17481	0.595213	-1.214
N	1.165234	3.284635	1.49062
N	0.861988	-1.28921	0.872635
N	4.539065	2.519816	3.465825
N	4.416683	-1.62961	2.53737
C	4.470094	-2.06925	1.271082
C	5.608922	-2.66679	0.747222
C	6.730154	-2.79334	1.564973
C	6.685819	-2.30069	2.860903
C	5.515387	-1.70287	3.343392
C	5.339617	-1.11963	4.671195
C	6.357529	-1.12002	5.635798
C	6.141867	-0.55573	6.887231
C	4.900024	0.022138	7.193787
C	3.900616	0.030367	6.217725
C	4.072217	-0.52139	4.937831
C	4.655435	0.629926	8.544528
C	1.274407	0.369494	4.184533
C	1.52672	-1.00148	1.797753
C	3.669455	3.082548	4.318328
C	4.030686	3.438866	5.611008
C	5.335666	3.187296	6.030047
C	6.222492	2.571069	5.159612
C	5.809455	2.224654	3.867721
C	6.624115	1.541741	2.866204
C	7.963956	1.195215	3.09255
C	8.699246	0.546643	2.107968
C	8.102231	0.231049	0.877504
C	6.762278	0.567969	0.671703
C	5.976743	1.21941	1.636459
C	8.889218	-0.46573	-0.19431

C	3.576487	1.082438	-0.22069
C	2.19045	2.710372	1.501984
H	3.564549	-1.91274	0.683957
H	5.612467	-2.99728	-0.28938
H	7.649179	-3.24057	1.183012
H	7.567378	-2.34723	3.49743
H	7.335316	-1.55266	5.409734
H	6.942821	-0.54957	7.631101
H	2.944182	0.505979	6.452208
H	5.560503	1.107067	8.948022
H	3.86358	1.388715	8.499813
H	4.336574	-0.1216	9.282993
H	2.661461	3.226421	3.929158
H	3.288143	3.878506	6.273569
H	5.651339	3.435453	7.044531
H	7.230007	2.321559	5.486766
H	8.441121	1.421322	4.049392
H	9.74026	0.269938	2.294033
H	6.294541	0.293928	-0.27806
H	8.229053	-1.02161	-0.87258
H	9.459315	0.243622	-0.81371
H	9.616704	-1.17433	0.227811

Table 11. Cartesian coordinates of the optimized excited triplet state dimer structure of **4** ($[Pt(CN)_2(ptpy)]^-$).

Pt	2.804174	-0.40297	3.24931
Pt	3.939878	1.692682	1.60447
N	0.36598	1.019669	4.555765
N	3.174831	0.595214	-1.21395
N	1.165203	3.284652	1.490602
N	0.861949	-1.28922	0.872615
N	4.645524	2.567628	3.377295
N	4.432195	-1.60142	2.606412
C	4.475362	-2.2869	1.45402
C	5.531822	-3.12757	1.138083
C	6.589768	-3.24574	2.048752
C	6.566975	-2.48999	3.210085
C	5.467821	-1.66681	3.490857
C	5.294239	-0.86062	4.700803
C	6.258808	-0.79388	5.718285
C	6.026902	-0.02535	6.850071
C	4.822599	0.685154	6.992203
C	3.869676	0.608496	5.977355
C	4.071224	-0.14489	4.811455
C	4.59253	1.571619	8.187704
C	1.309053	0.5561	4.052815
C	1.572625	-0.91095	1.711366
C	3.93069	3.363991	4.197997
C	4.478084	3.967497	5.312021
C	5.838757	3.731242	5.615146
C	6.556621	2.871322	4.804651
C	5.963695	2.291289	3.671417
C	6.622488	1.417833	2.717871
C	7.967032	1.009213	2.833008
C	8.534536	0.185525	1.87648
C	7.780524	-0.24959	0.765819
C	6.45583	0.161844	0.655138
C	5.835542	0.984855	1.610209
C	8.389247	-1.18718	-0.24191

C	3.464589	0.950469	-0.14258
C	2.141784	2.659913	1.58298
H	3.629971	-2.13558	0.786761
H	5.52166	-3.66882	0.19793
H	7.425553	-3.91228	1.848361
H	7.39284	-2.53642	3.911846
H	7.202616	-1.32756	5.624363
H	6.784103	0.034811	7.631264
H	2.939697	1.165009	6.086732
H	5.216136	1.274813	9.039888
H	4.835286	2.612242	7.93359
H	3.543424	1.551543	8.503793
H	2.887386	3.495713	3.922686
H	3.85699	4.606018	5.931676
H	6.309357	4.19315	6.480354
H	7.592538	2.640286	5.033773
H	8.567365	1.324993	3.684828
H	9.57099	-0.13614	1.982507
H	5.87104	-0.17474	-0.20071
H	7.760521	-1.267	-1.13513
H	9.38933	-0.85747	-0.55532
H	8.49706	-2.20018	0.175082

Table 12. Cartesian coordinates of the optimized ground state dimer structure of **1** ($[Pt(CN)_2(mpi)]^-$).

Pt	3.097825	-0.61216	5.800151
Pt	5.409762	-3.32632	5.28638
N	6.609251	-0.5935	4.1613
N	2.331829	-1.22206	3.065483
N	1.641342	-2.93115	4.185916
N	5.721532	-1.95334	2.742774
N	4.674042	1.247256	7.841859
N	2.318995	-2.47778	8.285178
N	6.712558	-2.40081	8.062641
N	4.105126	-5.65083	7.010153
C	2.25377	-1.7312	4.340268
C	1.422317	-3.88082	5.264261
H	0.844148	-4.72158	4.867714
H	2.379262	-4.24281	5.658886
H	0.888057	-3.39827	6.086077
C	5.054913	-3.13849	2.348918
C	3.76917	-5.48921	1.743876
H	3.25902	-6.42704	1.510112
C	4.099567	-4.60897	0.713234
H	3.853526	-4.84555	-0.3231
C	4.035016	1.848198	4.006415
H	4.427311	2.325968	4.908274
C	4.743181	-3.99404	3.431558
C	6.987559	0.063027	5.399319
H	7.956341	0.557734	5.26428
H	6.219656	0.791676	5.683048
H	7.048955	-0.67889	6.199368
C	1.360928	-3.17157	2.853856
H	0.930835	-4.10788	2.525012
C	4.630269	-4.8414	6.337866
C	3.656544	1.928517	1.609947
H	3.743224	2.441793	0.651087
C	4.086186	-5.18068	3.072367
H	3.817933	-5.8844	3.863837

C	3.435838	0.584065	4.126782
C	4.146086	2.512275	2.778538
H	4.620044	3.495915	2.733184
C	6.65912	0.015297	2.919616
H	7.035025	1.021893	2.796253
C	6.219748	-2.70065	7.037387
C	2.948241	0.043512	2.912499
C	3.046157	0.672942	1.675815
H	2.656906	0.198985	0.771389
C	2.619911	-1.80686	7.367209
C	1.790488	-2.09406	2.14409
H	1.80066	-1.90936	1.079133
C	4.75256	-3.41175	1.018558
H	5.017175	-2.70799	0.225518
C	6.107176	-0.84253	2.022144
H	5.919916	-0.73209	0.963175
C	4.056343	0.589408	7.087111
C	6.021625	-1.81301	4.078739

Table 13. Cartesian coordinates of the optimized excited triplet state dimer structure of **1** ($[Pt(CN)_2(mpi)]^-$).

Pt	3.365817	-0.81446	5.779368
Pt	5.25692	-3.1827	5.34291
N	6.89087	-0.75085	4.189691
N	2.48655	-1.28588	3.077238
N	1.565439	-2.8774	4.220892
N	5.809682	-1.98879	2.779189
N	4.674062	1.247299	7.841921
N	2.319	-2.47776	8.285127
N	6.712508	-2.40081	8.062581
N	4.10515	-5.6509	7.010202
C	2.378153	-1.7987	4.346146
C	1.25298	-3.79207	5.307512
H	0.668413	-4.61856	4.895318
H	2.1768	-4.17298	5.752187
H	0.690263	-3.27433	6.086921
C	5.005765	-3.08112	2.412139
C	3.520587	-5.34149	1.883989
H	2.943267	-6.24181	1.679955
C	3.945978	-4.53376	0.823881
H	3.700883	-4.79379	-0.20369
C	4.543606	1.540132	4.047787
H	4.983436	1.951912	4.955132
C	4.576483	-3.85546	3.524633
C	7.334037	-0.15712	5.440819
H	7.909723	0.741427	5.204621
H	6.467157	0.105261	6.054781
H	7.944123	-0.86908	6.00006
C	1.202924	-3.0511	2.901248
H	0.608735	-3.89483	2.585481
C	4.475895	-4.72822	6.400948
C	4.13681	1.720184	1.659934
H	4.261658	2.246846	0.716195
C	3.826571	-4.99687	3.20521
H	3.48744	-5.63825	4.017688

C	3.822301	0.34073	4.140448
C	4.695385	2.22693	2.837975
H	5.256297	3.159804	2.812764
C	7.088392	-0.2172	2.93282
H	7.651174	0.692074	2.787263
C	6.151538	-2.61988	7.067383
C	3.253899	-0.11932	2.921627
C	3.405533	0.531403	1.699562
H	2.956412	0.12789	0.79359
C	2.722924	-1.89595	7.362402
C	1.768545	-2.05334	2.175516
H	1.763842	-1.8666	1.114057
C	4.698581	-3.38779	1.088747
H	5.045895	-2.75379	0.274609
C	6.42237	-0.99157	2.038662
H	6.293108	-0.88311	0.97415
C	4.252353	0.455067	7.096205
C	6.082662	-1.83726	4.115855

Table 14. Calculated emission wavelength and observed emission wavelength.

Complex anion	Structure	Wavelength (calc)	Wavelength (obs)
(**4**)$[Pt(CN)_2(ptpy)]^-$	Monomer	529	487
	Dimer	567	560
(**1**) $[Pt(CN)_2(mpi)]^-$	Monomer	444	438
	dimer	472	505

4-4. Conclusion

In conclusion, two novel ionic liquids based on luminescent anionic Pt(II) complexes with different cyclometalating ligands were synthesized. These ionic liquids exhibited thermochromic luminescence with different color variations. The thermochromic luminescence is attributed to two different emissive states of the monomeric and dimeric forms of square planar Pt(II) complexes. The co-existence of monomeric and aggregated forms in disordered liquid and glass phases give rise to the dual emissions from both ^{3}LC and ^{3}MMLCT excited states, though the spectral changes at the liquid-glass phase transition points were not distinct. Our present results support for the thermochromic dual emission properties of anionic Pt(II) complex-based ionic liquids. The new type of luminescent ionic liquid systems enables emission color tune-up freely, which will be important in developing luminescent soft materials.

4-5. References

1 (*a*) J. P. Hallett and T. Welton, *Chem. Rev*. 2011, **111**, 3508; (*b*) P. Wasserscheid and W. Keim, *Angew. Chem. Int. Ed.*, 2000, **39**, 3772;

2 (*a*) M. Armand, F. Endres, D. R. MacFarlane, H. Ohno and B. Scrosati, *Nat. Mat.* 2009, **8**, 621; (*b*) S.-G. Lee, *Chem. Commun*., 2006, 1049.

3 M. Watanabe, M. L. Thomas, S. Zhang, K. Ueno, T. Yasuda and K Dokko, Chem. Rev. 2017, 117, 7190−7239

4 (*a*) S. Tang, A. Babai and A.-V. Mudring, *Angew. Chem. Int. Ed*., 2008, **47**, 7631; (*b*) A. Getsis, S. Tang and A.-V. Mudring, *Eur. J. Inorg. Chem*., 2010, 2172; (c) S. Pitula and A.-V. Mudring, *Chem. Eur. J*. 2010, **16**, 3355; (d) S. Gago, L. Cabrita, J. C. Lima, L. C. Branco and F. Pina, *Dalton Trans.*, 2013, **42**, 6213; (e) E. T. Spielberg, E. Edengeiser, B. Mallick, M. Havenith and A.-V. Mudring, *Chem. Eur. J.* 2014, **20**, 5338; (*f*) A. Tokarev, J. Larionova, Y. Guari, J. M. López-de-Luzuriaga, M. Monge, P. Dieudonné and C. Blanc, *Dalton Trans*., 2010, **39**, 10574; (*g*) Y. Yoshida, J. Fujii, G. Saito, T. Hiramatsu and N. Sato, *J. Mater. Chem*., 2006, **16**, 724; (h) Z.-P. Wang, J.-Y. Wang, J.-R. Li, M.-L. Feng, G.-D. Zou and X.-Y. Huang, *Chem. Commun.*, 2015, **51**, 3094.

5 T. Ogawa, M. Yoshida, H. Ohara, A. Kobayashi and M. Kato, Chem. Commun. 2015, 51, 13377–13380.

6 (*a*) M. Kato, *Bull. Chem. Soc. Jpn*., 2007, **8**, 287; (*b*) B. Ma, P. I. Djurovich and M. E. Thompson, *Coord. Chem. Rev*., 2005, **249**, 1501; (*c*) K. M.-C. G Wong and V. W.-W. Yam, *Acc. Chem. Res.*, 2011, **44**, 424; (*d*) A. Kobayashi and M. Kato, *Eur. J. Inorg. Chem.*, 2014, **27**, 4469.

7 (*a*) B. W. D'Andrade, J. Brooks, V. Adamovich, M. E. Thompson and S. R. Forrest, *Adv. Mater.*, 2002, **14**, 1032; (*b*) J. Kalonowski, M. Cocchi, D. Virgili, V. Fattori and J. A. G. Williams, *Adv. Mater*., 2007, **19**, 4000; (*c*) J. Kalinowski, M. Cocchi, L. Murphy, J. A. G. Williams and V. Fattori, *Chem. Phys.*, 2010, **378**, 47; (*d*) L. Murphy, P. Brulatti, V. Fattori, M. Cocchi and J. A. G. Williams, *Chem. Commun*., 2012, **48**, 5817; (*e*) G. Zhou, Q. Wang, X. Wang, C.-L. Ho, W.-Y. Wong, D. Ma, L. Wang and Z. Lin, *J. Mater. Chem.*, 2010, **20**, 7472.

8 (a) W. R. Dawson and M. W. Windsor, *J. Phys. Chem*., 1968, **72**, 325; (b) W. H. Melhuish, *J. Phys. Chem*., 1961, **65**, 229.

9 CrystalClear, Rigaku Corporation, Tokyo196-8666, Japan, 2000-2015.

10 SHELXS-2013: G. M. Sheldrick, Acta Cryst., 2008, A64, 112.

11 SHELXL-2014: G. M. Sheldrick, Acta Cryst., 2008, A64, 112.

12 *CrystalStructure 4.2.5*, Rigaku Corporation, Tokyo196-8666, Japan, 2000-2017.

13 R. Costa, E. Ortí, H. J. Bolink, F. Monti, G. Accorsi and N. Armaroli, *Angew. Chem. Int. Ed*., 2012, **51**, 8178.

14 J. Forniés, S. Fuertes, J. A. López, A. Martín and V. Sicilia, *Inorg. Chem*., 2008, **47**, 7166

15 S. Fuertes, A. J. Chueca, L. Arnal, A. Martín, U. Giovanella, C. Botta and Violeta Sicilia, *Inorg. Chem.*, 2017, **56**, 4829.

16 Gaussian 16, Revision A.03, M. J. Frisch, G. W. Trucks, H. B. Schlegel, G. E. Scuseria, M. A. Robb, J. R. Cheeseman, G. Scalmani, V. Barone, G. A. Petersson, H. Nakatsuji, X. Li, M. Caricato, A. V. Marenich, J. Bloino, B. G. Janesko, R. Gomperts, B. Mennucci, H. P. Hratchian, J. V. Ortiz, A. F. Izmaylov, J. L. Sonnenberg, D. Williams-Young, F. Ding, F. Lipparini, F. Egidi, J. Goings, B. Peng, A. Petrone, T. Henderson, D. Ranasinghe, V. G. Zakrzewski, J. Gao, N. Rega, G. Zheng, W. Liang, M. Hada, M. Ehara, K. Toyota, R. Fukuda, J. Hasegawa, M. Ishida, T. Nakajima, Y. Honda, O. Kitao, H. Nakai, T. Vreven, K. Throssell, J. A. Montgomery, Jr., J. E. Peralta, F. Ogliaro, M. J. Bearpark, J. J. Heyd, E. N. Brothers, K. N. Kudin, V. N. Staroverov, T. A. Keith, R. Kobayashi, J. Normand, K. Raghavachari, A. P. Rendell, J. C. Burant, S. S. Iyengar, J. Tomasi, M. Cossi, J. M. Millam, M. Klene, C. Adamo, R. Cammi, J. W. Ochterski, R. L. Martin, K. Morokuma, O. Farkas, J. B. Foresman, and D. J. Fox, Gaussian, Inc., Wallingford CT, 2016.

17 Y. Zhao, D. G. Truhlar, *Theor. Chem. Acc.*, 2008, **120**, 215.

18 Y. Zhao, N. E. Schultz, D. G. Truhlar, D. G. *J. Chem. Theory Comput.* 2006, **2**, 364.

19 (a) P. Fuentealba, H. Preuss, H. Stoll, L. Vonszentpaly, *Chem. Phys. Lett.* 1982, **89**, 418; (b) T. H. Dunning, Jr., P. J. Hay, *Modern Theoretical Chemistry*; Plenum: New York, 1977; **3**, 1.

20 (a) R. Ditchfield, W. J. Hehre, J. A. Pople, *J. Chem. Phys.*, 1971, **54**, 724; (b) W. J. Hehre, R. Ditchfield, J. A. Pople, J. Chem. Phys., 1972, **56**, 2257; (c) P. C. Hariharan, J. A. Pople, *Theor. Chem. Acc.*, 1973, **28**, 213; (d) P. C. Hariharan, J. A. Pople, *Mol. Phys.* 1974, **27**, 209; (e) R. C. Binning Jr., L. A. Curtiss, *J. Comp. Chem.* 1990, **11**, 1206.

21 N. J. Turro, Modern Molecular Photochemistry, University Science Books, Mill Valley, 1991.

Chapter 5.

Phosphorescence Properties of Platinum(II) Complexes with a Fluorine Substituted Tridentate Diphenylpyridyl Ligand in the Solid State.

5-1 Introduction

Luminescent Pt(II) metal complexes have been studied because of their potential to be applied for many applications such as bio-imaging material,[1] dye for solar cells,[2] chemical sensor,[3] and light emitting diode,[4] The luminescence properties of Pt(II) complexes attributed to efficient spin-orbit coupling of heavy platinum atoms,[5] the almost luminescence of the Pt(II) complexes have been assigned to phosphorescence from excited triplet states of ligand centered (^{3}LC) or metal-metal-to-ligand charge transfer states (^{3}MMLCT).[6] The luminescent quantum yield of the Pt(II) complexes is strongly dependent on their ligand field strength and coordination structure rigidity. However, the Pt(II) complexes with tridentate 2,6-diphenylpyridyl ligands (NBu_4)[Pt(C^N^C)(L)] : HC^N^CH = 2,6-diphenylpyridine; L = alkynyl, CN^-, S-2Py$^-$, or acetonyl) have been reported as weakly emissive compounds in both solid and solution states by Berenguer and co-workers, even though the complexes might fulfill the requirement of intense emissive Pt(II) complexes.[7] The emissive states were assigned to ^{3}LC in glassy CH_2Cl_2 solution at 77K. On the other hand, the related tridentate N^C^N (N^CH^N = 2,6-dipyridilbenzene) cyclometalating ligands afford highly emissive Pt(II) complexes in not only rigid media but also fluid solution.[8] Based on the number of strong s donor C^- of phenyl ring, The C^N^C coordination ligands should provide stronger ligands field than that of N^C^N ligands. However, the $[Pt(C^N^C)L]^-$ complexes were non-emissive in fluid solution and weakly emissive in solid states at room temperature. To understand this counterintuitive emission behavior, Che and co-worker reported theoretical analysis for non-emissive [Pt(C^N^C)L] (L = CNPh) and other related non-emissive Pt(II) complexes with tridentate ligands as well as strong emissive Pt(II) complexes. It was found that the optimized excited triplet structures of non-emissive and weakly-emissive Pt(II) complexes adopted distorted coordination geometry.[9] Furthermore, spin-orbit coupling time dependent density functional theory (SOC-TDDFT) suggested the emissive states can be assigned to the ^{3}MLCT states.

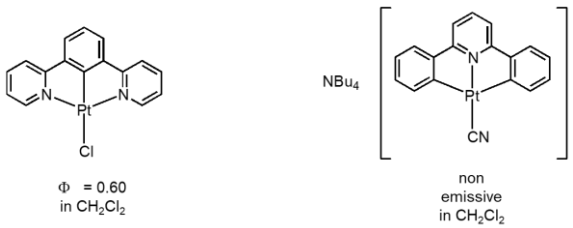

Scheme 1. Structural formula of Pt(II) N^C^N and C^N^C cyclometallated complexes

In order to obtain further insight of these tridentate C^N^C ligands, the molecular orbital should be perturbated by some chemical substitution. The ^{3}LC emission properties of Pt(II) complexes can be controlled by modifications of the ligands. An approach to perturbate emission colors without

changing the parent molecular structure is substitution with donor and/or acceptor groups or extending π-system of the ligands. Especially, substitution of fluorine atoms on the phenyl ring of phenylpyridine is an outstanding example for hypsochromic shift of emission wavelength of cyclometalated transition metal complexes.[10] The electron-withdrawing property of fluorine atom contribute to stabilization of energy level of HOMO which electron density is localized on phenyl ring in the case of cyclometalated ligands. In this chapter, the anionic Pt(II) complexes with a fluorine substituted tridentate ligand (dFphpy = 2,6-bis(2,6-difluorophenyl)-pyridine) were synthesized and characterized. The crystal structures and photophysical properties of the complexes are reported.

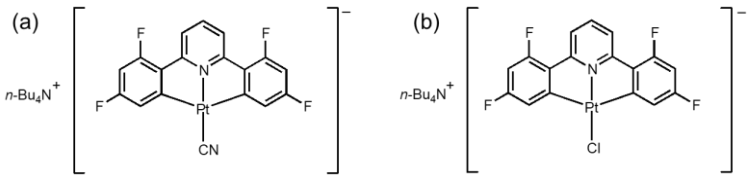

Scheme 2. Structural formula of complexes **1** (a) and **2** (b).

5-2 Experimental

5-2-1 Materials

All reagents were purchased from Wako Pure Chemical Industry, Kanto Chemical or Tokyo Chemical Industry. All reagents were used without further purification unless otherwise noted. The solvents for spectroscopic measurements were collected with spectroscopic grade CH_3CN, CH_2Cl_2, THF, Acetone and CH_3OH. The ligand dFphpy was synthesized by reported method.[11]

5-2-2 Physical measurements

^1H NMR spectra were collected on a JEOL EX-270 NMR spectrometer (270 MHz). Elemental analysis was measured through the analysis center in Hokkaido University. Absorption spectra were measured using a Shimadzu UV-2500PC Spectrophotometer using quartz cells with a thickness of 1 cm.

5-2-3 Synthesis

[Pt(dFphpy)(DMSO)]

$K_2[PtCl_4]$ (638 mg, 1.5 mmol) was added to a solution of dFphpy (606 mg, 2.0 mmol) in glacial acetic acid. The reaction mixture was stirred at 80°C for 3days. The reaction mixture was filtered and washed with water, ethanol, and Et_2O. Then the green powder was dissolved in hot DMSO (12 mL) at 100°C for 5 min. After cooling to ambient temperature, water (80 mL) was added to reaction mixture. The yellow powder was corrected and washed with water. The crude products were purified by recrystallization from CH_2Cl_2/Et_2O.

Yield, 305 mg (0.515 mmol, 33%), ^1H NMR (CD_3CN, 270 MHz): δ = 7.74-7.70 (m, 3H), 7.35 (dd, J = 8.6, 2.2 Hz, 2H), 6.58 (ddd, J = 12.2, 8.3, 2.2 Hz, 2H), 3.71 (t, J = 12.7 Hz, 6H).

***n*-Bu$_4$N[Pt(dFphpy)CN] (1)**

[Pt(dFphpy)(DMSO)] (103 mg, 0.18 mmol) was added to MeOH (50 mL) solution of *n*-$Bu_4N(CN)$ (58 mg, 0.21 mmol), and the mixture was stirred for 4 h at room temperature. Then, the solvent was evaporated to dryness and the solid residue was washed with water and Et_2O. After the recrystallization from CH_2Cl_2/Et_2O, pale yellow crystals were obtained.

Yield, 95 mg (0.13 mmol, 70%). ^1H NMR (CD_3CN, 270 MHz): δ = 7.73-7.58(m, 3H), 7.34 (tdd, J = 21.6, 7.5, 2.6 Hz, 2H), 6.49 (ddd, J = 12.7, 9.2, 2.6 Hz, 2H), 3.10-3.04 (m, 8H), 1.68-1.53 (m, 8H), 1.36 (sext, J = 7.3 Hz, 8H), 0.96 (t, J = 7.4 Hz, 12H). Anal. Calcd for $C_{34}H_{43}F_4N_3Pt$: C, 53.40; H, 5.67; N, 5.49%. Found: C, 53.32; H, 5.62; N, 5.45%.

***n*-Bu$_4$N[Pt(dFphpy)Cl] (2)**

[Pt(dFphpy)(DMSO)] (103 mg, 0.18 mmol) was added to MeCN (50 mL) solution of *n*-Bu$_4$N(Cl) (58 mg, 0.21 mmol), and the mixture was stirred for 24 h at room temperature. Then, the solvent was evaporated to dryness and the solid residue was washed with water and Et$_2$O. After the recrystallization from CH_2Cl_2/Et$_2$O, pale yellow crystals were obtained.

Yield, 58 mg (0.074 mmol, 41%). ^{1}H NMR ($CDCl_3$, 270 MHz): δ = 7.58-7.52 (m, 3H), 7.50 (tdd, J = 15.8, 7.5, 2.6 Hz, 2H), 6.41 (ddd, J = 12.2, 9.2, 2.6 Hz, 2H), 3.18-3.08 (m, 8H), 1.48-1.34 m, 8H), 1.23sext, J = 7.7 Hz, 8H), 0.86 (t, J = 7.4 Hz, 12H). Anal. Calcd for $C_{33}H_{43}ClF_4N_2Pt$: C, 51.19; H, 5.60; N, 3.62%. Found: C, 51.12; H, 5.58; N, 3.57%.

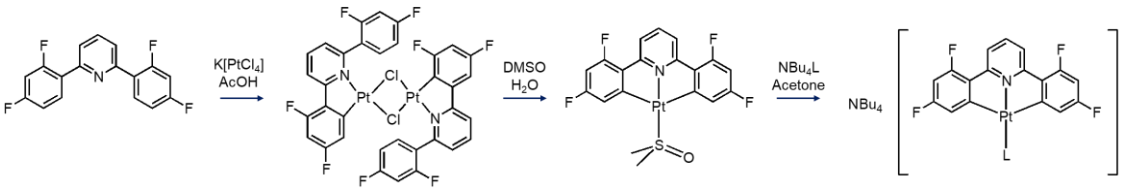

Scheme 3. Synthetic scheme of Pt(II) complexes with fluorine substituted C^N^C tridentate ligands.

5-2-4 Luminescence measurements

Luminescence spectra were collected using a JASCO FR-6600 spectrofluorometer at room temperature and 77 K. Slit widths of the excitation and emission light were 5 or 6 nm. Luminescence quantum yields were measured on a Hamamatsu Photonics C9920-02 absolute photoluminescence quantum yield measurement system equipped with an integrating sphere apparatus and 150 W continuous weave Xenon light source. Hamamatsu Photonics A10095-03 non-luminescent quartz sample holder was used for absolute photoluminescence quantum yield measurements. The accuracy of the instrument was confirmed by the measurement of quantum yield of anthracene in ethanol solution (Φ = 0.27).[12] Emission life time measurements were performed in a Hamamatsu Photonics, C4334 system equipped with a streak camera as a photo detector and a nitrogen laser for the 337 nm excitation. Liquid N_2 cryostat (Optistat-DN optical Dewar and ITC-503 temperature controller, Oxford Instruments) was used for the temperature control. Temperature-dependent data of the emission lifetimes were fitted by Origin2017 software using equation 5-1.

5-2-5. Single crystal X-ray diffraction measurements

All single crystal X-ray diffraction measurements were measured using a Rigaku AFC-7R diffractometer with a Mercury CCD area detector and graphite monochromatized Mo Kα radiation (λ = 0.71069 Å) at 150 K. Each single-crystal was mounted on a MicroMount using liquid paraffin. These crystals were cooled using a N_2-flow type temperature controller. Diffraction data were collected and processed using the Crystal-Clear software.[13] The structures were solved by direct methods SIR2011[14]. Structural refinements were conducted by the full-matrix least-squares method using SHELXL2013.[15] Non-hydrogen atoms were refined anisotropically, and all hydrogen atoms were refined using the rigid model. All calculations were performed using the CrystalStructure crystallographic software package[16] except for refinement. The crystallographic data of **1** and **2** are summarized in Table 1.

Table 1. Crystal Data for complexes **1** and **2**

	1	**2**
Formula	$C_{34}H_{43}F_4N_3Pt$	$C_{33}H_{43}ClF_4N_2Pt$
Formula Weight	764.82	774.25
Crystal system	monoclinic	Monoclinic
Space group	$P2_1/a$	$P2_1/c$
a (Å)	17.545(3)	10.159(1)
b (Å)	18.770(3)	18.375(2)
c (Å)	19.700(4)	16.916(2)
α (°)	90	90
β (°)	102.168(3)	94.697(2)
γ (°)	90	90
V (Å^3)	6342(2)	3147.3(6)
T (K)	150	150
Z	8	4
D_{calc} (g cm^{-3})	1.602	1.634
F(000)	3056.00	1544.00
measured refl.	48794	24898
unique refl.	14393	7181
GOF on F^2	1.017	1.094
R_{int}	0.0527	0.0241
R_1[a]	0.0517	0.0242
wR_2[b](all data)	0.1480	0.0613

[a] $R_1 = \Sigma||F_o| - |F_c||/\Sigma|F_o|$. [b] $wR_2 = [\Sigma w(F_o^2 - F_c^2)/\Sigma w(F_o)^2]^{1/2}$, $w = [\sigma_c^2(F_o^2) + (xP)^2 + yP]^{-1}$, $P = (F_o^2 - 2F_c^2)/3$.

5-2-6. Computational methods

Density functional theory (DFT) calculations for the complexes were performed using the Gaussian software package (G 09).[17] The M06 hybrid function[18] was applied for geometry optimization of singlet states. The 6-31G** atomic orbital basis set[19] was used for light atoms (H, N and C). On the other hands, the SDD basis set[20] was applied for heavy Pt atoms. The tenth lowest singlet electronic excitations were calculated for the ground state geometry using the time-dependent density functional theory (TD-DFT) calculations. All orbitals are visualized by GaussView 0.5 software package (isovalue = 0.02).[21]

5-3 Results and discussion

5-3-1. Crystal structures

The single crystals suitable for single crystal X-ray diffraction measurements were obtained from slow Et_2O vapor diffusion into complex solution of CH_3CN (**1**) and CH_2Cl_2 (**2**). The resulting molecular structures are summarized in Table 1. In the unit cell, two and one crystallographically independent Pt complexes were observed for complex **1** and **2** respectively. Both of two Pt(II) complexes in crystal structure of **1** show the identical coordination structure within experimental error. Therefore, one of them is considered in following discussion (Figure 1). The coordination geometry of complex **1** and **2** were square planar geometry as expected. The sum of the bond angles of coordination geometry (360.1 (**1**), 360.0 (**2**)) revealed that the Pt complexes are highly planar. In comparison with the structure of Pt complex with fluorine unsubstituted ligand and CN^- ligand, each of three bond lengths between tridentate ligand and Pt center of complex **1** is slightly shorter than that of non-substituted compound due to the electron withdrawing property of fluorine atom. The Pt-N bond of complex **1** (1.999(6) Å) is longer than that of complex **2** (1.962(2) Å), which was caused by the trans influence of the monodentate CN^- and Cl^-. The strong σ donor ability of CN^- ligand prolongs the bond length of trans position Pt-N bond than that of Cl^- atom.

The packing structure of **1** and **2** were presented in Figure 2, the complex anions were surrounded by bulky *n*-tetrabutyl ammonium cations. These packing structures were frequently observed in anionic Pt(II) complexes with the *n*-Bu_4N^+ cation.[22] Therefore, no Pt-Pt or π-π intermolecular interaction was observed in the crystalline states of complexes **1** and **2**.

Table 2. Selected bond lengths for the complexes **1** and **2**.

bond (Å)	**1**	**2**
Pt(1)–N(1)	1.999(6)	1.962(2)
Pt(1)–C(1)	2.042(6)	2.050(3)
Pt(1)–C(2)	2.045(7)	2.054(3)
Pt(1)–C(3)	1.957(6)	---
Pt(1)-Cl(1)	---	2.3090(8)

Table 3. Selected bond angles for the complexes **1** and **2**.

angle (°)	**1**	**2**
N(1)–Pt(1)–C(1)	80.6(2)	86.4(3)
N(1)–Pt(1)–C(2)	81.2(3)	79.0(3)
C(2)–Pt(1)–C(3)	161.8(3)	101.3(3)
N(1)–Pt(1)–C(3)	177.0(2)	---
N(1)–Pt(1)–Cl(1)	---	178.56(7)

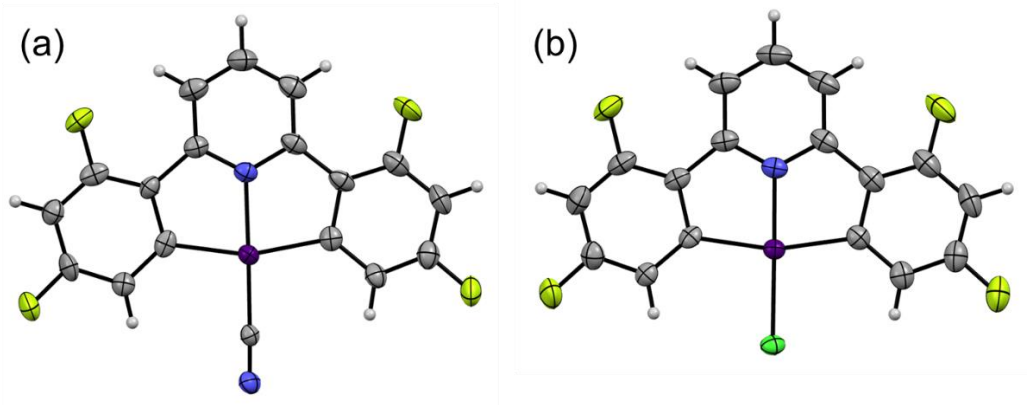

Figure 1. ORTEP drawings of complex anion of (a) **1** and (b) **2**. Displacement parameters are drawn at the 50% probability level. Color code: Pt, purple; C, grey; N, blue; F, yellow; Cl, green; H, White

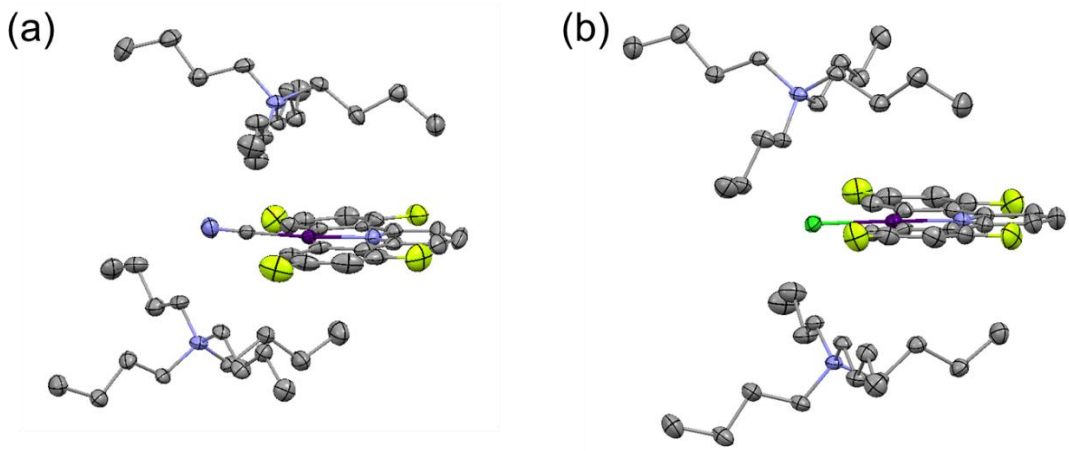

Figure 2. Packing structures of (a) **1** and (b) **2**. Hydrogen atoms are omitted for clarity.

5-3-2. Absorption spectra and solvatochromic properties

The absorption spectra of complex **1** and **2** were presented in Figure 3. The spectra both of complexes exhibited very similar shape in the regime 300–370 nm. The intense absorption bands at shorter than 300 nm are assigned to ligand-centered absorption (^{1}LC). The moderate intense band between 300–370 nm is assigned to inter-ligand charge transfer (^{1}ILCT) and metal-to-ligand charge transfer (^{1}MLCT) absorption likewise square planar Pt(II) complexes reported so far. The most longer-wavelength spin allowed absorption bands show slight difference between two complexes (380–450 nm). The molecular structural difference of two complex is monodentate anionic ligands (CN^- and Cl^-), therefore, the absorption band can be assigned to ^{1}MLCT absorption. The solvatochromic behavior of the complexes were determined by absorption spectra measured in several solvents (Figure 4). The absorption maxima of ^{1}MLCT band show negative solvatochromic behavior with increasing acceptor power of the solvents (Table 4). The linear correlation between acceptor number and energy of ^{1}MLCT absorption maxima revealed that the electron negatively charged Pt anionic complexes are well affected by the electrophilic property of solvents.

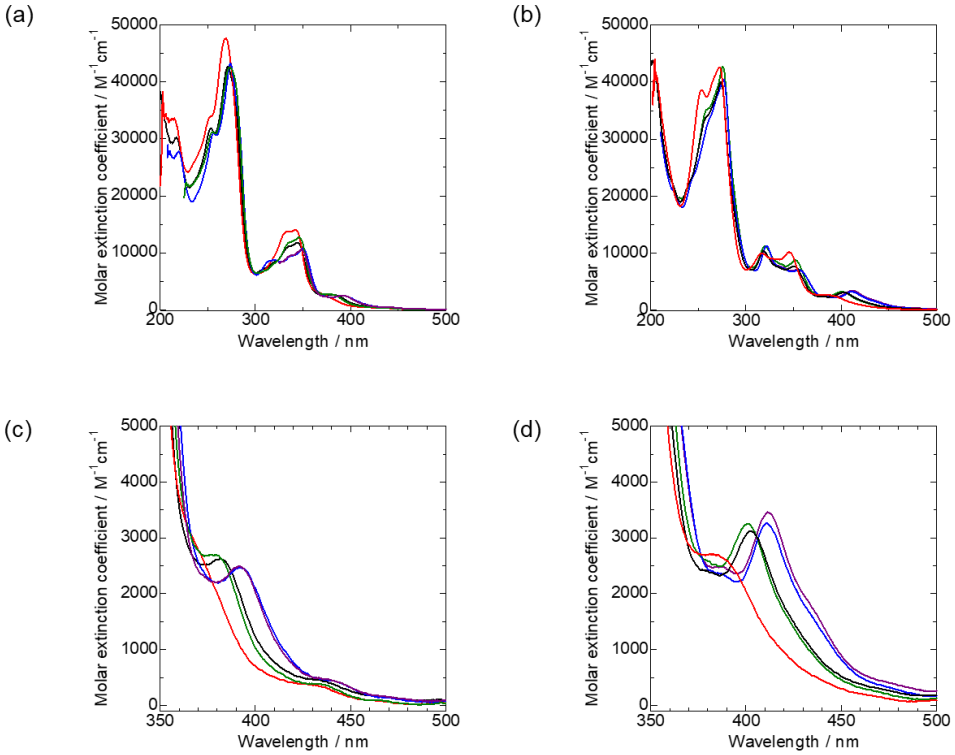

Figure 3. Absorption spectra of (a) **1** and (b) **2**, and enlarged MLCT absorption bands (c) **1** and (d) **2** in acetonitrile (black), methanol (red), dichloromethane (green), acetone (purple) and tetrahydrofuran (blue).

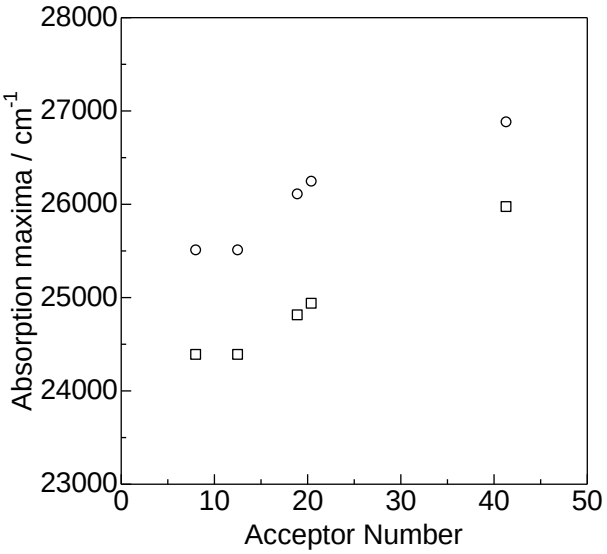

Figure 4. Plot of absorption maxima of ^{1}MLCT absorption vs acceptor number (circle (**1**) and square (**2**))

Table 4. Absorption properties of the complexes **1** and **2** in various solvents.

Solvent	Absorption maxima		E_T value / kcal mol	Acceptor number	Donor number
	Complex **1**	Complex **2**			
MeOH	372 nm (sh)	385 nm (sh)	55.4	41.3	30.0
CH_2Cl_2	381 nm	401 nm	40.7	20.4	1.0
MeCN	383 nm	403 nm	45.6	18.9	14.1
Acetone	392 nm	410 nm	42.2	12.5	17.0
THF	392 nm	410 nm	37.4	8.0	20.0

5-3-3. Photoluminescence properties

In order to discuss the effect of fluorine atom substitution, the photoluminescence spectra were measured in several organic solvents. The reported non-substituted (*n*-Bu_4N)[Pt(C^N^C)(L)] complexes exhibit ^{3}LC emission in fluid solution, however, the complexes **1** and **2** showed no detectable emission in fluid solution. On the other hand, the detectable photoluminescence was observed in the solid state. Therefore, the following photoluminescence properties were described in the solid state. The emission spectra in the solid state were shown in Figure 5, the broad weak emission with the emission maxima at 609 (**1**) and 627 (**2**) nm were observed at room temperature. The emission maximum of corresponding (*n*-Bu_4N)[Pt(C^N^C)(CN)] in the solid state at room temperature is 590 nm. The emission maximum of complex **1** was slightly longer wavelength shifted than that of non-substituted complex, which suggest the lowest excited triplet state of complex **1** is less contributed from inter ligand charge transfer and ligand center states. The emission lifetimes were less than microsecond (τ = 170 (**1**), 77 (**2**) ns) and the emission quantum yields were very low value (Φ = 0.02(**1**), 0.01(**2**)), which clearly presented the emission efficiency was not improved by the fluorine substitution to the tridentate C^N^C ligand. The emission quantum yield increased to 0.25 (**1**) and 0.13 (**2**) with temperature decreasing, and lifetimes also increased to 3.9 (**1**) and 2.2 (**2**) μs at 77 K. These weak broad emissions can be assigned to ^{3}MLCT emission in Pt(II) complexes. Further discussion is described in following temperature dependence and theoretical calculations section.

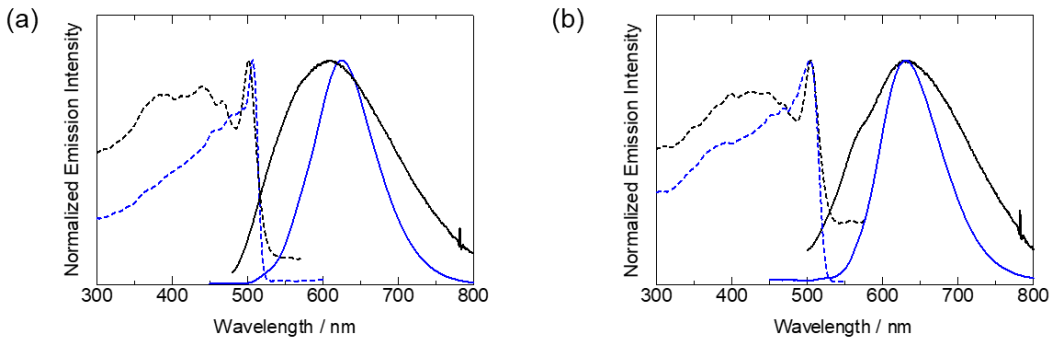

Figure 5. Emission (solid lines) and excitation (dotted lines) spectra of (a) **1** and (b) **2** at room temperature and 77 K (blue) (solid state; λ_{ex} = 400, λ_{em} = 620 nm).

Table 5. Luminescence properties of the complexes **1** and **2**.

Complex	Temp. (K)	λ_{em} (nm)	Φ	τ (μs)	k_r (s^{-1})	k_{nr} (s^{-1})
1	298	609	0.02	0.17	117647	5764705
	77	624	0.25	3.9	64102	192307
2	298	627	0.01	0.077	129870	12857142
	77	630	0.13	2.2	59090	395454

5-3-4. Temperature dependence of photoluminescence properties.

To obtain the information for non-radiative decay pathways, temperature dependence of emission lifetimes was measured. To analyze activation energy and rate constant from emissive triplet state to non-emissive states, resulting emission decay was analyzed using equation 1, where, τ, k_0, k_1, ΔE, k_B, T were observed emission lifetimes, temperature independent rate constant, rate constant of decay process with energy barrier, activation energy, Boltzmann constant, and temperature.[23]

$$\tau^{-1} = k_{obs} = k_0 + k_1 \exp\left(\frac{-\Delta E}{k_B T}\right) \quad \text{(eq. 1)}$$

The fitting results exhibit small activation energy (860 cm^{-1} for both **1** and **2**) and 10^8 orders of k_1 (Table 6). Such small activation energies are good agreement with the low quantum yield of both complexes at room temperature. Several Pt(II) complexes have been analyzed using either Arrhenius or Boltzmann equation to obtain their non-radiative pathways. Most of the case, it was found that 2000-3000 cm^{-1} higher lying metal-center (^{3}MC) excited states with the rate constant of $10^{10\sim11}$ s^{-1} order.[23] However, in the case of complex **1** and **2**, the much slow 10^8 order of rate constants suggest that the dominant non-radiative process is not higher lying ^{3}MC states. Therefore, other mechanism of non-radiative pathways is needed to explain the non-radiative pathway for complexes **1** and **2**. In order to obtain further information of excited triplet states, the computational studies were carried out and discussed in next section.

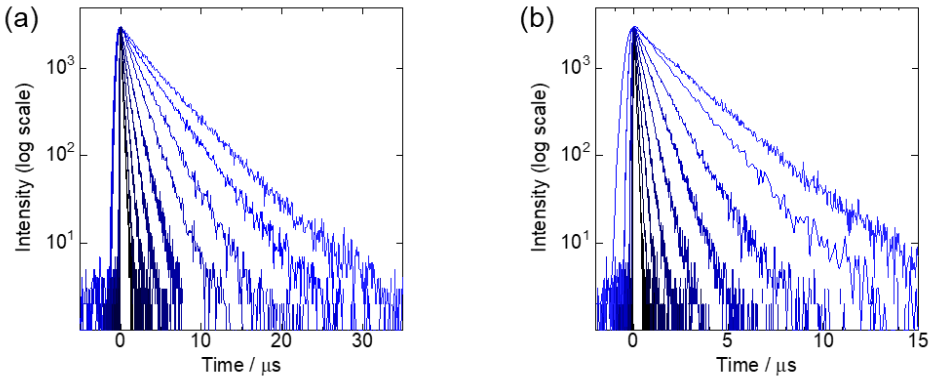

Figure 6. Temperature dependence of emission decays for complexes **1** and **2** at 298–77 K in the solid state. (at 77, 100, 130, 160, 190, 220, 250, 280, and 298 K)

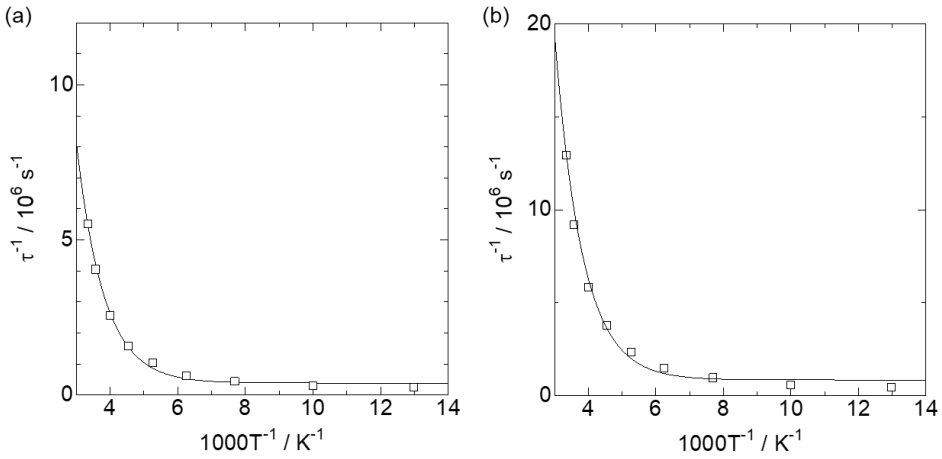

Figure 7. The plots of emission lifetimes vs temperature in reciprocal scale for **1** and **2**. The solid lines were described from the results of fit using eq 1.

Table 6. Fitting results of temperature dependent lifetime measurement.

Complex	k_0 (s^{-1})	k_1 (s^{-1})	ΔE_1 (cm^{-1})
1	3.8×10^5	3.1×10^8	860
2	8.5×10^5	7.3×10^8	860

5-3-5. Computational studies.

Density functional theory (DFT) and time-dependent DFT (TD-DFT) were used to study the ground state and lowest singlet and triplets excited states of two complexes. Starting from the ground state optimized structures, vertical excitation energies were calculated by using TD-DFT and summarized in Tables 7 and 8. The lowest excited states (389 (**1**) and 396 (**2**) nm) with weak oscillator strength exhibited good agreement with experimental absorption spectrum of ^{1}MLCT bands (372-‑392 (**1**) and 385–410 (**2**) nm), and these calculated excited states can be assigned to ^{1}MLCT by orbital contributions (Figures 8 and 9).

For excited triplet states, TD-DFT calculations were conducted with structure optimization. Two distinct triplet state structure were obtained in **2** depending on the initial structure (Figure 10). Planar structure has similar energy value (602 nm (**2**)) to experimental wavelength (627 nm (**2**)), the other is bent structure and the excitation energy (1097 nm) is much smaller than that of planar structure. Only bent structure was obtained from planar and bent initial structure, and energy value is far from experimental value. To obtain information of planar excited triplet structure of **1**, the coordination dihedral angle C-Pt-N-C frozen calculation was performed, and resulting energy value revealed the better agreement with experimental results. Calculated total energies of bent triplet states are 2400 cm^{-1} stable from that of planar excited triplet states (Table 9). In order to rationalize the nature of the emission, the triplet structures using single-point energy calculations have been checked. The Kohn-Sham orbitals corresponding to excited electron and hole revealed that the excited state characters of planar triplet states can be assigned to ^{3}MLCT excited states. On the other hand, contributions of Pt(II) atoms increased significantly in the case of bent structure, therefore, the excited states of bent structure were assigned to lower lying metal center states (^{3}MC) (Figure 11).

Table 7. selected excited singlet states of TD-DFT calculations for complex **1**.

Excited states	Energy / eV(nm)	Oscillator strengths	Major contributions (%)
1	2.86 (433)	0.00	HOMO−1-LUMO (99)
2	2.88 (431)	0.00	HOMO-LUMO (98)
3	3.19 (389)	0.01	HOMO−2-LUMO (99)
4	3.40 (365)	0.01	HOMO−3-LUMO (73)
			HOMO−1-LUMO+1 (23)
5	3.45 (360)	0.00	HOMO−2-LUMO+1 (98)

Table 8. selected excited singlet states of TD-DFT calculations for complex **2**.

Excited states	Energy / eV(nm)	Oscillator strengths	Major contributions (%)
1	2.60 (476)	0.00	HOMO-LUMO (98)
2	2.81 (441)	0.00	HOMO−1-LUMO (99)
3	3.10 (400)	0.00	HOMO−3-LUMO (91)
			HOMO-LUMO+1 (8)
4	3.13 (396)	0.02	HOMO−2-LUMO (85)
			HOMO−1-LUMO+1 (11)
5	3.07 (391)	0.00	HOMO−3-LUMO (8)
			HOMO-LUMO+1 (90)

Figure 8. Selected molecular orbitals for the ground state of complex **1** calculated by DFT method at the M06 level (isovalue = 0.02), combined with the energy (eV).

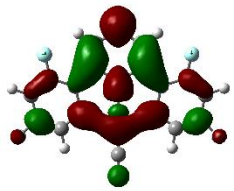	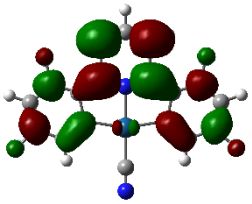		
LUMO 1.18 eV	LUMO+1 1.63 eV		
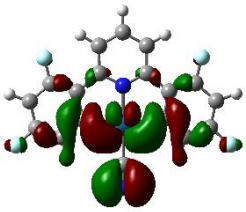	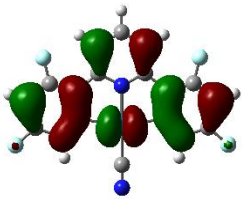	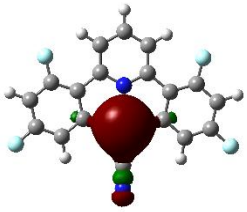	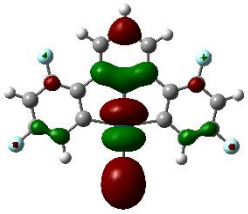
HOMO −2.86 eV	HOMO−1 −2.88 eV	HOMO−2 −3.20 eV	HOMO−3 −3.26 eV

Figure 9. Selected molecular orbitals for the ground state of complex **2** calculated by DFT method at the M06 level (isovalue = 0.02), combined with the energy (eV).

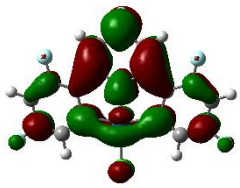	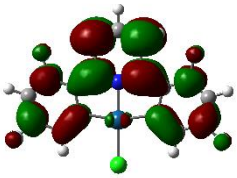		
LUMO 1.35 eV	LUMO+1 1.76 eV		
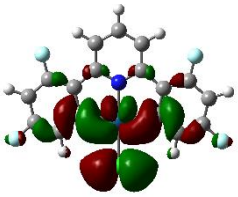	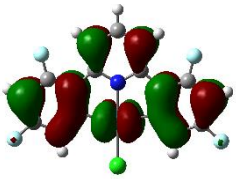	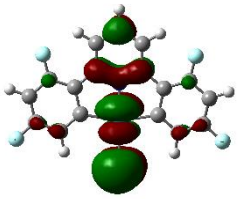	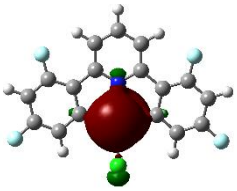
HOMO −2.42 eV	HOMO−1 −2.69 eV	HOMO−2 −2.71 eV	HOMO−3 −3.03 eV

Table 9. Lowest excited triplet states of TD-DFT calculations for complexes **1** and **2**.

complex	structure	Energy / eV(nm)	Total energy (Hatree)	Orbital contributions (%)
1	flat	2.18 (568)	-1317.6874	92-93 (71)
	bent	1.34 (925)	-1317.6983	92-93 (96)
2	flat	2.06 (602)	-1685.0925	93-95 (86)
	bent	1.13 (1097)	-1685.1036	94-95 (95)

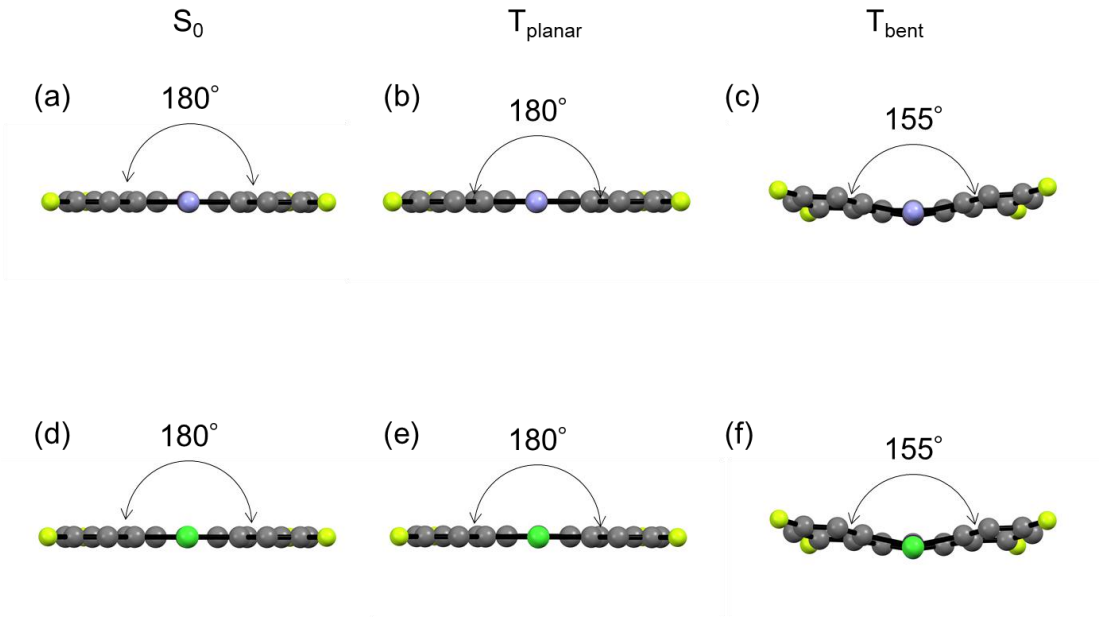

Figure 10. Ground state structure, planar and bent triplet states of complexes **1** (a-c) and **2** (d-f).

Figure 11. Kohn Sham orbitals of planar and bent structure of triplet states for complexes **1** and **2**.

Complex **1**		Complex **2**	
Planar	Bent	Planar	Bent
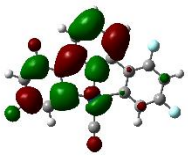	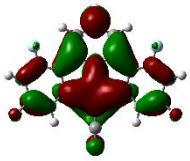	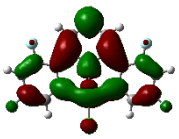	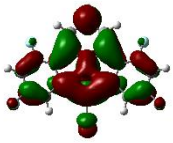
93	93	95	95
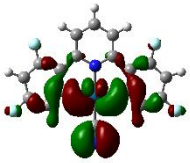	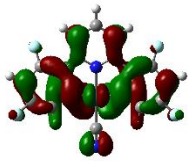	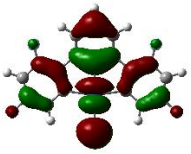	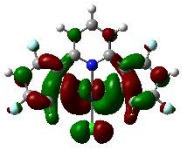
92	92	93	94

5-3-6. **Assignments of the excited triplet states**

Based on the both experimental results and computational experiments, the energy diagram of the complexes were proposed as shown in Figure 12. The localized minimum emissive ^{3}MLCT states were quenched via lower lying triplet states with small activation energy. The bent structure of lowest triplet states might have fast non-radiative decay pathways, therefore, the photoluminescence quantum yields of complexes in the solid states are very low at room temperature. It has been reported that ^{3}MLCT emitters of Pt(II) complexes frequently access to higher and lower lying ^{3}MC states.[24] The ^{3}MLCT states of Pt(II) complexes are less emissive than that of Ru(II) and Ir(III) complexes.

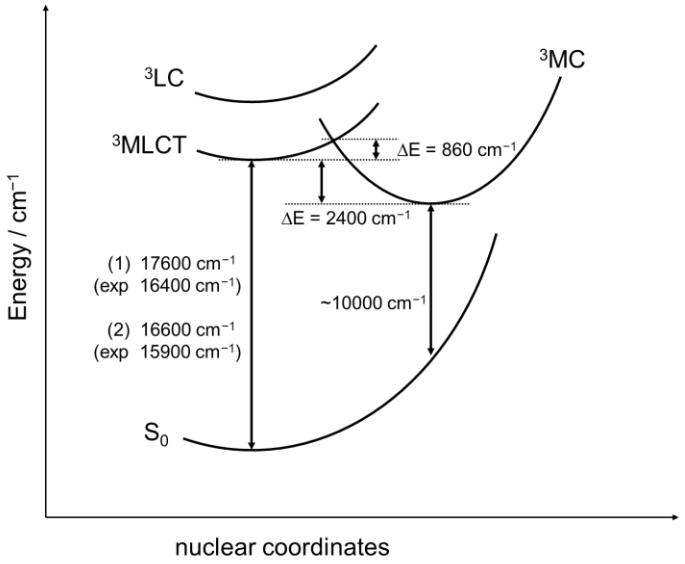

Figure 12. Energy diagrams of excited triplet states of complexes **1** and **2**.

5-4. Conclusion

In this chapter, the weakly emissive C^N^C cyclometalated Pt(II) complexes were studied to describe further criteria to design phosphorescence Pt(II) complexes with high quantum yield. The emissive states of **1** and **2** can be assigned to ^{3}MLCT. The very small activation energy to non-radiative states was obtained by temperature dependence of emission lifetime. Furthermore, theoretical calculations also suggest the presence of such two different triplet states. Therefore, it was not emphasized criteria to make intense phosphorescence Pt(II) complexes that the ^{3}MLCT cannot be used for strong emitters. To prevent making the lowest triplet MLCT states, energy levels of ligand especially HOMO should be taken into consideration.

1 (*a*) Q. Zhao, C. Huang and F. Li, *Chem. Soc. Rev*., 2011, **40**, 2508–2524; (*b*) K. K.-W. Lo and S. P.-Y. Li, *RSC Adv.*, 2014, **4**, 10560–10585.

2 (*a*) Y.-J. Yuan, Z.-T. Yu, D.-Q. Chen and Z.-G. Zou, *Chem. Soc. Rev*., 2017, 46, 603–631; (*b*) P. D. Frischmann, K. Mahata and F. Würthner, *Chem. Soc. Rev*., 2013, **42**, 1847–1870.

3 (*a*) O. S. Wenger, *Chem. Rev*., 2013, **113**, 3686−3733; (*b*) Anna J. McConnell, Christopher S. Wood, Prakash P. Neelakandan, and Jonathan R. Nitschke, *Chem. Rev*. 2015, **115**, 7729−7793.

4 (*a*) H. Yersin, A. F. Rausch, R. Czerwieniec, T. Hofbeck, T. Fischer, *Coord. Chem. Rev*., 2011, **255**, 2622–2652; (*b*) Y. Chi and P.-T. Chou, *Chem. Soc. Rev.*, 2010, **39**, 638–655.

5 J. Kalinowski, V. Fattori, M. Cocchi, J. A. G. Williams, *Coord. Chem. Rev*., 2011, **255**, 2401–2425.

6 J. A. G. Williams, *Top. Curr. Chem*., 2007, **281**, 205.

7 J. R. Berenguer, E. Lalinde and J. Torroba, *Inorg. Chem.*, 2007, **46**, 9919

8 J. A. G. Williams, A. Beeby, E. S. Davies, J. A. Weinstein, C. Wilson, *Inorg. Chem.* 2003, **42**, 8609.

9 G. So-Ming and C.-M. Che, *Chem. Eur. J.*, 2009, **15**, 7225.

10 (a) J. Brooks, Y. Babayan, S. Lamansky, P. I. Djurovich, I. Tsyba, R. Bau and M. E. Thompson, *Inorg. Chem*., 2002, **41**, 3055; (b) A. F. Rausch, L. Murphy, J. A. G. Williams, and H. Yersin, *Inorg. Chem*., 2012, **51**, 312; (c) A. F. Rausch, U. V. Monkowius, M. Zabel, and H. Yersin, *Inorg. Chem*., 2010, **49**, 7818.

11 A. J. Wilkinson, H. Puschmann, J. A. K. Howard, C. E. Foster, and J. A. G. Williams., *Inorg. Chem.*, 2006, **45**, 8685.

12 (a) W. R. Dawson and M. W. Windsor, *J. Phys. Chem*., 1968, **72**, 325; (b) W. H. Melhuish, *J. Phys. Chem*., 1961, **65**, 229.

13 CrystalClear: Data Collection and Processing Software, Rigaku Corporation (1998-2014). Tokyo 196-8666, Japan.

14 SIR2011: Burla, M. C., Caliandro, R., Camalli, M., Carrozzini, B., Cascarano, G. L., Giacovazzo, C., Mallamo, M., Mazzone, A., Polidori, G. and Spagna, R. (2012). J. Appl. Cryst. 45, 357-361.

15 SHELXL2013: Sheldrick, G. M. (2008). Acta Cryst. A64, 112-122.

16 *CrystalStructure 4.2.5*, Rigaku Corporation, Tokyo196-8666, Japan, 2000-2017.

17 M. J. Frisch, G. W. Trucks, H. B. Schlegel, G. E. Scuseria, M. A. Robb, J. R. Cheeseman, G. Scalmani, V. Barone, B. Mennucci, G. A. Petersson, H. Nakatsuji, M. Caricato, X. Li, H. P. Hratchian, A. F. Izmaylov, J. Bloino, G. Zheng, J. L. Sonnenberg, M. Hada, M. Ehara, K. Toyota, R. Fukuda, J. Hasegawa, M. Ishida, T. Nakajima, Y. Honda, O. Kitao, H. Nakai, T. Vreven, J. A. Montgomery, Jr., J. E. Peralta, F. Ogliaro, M. Bearpark, J. J. Heyd, E. Brothers, K. N. Kudin, V. N. Staroverov, R. Kobayashi, J. Normand, K. Raghavachari, A. Rendell, J.

C. Burant, S. S. Iyengar, J. Tomasi, M. Cossi, N. Rega, J. M. Millam, M. Klene, J. E. Knox, J. B. Cross, V. Bakken, C. Adamo, J. Jaramillo, R. Gomperts, R. E. Stratmann, O. Yazyev, A. J. Austin, R. Cammi, C. Pomelli, J. W. Ochterski, R. L. Martin, K. Morokuma, V. G. Zakrzewski, G. A. Voth, P. Salvador, J. J. Dannenberg, S. Dapprich, A. D. Daniels, Ö. Farkas, J. B. Foresman, J. V. Ortiz, J. Cioslowski, and D. J. Fox, GAUSSIAN 09 (Revision E.01), Gaussian, Inc., Wallingford, CT, 2009.

18 Y. Zhao and D. G. Truhlar, *Theor. Chem. Account*, 2008, **120**, 215.

19 (*a*) R. Ditchfield, W. J. Hehre, and J. A. Pople, *J. Chem. Phys.*, 1971, **54**, 724–728; (*b*) W. J. Hehre, R. Ditchfield, and J. A. Pople, *J. Chem. Phys.*, 1972, **56**, 2257–2261; (*c*) P. C. Hariharan and J. A. Pople, *Theor. Chem. Acc*., 1973, **28**, 213–222; (*d*) P. C. Hariharan and J. A. Pople, Mol. Phys., 1974, **27**, 209-214; (e) R. C. Binning Jr. and L. A. Curtiss, *J. Comp. Chem.*, 1990, **11**, 1206–1216.

20 (*a*) P. Fuentealba, H. Preuss, H. Stoll, and L. Vonszentpaly, *Chem. Phys. Lett.*, 1982, **89**, 418–422; (*b*) T. H. Dunning Jr., P. J. Hay, *Modern Theoretical Chemistry*; Plenum: New York, *1977*, **3**, 1–28.

21 R. Dennington, T. Keith, and J. Millam, GaussView 05, Semichem Inc., Shawnee Mission, KS, 2009.

22 (a) J. Forniés, S. Fuertes, J. A. López, A. Martín and V. Sicilia, *Inorg. Chem*., 2008, **47**, 7166-7176; (b) T. Ogawa, M. Yoshida, H. Ohara, A. Kobayashi and M. Kato, *Chem. Commun.*, 2015, **51**, 13377.

23 (*a*) C. B. Blanton, Z. Murtaza, R. J. Shaver, and D. P. Rillema, *Inorg. Chem*., 1992, **31**, 3230-3235; (*b*) F. Barigelletti, J. D. Sandrini, M. Maestri, V. Balzani, A. von Zelewsky, L. Chassot, P. Jolliet and U. Maeder, *Inorg. Chem*., 1988, **27**, 3644−3647.

24 W. B. Connick, V. M. Miskowski, V. H. Houlding and H. B. Gray, *Inorg. Chem*., 2000, **39**, 2585.

Chapter 6.
General Conclusion

The studies in this thesis demonstrated the state of matter and photophysical properties of anionic Pt(II) complexes controlled by counter ions. In comparison with neutral complexes, it was clearly indicated that ionic complexes have advantageous to control state of matter, crystalline structure as well as phosphorescence properties of the Pt(II) complexes. The condensed liquid states were discovered when imidazolium cations are used as the counter cation of anionic Pt(II) complexes. On the other hand, the tetra *n*-butyl ammonium cation affords rigid packing structure without any Pt-Pt or π-π interactions between Pt(II) complex anions. Using such crystalline states, detailed phosphorescence properties can be determined easily, although the luminescence cannot be observed in fluid solutions.

In chapter 1, the background and purpose of this thesis were described. The phosphorescence properties of Pt(II) and other metal complexes, soft materials composed of metal complexes and outline of this thesis were summarized.

In chapter 2, anionic complex with imidazolium cation formed liquid phase at room temperature. Resulting ionic liquid Pt(II) complexes exhibit glass transition during cooling process, and no crystalline states were observed in the measurement conditions. The resulting ionic liquid Pt(II) complexes exhibit both emission from monomer (^{3}LC) and dimer (^{3}MMLCT). The temperature dependence of intensity of two distinct emission affords thermochromic luminescence properties. These photophysical properties were attributed to co-existence of monomer and dimer species in liquid state and amorphous glass states.

In chapter 3, novel anionic Pt(II) complexes with N-heterocyclic carbene (NHC) ligands were synthesized as tetrabutyl ammonium salts. The intense phosphorescence of anionic Pt(II) complexes was assigned to ^{3}LC. Temperature dependence of phosphorescence lifetime reveals that the detailed photophysical properties depend on the emission energy of Pt(II) NHC complexes. Furthermore, effects of π extension regioselectivity was determined by theoretical calculations. These results contribute to design phosphorescence properties of novel Pt(II) NHC complexes.

In chapter 4, two another ionic liquid Pt(II) complexes were synthesized. The thermochromic luminescence behavior and similar phase transition behavior were observed likewise first ionic liquid Pt(II) complexes reported in chapter 2. These two another example support the generality of thermochromic luminescence behavior of ionic liquid Pt(II) complexes. The emission color can be tuned by emission wavelength of ^{3}LC and ^{3}MMLCT.

In chapter 5, fluorine substituted tridentate C^N^C cyclometalated Pt(II) complexes were studied to obtain further information of weak emissive anionic Pt(II) complexes with C^N^C ligands. The emission in solid states can be assigned to ^{3}MLCT states. There are another lower lying triplet states with bent coordination structure, which might contribute to fast non-radiative decay pathways. This result suggests that tridentate ligands are not always rigid at excited triplet states. In Pt(II) complexes, ^{3}MLCT states are close to ^{3}MC states, therefore, the most ^{3}MLCT emission is weak. To make intense

phosphorescence of Pt(II) complexes, the HOMOs should consist of orbitals from ligand.

Among these results, it was demonstrated that anionic Pt(II) complexes are advantageous to control not only the state of matter and crystal structure but also phosphorescence properties by various counter cations. Although the interest to phosphorescent ionic soft material and solid material is still not high, these results provide some knowledge about design of phosphorescent ionic materials.

Acknowledgements

The studies presented in this thesis were carried out at the Department of Chemistry, Faculty of Science, Hokkaido university during April 2012-March 2018.

The author would like to express greatest profound appreciation to Professor Masako Kato (Hokkaido University) for the best research environment and warm encouragements.

The author would like to express deepest gratitude to Professor Ho-Chol Chang (present affiliation Chuo University) for earnest guidance and valuable discussions.

The author would also like to express deepest appreciation to Associate Professor Atsushi Kobayashi (Hokkaido University) for his numerous discussions and devoted attitude to education.

Furthermore, the author is deeply grateful to Assistant Professor Masaki Yoshida (Hokkaido University) for his helpful discussion and encouragements.

The author would also like to show greatest appreciation to Assistant Professor W. M. C. Sameera for his valuable comments and discussions as well as support for advanced calculations.

The author would like to gratefully acknowledge to Assistant Professor Takeshi Matsumoto (present affiliation Chuo University) for his helpful discussions and supports with outstanding experimental techniques.

The author would also like to express gratitude to Professor Felix N. Castellano, Dr. Karim El-Roz, and Dr. Petr Koutnik (all North Carolina State University) for supervision and warm hospitality during visiting their research group (January 2017- March 2017).

Moreover, the author would like to express his gratitude to Professor Noboru Kitamura, Professor Sadamu Takeda, and Professor Toshihiro Shimada (all Hokkaido University) for reviewing this thesis.

The author also gratefully acknowledges to Professor Sadamu Takeda, Dr. Tomonori Ikegami and Mr. Jun-ya Okamoto for their support with DSC measurements. The author would like to acknowledge to Professor Noboru Kitamura and Mr. Soichiro Akagi for their support with emission lifetime measurement below 77 K.

I would like to acknowledge to Dr. Tadashi Ohba, Dr. Hiroki Ohara, Dr. Masanori Wakizaka and Dr. Hirotaka Honda (all Hokkaido University) for helpful advice and valuable comments as well as numerous words of encouragement.

The author deeply grateful to Dr. Yasuhiro Shigeta for helpful discussion, best friendship as well as dedicated supports.

The author also deeply grateful to Dr. Masataka Imai for best friendship and valuable supports.

The author also grateful to Dr. Kana Sato (Sawaguchi), Dr. Erika Saito, and Ms. Panyi Liang (all Hokkaido University) as well as all member of the Kato group for helpful cooperation in the laboratory.

This work was financially supported by the KAKENHI Grant Number JP 16J01368 from the JSPS.

Finally, I would like to express special thanks to my family (Dr. Hideo Ogawa, Mrs. Mikako Ogawa, Mr. Seiji Ogawa and Ms. Eri Ogawa) and friends for their supports and encouragements.

Tomohiro Ogawa
Graduate School of Chemical Sciences and Engineering
Hokkaido University